# Orbital control and climate feedbacks on ice age cycles during Plio-Pliestocene

by

Shih-Yu Lee

A dissertation submitted in partial fulfillment
of the requirements for the degree of
Doctor of Philosophy
(Oceanography: Marine Geology and Geochemistry)
in The University of Michigan
2008

Doctoral Committee:

Associate Professor Christopher J. Poulsen, Chair
Professor Philip A. Meyers
Professor Joyce E. Penner
Professor David K. Rea
Assistant Professor Ingrid L. Hendy
Assistant Professor Xianglei Huang

To Mom and to Min-John for all their love and support.
And to my grandparents, who I know would
have been so pleased.
- 謝謝 -

Acknowledgements

First and foremost I want to thank my advisor Chris Poulsen. It has been an honor to be his first PhD student. He has shown me an excellent role model of how good science and quality life work together. I deeply appreciate all his time, discussion, and funding to make my PhD experience inspirational and enjoyable. His enthusiasm for research was contagious and motivational for me, even during the tough times of this pursuit. I am also thankful for his assistance during the initial stages of this program as I was very much under-prepared. He demonstrated great patience as I figured out what I was doing.

For this dissertation, I would like to thank my committee members: Chris, Dr. Joyce Penner, Dr. Ingrid Hendy, Dr. Xianglei Huang, Dr. Phil Meyers, and Dr. Dave Rea for all their time, helpful comments, and insightful questions. I also gratefully acknowledge the funding sources that made my graduate study possible. My dissertation work was supported by the National Science Foundation, the University of Michigan, and the Barbour fellowship.

My time in Ann Arbor was made enjoyable in large part due to many friends that became a part of my life. I am grateful for times spent with roommates and my lunch gangs, for my running buddies and our memorable jogs in freezing Michigan winters, for Andrea and Mark's hospitality when I was transforming myself from a foreigner and getting to know American culture, and

for many other people and memories. My graduate student life was also enriched by members of Poulsen's research group. The group has been a source of friendship as well as good advice: Dan Horton's amazing ability to decipher what I really want to say in everyday life and papers. Jing Zhou's cheerful smiles constantly light me up. I also have had pleasure to work with Tran Huynh and Tom Foster who were very helpful when I started graduate school in the US.

My adventure to America was deeply blessed by many other individuals. CAH has been a friend as well as a mentor over these years. Sinsin is my silent hero. Thelyra and Vicky are my forever cheer team since college. XFP and PP always greet me with open arms and warm hearts wherever they are.

Lastly, I would like to thank my family for all their love, support, and encouragement. For my mom who raised me with a love of enjoying life and unconditionally supporting me in all my pursuits. For my brother Min-John who has been so loving, supportive, and encouraging of every aspect in my life. Thank you.

Table of Contents


Dedication ii
Acknowledgements iii
List of Figures vi
List of Tables xi
Abstract xii
Chapter
I. Introduction 1
II. Tropical Pacific climate response to obliquity forcing in the Pleistocene 11
III. Sea ice control of Plio-Pleistocene Tropical Pacific climate evolution 44
IV. Amplification of obliquity forcing through mean-annual and seasonal atmospheric feedbacks 75
V. Obliquity and precessional forcing of continental snow fall and melt 101
VI. Summary 139

List of Figures

Figures 2-1. Seasonal (left) and mean-annual (right) solar insolation difference between HOBL and LOBL. Under high obliquity, seasonal and annual meridional insolation gradients are reduced. The contour interval is 10 $Wm^{-2}$. 32

Figure 2-2. (a) Simulated mean-annual sea-surface temperature in the glacial HOBL experiment. Glacial tropical SSTs are approximately 4 °C cooler than modern SSTs. (b) Surface and (c) subsurface (30-100 m) temperature differences between the HOBL and LOBL (HOBL – LOBL) experiments. In response to an increase in obliquity, tropical SSTs cool by up to 0.6 °C, but tropical subsurface waters warm by up to 0.8 °C. Southern hemisphere water particle paths calculated using a Lagrangian transport model are shown in (c). The thick black (blue) line represents the particle trajectory in the HOBL (LOBL) experiment. The length of the trajectory indicates the speed of the flow. Thus, the trajectories indicate that flow through the subtropical gyre is faster in the LOBL experiment than the HOBL experiment. The contour interval is 3 °C in (a) and 0.2 °C in (b) and (c); the blue area in (b) and (c) represents a temperature decrease. 33

Figure 2-3. Simulated seasonal sea-surface temperature (°C) difference between HOBL and LOBL (HOBL – LOBL) experiments. Seasonal differences are linked to seasonal insolation differences or dynamical responses to seasonal insolation differences (see text). The contour interval is 0.2 °C; lower temperatures are indicated by dashed contour. (DJF = December, January, February; MAM=March, April, May; JJA=June, July, August; SON=September, October, November) 34

Figure 2-4. Seasonal and mean-annual differences in near-surface wind (vectors) and surface-level pressure (SLP) (contours) between HOBL and LOBL (HOBL-LOBL). Seasonal differences in insolation forcing generate SLP and near-surface wind anomalies. For example, in MAM, subtropical heating (cooling) intensifies (reduces) the subtropical high, leading to stronger (weaker) trades in the northern (southern) hemisphere. Only wind vector differences greater than 0.5 $ms^{-1}$ in (a)-(d) and 0.25 $ms^{-1}$ in (e) are displayed. The SLP contour interval is 0.5 mb; the dashed contours represent a decrease in SLP. Acronyms for the seasons are the same as in Fig. 3; ANN=mean-annual. 35

Figure 2-5. (a) Mean-annual subsurface (30-100m) flow in the HOBL experiment. (b) Difference in the subsurface flow between the HOBL and LOBL (HOBL – LOBL) experiments. As indicated by their reversal in the difference plot, the subtropical gyres slow, while the Northern Equatorial Counter Current and Southern Equatorial Current increase in speed. Note the different between the reference vectors between panels. Reference vectors are in cm $s^{-1}$. 36

Figure 2-6. (a) Difference (HOBL – LOBL) in zonal-average mean-annual surface wind ($ms^{-1}$) over the Pacific (120°E-90°W). As indicated by the positive (eastward) wind difference, in the northern hemisphere, the off-equatorial trade winds weaken around 15° and intensify near 30° in the HOBL experiment. (b) Schematic displaying the affect of the change in zonal wind stress on the equatorial currents, according to Sverdrup theory. The solid line represents the change in relative sea -level height due to the changes in zonal wind with latitude. The symbols represent the relative change in current direction. Note that the SEC and the NECC both strengthen; the NEC weakens. 37

Figure 2-7. Cross-section of seawater temperature difference (HOBL – LOBL) in the eastern South Pacific (77.4°W – 91.4W). The contour interval is 0.2 °C. 38

Figure 2-8. Seasonal (DJF and JJA) sea-ice distributions in the southern hemisphere for the HOBL (left column) and LOBL (right column) experiments. Note that the sea-ice distribution is farthest equatorward in the LOBL experiments. The polar projection map begins at 30 °S; the continents are shaded gray. 39

Figure. 3-1. Mean Southern Hemisphere winter (June-July-August) sea-ice distribution for the LGM-ICE (left), MOD-ICE (middle), and NO-ICE (right) experiments. The LGM-ICE winter sea-ice extent is approximately 95% greater than the MOD-ICE. NO-ICE has no sea ice by design (see Section 2.2). The polar projection map begins at 30°S. 60

Figure. 3-2. Simulated mean-annual sea surface temperatures in LGM -ICE (dotted), MOD-ICE (dashed), and NO-ICE (solid) experiments. LGM-ICE and MOD-ICE SSTs are approximately 10 and 6°C cooler than NO-ICE at 45°S. 61

Figure. 3-3. Mean-annual SST differences (°C) in the equatorial Pacific Ocean between (a) the LGM-ICE and NO-ICE experiments, and (c) the MOD-ICE and NO-ICE experiments. In both cases, the presence of high-latitude sea ice causes tropical cooling with greater cooling in the EEP, intensifying the east-west tropical SST gradient. Cross

section of mean-annual seawater temperature difference (°C) between (b) the LGM-ICE and NO-ICE experiments, and (d) the MOD-ICE and NO-ICE experiments. Pacific temperature differences are averaged between 10°N-10°S. Note that much colder waters are upwelled in the EEP in the experiments with sea ice. The contour interval is 0.5°C. 62

Figure. 3-4. Mean-annual sea water temperature differences (°C) in (a) the eastern equatorial Pacific upper ocean and (b) the global deep-ocean through time (model year). The EEP upper ocean temperature difference were calculated between the sea surface and a depth of 150m for the domain within 3.5°S – 3.5°N and 92°E - 103°E (Fig. 3-3a). The global deep ocean temperature differences were calculated between 200-5000 m. 63

Figure. 3-5. Mean-annual vertical pressure velocity (Pa $s^{-1}$) (contours) and zonal velocity ($ms^{-1}$) (color contours) differences between the LGM-ICE and MOD-ICE experiments. Positive (negative) vertical velocity differences indicate enhanced subsidence (upward motion). Positive (negative) zonal velocity indicates increased eastward (westward) flow. Note from the vertical velocity differences that EEP subsidence and WEP upward motion is enhanced. Also, zonal velocity differences show an increase in the Trades and westward flow aloft. 64

Figure. 3-6. Mean-annual SST differences (°C) in the equatorial Pacific Ocean between (a) the NO-ICE and NO-ICE380 experiments and, (b) the LGM-ICE and LGM-ICE380 experiments. Note that equatorial Pacific SST gradient is strengthened only with the presence of sea ice. The contour interval is 0.2 °C. 65

Figure 4-1. Mean monthly and annual (right column) insolation difference ($Wm^{-2}$) between ΔTOTAL (A. *lobl – hobl*) and ΔMA (B. *higrad – lograd*) experiments. The insolation difference in ΔMA yields the climate response to obliquity's mean-annual forcing. Contour interval is 10 $Wm^{-2}$. Although seasonal insolation differs between these experiments sets, mean-annual insolation is identical between ΔTOTAL and ΔMA. 91

Figure 4-2. Continental snowfall response to orbital forcing. Zonally averaged half-year (December through May and June through November) differences in total snowfall (cm): (a) ΔTOTAL (*lobl-hobl*), (b) ΔMA (*higrad-lograd*), and (c) ΔSEA (ΔTOTAL - ΔMA) 92

Figure 4-3. Differences in January-February-March atmospheric conditions over North America due to a decrease in obliquity (ΔTOTAL) (a) surface air temperature (in degree Celsius), (b) lower tropospheric wind (vectors; averaged from surface to 750 mb) and surface level pressure (contour; in mb), (c) lower tropospheric (750 mb) air temperature

(in degrees Celsius), (d) latent heat flux (in $Wm^{-2}$), (e) relative humidity (in %), and (f) continental snowfall rate (in cm $month^{-1}$). 93

Figure 4-4. Differences in zonally-averaged June-July-August (a) continental surface air temperature (in degree Celsius), (b) continental rainfall rate (in cm $month^{-1}$), and (c) continental snowfall rate (in cm $day^{-1}$) between experimental sets. Results from ΔTOTAL and ΔMA experiments are shown in red-solid and black-dash line, respectively. 94

Figure 4-5. Response of vapor transports and tropospheric relative humidity to orbital changes. (a-b) Difference maps in lower tropospheric (750 mb) June-July-August relative humidity (%) as a result of a decrease in air temperature and an increase in vapor tranport in (a) ΔTOTAL and (b) ΔMA. The polar projection map begins at 30ºN and the contour interval is 4%. (c-d) Difference in zonal-average June-July-August atmospheric meridional vapor transport (g $kg^{-1}$ m $s^{-1}$) by (A) all processes (mean meridional + stationary eddies + transient eddies) and through (B) transient eddies between experimental sets. Results from ΔTOTAL and ΔMA experiments are shown in red and black line, respectively. Positive values represent an increase in the northward vapor transport or a reduction in the southward vapor transport. 95

Figure 4-6. Zonally averaged half-year continental snowfall response to precessional forcing. Snowfall differences is shown in cm. 96

Figure 5-1. June 21 insolation at 65ºN for the past 1 million years. Insolation was calculated for orbits with (A) fixed (23.5°) obliquity and time varying eccentricity and precession, (B) fixed eccentricity/precession and time varying obliquity, and (C) time varying eccentricity, precession, and obliquity. The summer insolation at 65ºN is dominated by precession signal. The insolation records were created using code contributed to us by D. Pollard (personal communication) and based on celestial mechanics from Danby (1967) using the orbital solutions of Berger (1991). 122

Figure 5-2. Mean monthly insolation difference ($Wm^{-2}$) between obliquity (A. ∆obl-max = lobl-A – hobl-A) and precessional (B. ∆prec-max = nhcs-high – nhhs-high) experiments. Contour interval is 10 $Wm^{-2}$. 123

Figure 5-3. Cumulative continental snowfall responses to obliquity forcing. Zonally-averaged half-year (December through May and June through November) differences in total snowfall (cm) (A,D) ∆obl-max, (B,E) lobl-B – hobl-B, and (C,F) lobl-C – hobl-C. 124

Figure 5-4. Cumulative continental snowfall responses to precession forcing. Zonally-averaged half-year (December through May and June

through November) differences in total snowfall (cm) (A,D) ∆perc-max, (B,E) nhcs-med – nhhs-med, and (C,F) nhcs-low – nhhs-low. 125

Figure 5-5 Annual NH continental snowfall (cm) in each experiment. Note that the snowfall response to obliquity and precession in the model is largely linear. 126

Figure 5-6 Response of meridional vapor transport to orbital forcing. Differences in zonally average seasonal meridional (A-B) total vapor transport (including mean meridional circulation, stationary eddies, and transient eddies) between experiments (∆obl-max: red line; ∆prec -max: black line) and (C-D) transient eddy vapor transport (g $kg^{-1}$ m $s^{-1}$). Positive values represent an increase in the northward vapor transport or a reduction in the southward vapor transport. 127

Figure 5-7 Difference in total northward vapor transport over Northern Hemisphere continents. Difference in mean (A) December-January-February and (B) June-July-August meridonal vapor transport due to a reduction in obliquity (∆obl-max). Positive values represent greater northward vapor transport. In June-July-August, the enhanced northward transport corresponds to increase continental snowfall (Fig. 3A). The contour interval is 10 cm $s^{-1}$ g $kg^{-1}$. 128

Figure 5-8 Response of tropospheric relative humidity to orbital forcing. Difference maps of seasonal lower tropospheric (700mb) relative humidity (%) in (A,C) ∆prec-max and (B,D) ∆obl-max. The contour interval is 2%. The enhanced moisture transport through orbital-forced transient eddy activity can be recognized as increases in lower tropospheric relative humidity across North America. 129

Figure 5-9. Response of tropospheric specific humidity to orbital forcing. Difference maps of seasonal lower tropospheric (700mb) specific humidity (g $kg^{-1}$) in (A,C) ∆prec-max and (B,D) ∆obl-max. The contour interval is 0.4 g $kg^{-1}$. The different spatial pattern between relative and specific humidity indicates difference in saturation and moisture transport. 130

Figure 5-10 Spectral analyses of synthetic records contain both obliquity and precessional signals and random noise. (A) shows a spectral analysis of fix variance amplitude in obliquity band and 1x variance amplitude in precessional band. (B) shows a spectral analysis of fix variance amplitude in obliquity band and doubled variance amplitude in precessional band compare to (A). Note the significant increase of power variance at the precessional period from (A) to (B). The spectral analyses illustrate how increase in global ice volume variability in precessional band may have enhanced precessional power expression in global ice volume record after 1 Ma. 131

List of Tables

Table 3-1. Mean winter sea-ice extent ($10^7$ $km^2$) in MOD-ICE, LGM-ICE, and LGM-ICE380 experiments. See Section 2.2 for a description of our methodology for specifying the sea ice. (DJF=December, January, February; JJA=June, July, August; N.H.=northern hemisphere; S.H.=southern hemisphere) 66

Table 3-2. Summary of Last Glacial Maximum boundary conditions. 67

Table 3-3. Net sea surface energy fluxes in the EEP (3.5°S-3.5°N, 92°E-103°E) and the WEP (3.5°S-3.5°N, 150°W-164°W). The domain for the EEP and WEP area averages are illustrated in Fig. 2a (black boxes). Positive (negative) fluxes represent gain (loss) from the sea surface (in $Wm^{-2}$). Sea surface energy fluxes are calculated for the LGM-ICE (left column) and NO-ICE experiments (center column), and the difference between the two experiments (left column). (RAD= downward surface radiation; LWV=upward longwave flux; SHF= sensible heat flux; LHF=latent heat flux; OH=ocean heat flux) 68

Table 4-1. Numerical Climate Experiments. 97

Table 5-1. List of numerical climate experiments and orbital parameters. Orbital parameters were modified one at a time; other orbital settings were prescribed at present-day value with eccentricity of 0.017, obliquity of 23.45º, and precession of 168º. (nhcs = NH cold summer; nhhs = NH hot summer; hobl = high obliquity; lobl = low obliquity). 132

Table 5-2. Continental snowfall differences between experimental pairs. Positive (negative) numbers represent greater (less) continental snowfall (in cm $yr^{-1}$) relative to corresponding experiment.. 133

Table 5-3. Annual and seasonal PDD indexes for each experiment. The indexes are calculated by summing daily above-freezing temperatures over a year. In the NH, the indexes were derived from area north of 60ºN. 134

## Abstract

Orbital forcing of Pleistocene climate has been firmly established since the development of the benthic $\delta^{18}O$ record, a proxy for glacial ice volume, three decades ago. However, our understanding of ice age cycles and the involving feedback remains limited. Prediction based on Milankovitch theory that both ~21kyr and ~41kyr cycles exist in the ice volume record failed to explain Pleistocene benthic $\delta^{18}O$ record which is dominated by ~41kyr periodicity before 0.8 Ma. This failure of Milankovitch theory has inspired new hypotheses to account for the unexplained features of the ice volume record. The variety of these hypotheses indicates the complication of the climate-orbital linkage: instead of simple radiative forcing of high latitudes, internal climate feedbacks might play an important role in the cause of ice age cycles. However, these hypotheses are largely untested to date. Marine proxy records demonstrate tropical climate oscillations in accordance with high-latitude climate changes. Based on these records, tropical region has been recognized as a possible amplifier of the obliquity insolation change. Nevertheless, the pathways through which the high-latitude climate influenced tropical climate condition are not understood.

This study seeks to understand the climate response to obliquity forcing in coupled ocean-atmosphere simulations. Pleistocene experiments were developed and analyzed to determine the mechanisms that link high and low latitudes during the late Pliocene to early Pleistocene. Surface gyre circulation in the South Pacific was identified as an oceanic mechanism that connects high-latitude and tropical oceans. This mechanism, tight closely to South Ocean sea ice extent, explains much of the tropical climate variability in Plio-Pleistocene proxy records especially the obliquity imprints in tropical records. By comparing simulated climate response to obliquity and precessional forcing, this study test a couple existing hypotheses account for the prominence of obliquity period in Pleistocene ice volume record and identify factors that explain the large sensitivity of ice volume record to obliquity. Within an obliquity cycle, seasonal as well as mean-annual forcing are both important in changing high-latitude snowfall. Net global snowfall and Antarctic snow accumulation tend to magnify the influence of obliquity forcing on the glacial ice volume.

# Chapter I

## Introduction

The two interrelated goals of paleoclimate research are to reconstruct past climate conditions and to understand the dynamics of the global climate system. The enormous number of complex interactions operating on a wide variety of temporal and spatial scales within the climate system makes the second goal one of the most monumental tasks in the physical sciences. However, this goal is also one of the most pressing tasks, given the possibility that human activities may soon dramatically alter the planet's climate.

One of the most effective ways to study global climate dynamics is through numerical model simulation. Climate models, driven by fundamental physics such as conservation of momentum, energy, and mass, provide information about the climate response to climate forcings, and connections between different parts of the climate system. The results presented in this dissertation contribute to paleoclimate research by presenting the climate response to changes in incoming solar radiation (insolation) due to variations in Earth's orbit which are thought to be the major forcing on glacial-interglacial time scale and by providing internal mechanisms that interconnect climate sub-systems propagating the forcing. This work focuses on the Plio-Pleistocene, a

time interval when multiple of climate archives are available to constrain the experiments and when the Earth's climate experiences several dramatic but poorly understood changes, specifically the glacial cycle oscillations and a long-term cooling trend.

### *1. Plio-Pleistocene climate*

The glacial-interglacial cycles of the past ~2.7 Myr, represent one of the largest and most significant climate changes of the late Pliocene – early Pleistocene ice age. The prevailing theory of ice age cycles has been that major oscillations of global climate are caused by insolation variations at critical latitudes and seasons. In particular, the advances and retreats of ice sheets are thought to be sensitive to northern high latitudes summer insolation. If snow and ice survives the summer, the ice sheet will grow causing ice volume to increase (Milankovitch, 1948).

Variation of high-latitude summer insolation is dominated by the precession of equinoxes with a period of 21 kyr, combined with a secondary control by the change of Earth's axial tilt with a period of 41 kyr. Thus, Milankovitch theory would predict the existence of both ~21 kyr and ~41 kyr cycles in the ice volume record. This prediction, however, is contrary to the global ice volume and deep sea temperature record derived from $\delta^{18}O$ of benthic foraminifers which are dominated by 41 kyr power prior to ~0.8 Ma and 100 kyr power after ~0.8 Ma (Ruddiman et al., 1986; Martinson et al., 1987).

The failure of the Milankovitch theory to explain fundamental features of the Plio-Pleistocene ice volume record highlights gaps in our understanding of how orbital forcing influences climate and how it was expressed in climate records. Among these features, this study will focus on the prominence of the obliquity signal and the near absence of the precessional signal in the ice volume record. Although Hays et al. (1976) proposed a global ice-volume and high high-latitude summer insolation connection based on a statistical association between the two factors, a physical explanation for the cause of the ice-age cycles is still missing. To this end, a number of hypotheses have recently been presented in the literature to explain the strong obliquity signal. However, these hypotheses are largely untested to date.

The main objective of this study is to investigate mechanisms that might have been responsible for the obliquity signal observed in the climate records and to reconcile the apparently contradictory ice volume and insolation records with existing hypotheses. Marine proxy records from tropical Pacific preserve strong 41 kyr peridicities in Pleistocene seawater temperature and productivity that are attributed to fluctuations in Earth's obliquity (Clemens et al., 1991; Lea et al., 2000; Beaufort et al., 2001; Liu and Herbert, 2004; de Garidel-Thoron, 2005; Medina-Elizalde and Lea, 2005; Cleveland and Herbert, 2007). The source of the 41 kyr periodicities is paradoxical in light of the small influence of obliquity on low-latitude local insolation. Chapter 2 of this study identifies a connection between high-latitude and tropics through the Southern Pacific sub-tropical gyre circulation. This connection provides a possible solution for the paradoxical

tropical obliquity climate variability presented in literature. Following the hypotheses that strong obliquity responses in the late Pliocene and early Pleistocene may be associated with the mean-annual and seasonal spatial insolation distribution, Chapter 4 systematically quantifies the influence of both mean-annual and seasonal insolation changes resulting from Earth's obliquity on continental snowfall and determines the climate mechanisms that respond to these insolation variations. Finally, the continental snowfall responses to both obliquity and precessional forcings and an examination of the current hypotheses related to the cause of 41 kyr periodicity are presented in Chapter 5.

Another unanswered Plio-Pleistocene climate question is related to the caused of long-term global cooling trend of the last 4 Myr. An increase of benthic foraminifer $\delta^{18}O$ during Plio-Pleistocene indicates a decrease in deep ocean temperature and an increase in global ice volume (Zachos et al., 2001). However, the cause for this cooling remains a mystery. While a low atmospheric greenhouse gas concentration may cause such a cooling, $CO_2$ levels have remained relatively stable since 20 Ma (Pearson and Palmer, 2000). Tectonic ocean gateways have also been linked to the Plio-Pleistocene cooling. Closing of the Panama gateway at ~4 Ma might have influenced ocean circulation that increased the amount of poleward moisture transport to grow the Northern Hemisphere ice sheets (Haug and Tiedemann, 1998). The Achilles' heel of this theory is that the gateway closing led large ice sheets formation by 1 Ma and it fails to explain the continuous cooling trend after the onset of Northern Hemisphere glaciation at ~2.7 Ma.

During times when the North Hemisphere experienced major cryosphere expansion, tropical area was characterized by an increase in zonal thermal gradient. Marine proxies of sea surface temperature indicate that zonal thermal gradient of the tropical Pacific and Atlantic intensified through the past 4 Myr and peaked during Pleistocene glaciations (Ravelo et al., 2004). In the tropical Pacific, marine proxy records show that the east-west sea surface temperature gradient has likely increased by 2ºC over the past 1.75 Myr as the eastern equatorial Pacific gradually cooled (de Garidel-Thoron et al., 2005). Regarding to the importance of tropical ocean to the global exchange of heat, moisture, and momentum, little research has focused on tropical processes and there is currently little consensus on the cause of tropical climate variability during the Plio-Pleistocene. Chapter 3 of this study provides a new oceanic mechanism tied to the sea-ice expansion in the Southern Ocean that might explain the long term cooling trend and zonal thermal gradient enhancement in the tropics.

### *2. Climate modeling of orbital forcing*

Climate models are valuable tools in the search for physical explanations for the climate histories posed by proxy records. The climate response to orbital forcings has been explored in a number of energy-balance models (EBM). Early EBM experiments investigated climate sensitivity to changes in global mean-annual (e.g. Budyko, 1969; North, 1975) and seasonal (e.g. Thompson and Schneider, 1979; Suarez and Held, 1979) insolation forcing demonstrating an insolation-climate linkage. In the last two decades, glacial climate simulations

have been conducted using atmospheric general circulation models (AGCM). Many of the early AGCM studies attempted to simulate the climate conditions of the Last Glacial Maximum and termination (e.g. Manabe and Broccoli, 1985; Kutzbach and Guetter, 1986; Phillips and Held, 1994; Dong and Valdes, 1995). These studies identify the importance of orbital parameters for the initiation of glacial cooling (Kutzbach and Guetter, 1986; Dong and Valdes, 1995). However, a consistent feature of the EBMs and AGCMs is the simplified, non-dynamical representation of the oceans. This simplification of the ocean treatment may have important effect on the simulated equilibrium climate due to the large thermal inertia of world's ocean. Previous studies (Khodri et al., 2001; Harrison et al., 2003) demonstrate that ocean-atmosphere interaction plays a role in determining atmospheric temperature response to orbital forcing and coupled ocean-atmosphere models generally have a more realistic representation of dynamical processes.

Although many efforts have been made to advance our understanding of ice age climate, few studies have attempted to determine the climate sensitivity to orbital forcings using a coupled ocean-atmosphere model in a systematic fashion. As a result, many fundamental questions about the ice age cycles remain unclear. Previous simulations using AGCMs have shown that atmospheric changes alone fail to produce perennial snow and low surface temperatures in northern high-latitudes when forced by glacial orbital parameters (Rind et al., 1989; Oglesby, 1990). In contrast, it has been suggested that ocean feedbacks involving latent and sensible heat warming to the atmosphere during

fall and early winter led to a cooling of northern high-latitudes together with an increase in equator-to-pole atmospheric moisture transport (Khodri et al., 2001). The model experiments in this study were completed using the Fast Ocean Atmosphere Model version 1.5, a fully coupled ocean-atmosphere GCM. By having a better representation of oceanic dynamical processes, we believe that coupled GCM can provide the best first-order test of the role of insolation forcing in the climate system. This study attempts to determine the climate response to Pleistocene forcing through sensitivity experiments. We systematically varied orbital parameters over the full range of orbital variations for the last 5 million years (Berger, 1991) in order to examine the full spectrum of climate response to orbital forcings.

## REFERENCES


Beaufort, L., T. de Garidel-Thoron, A. C. Mix, and N. G. Pisias (2001), ENSO-like forcing on oceanic primary production during the Late Pleistocene, Science, 293, 2440-2444.

Berger, A., and M. F. Loutre (1991), Insolation Values for the Climate of the Last 10000000 Years, Quaternary Science Reviews, 10, 297-317.

Budyko, M. I. (1969), Effect of Solar Radiation Variations on Climate of Earth, Tellus, 21, 611-&.

Cleaveland, L. C., and T. D. Herbert (2007), Coherent obliquity band and heterogeneous precession band responses in early Pleistocene tropical sea surface temperatures, Paleoceanography, 22.

Clemens, S., W. Prell, D. Murray, G. Shimmield, and G. Weedon (1991), Forcing Mechanisms of the Indian-Ocean Monsoon, Nature, 353, 720-725.

de Garidel-Thoron, T., Y. Rosenthal, F. Bassinot, and L. Beaufort (2005), Stable sea surface temperatures in the western Pacific warm pool over the past 1.75 million years, Nature, 433, 294-298.

Dong, B. W., and P. J. Valdes (1995), Sensitivity Studies of Northern-Hemisphere Glaciation Using an Atmospheric General-Circulation Model, Journal of Climate, 8, 2471-2496.

Harrison, S. P., J. E. Kutzbach, Z. Liu, P. J. Bartlein, B. Otto-Bliesner, D. Muhs, I. C. Prentice, and R. S. Thompson (2003), Mid-Holocene climates of the Americas: a dynamical response to changed seasonality, Climate Dynamics, 20, 663-688.

Haug, G. H., and R. Tiedemann (1998), Effect of the formation of the Isthmus of Panama on Atlantic Ocean thermohaline circulation, Nature, 393, 673-676.

Hays, J. D., J. Imbrie, and N. J. Shackleton (1976), Variations in Earths Orbit - Pacemaker of Ice Ages, Science, 194, 1121-1132.

Khodri, M., Y. Leclainche, G. Ramstein, P. Braconnot, O. Marti, and E. Cortijo (2001), Simulating the amplification of orbital forcing by ocean feedbacks in the last glaciation, Nature, 410, 570-574.

Kutzbach, J. E., and P. J. Guetter (1986), The Influence of Changing Orbital Parameters and Surface Boundary-Conditions on Climate Simulations for the Past 18000 Years, Journal of the Atmospheric Sciences, 43, 1726-1759.

Lea, D. W., D. K. Pak, and H. J. Spero (2000), Climate impact of late quaternary equatorial Pacific sea surface temperature variations, Science, 289, 1719-1724.

Liu, Z. H., and T. D. Herbert (2004), High-latitude influence on the eastern equatorial Pacific climate in the early Pleistocene epoch, Nature, 427, 720-723.

Manabe, S., and A. J. Broccoli (1985), A Comparison of Climate Model Sensitivity with Data from the Last Glacial Maximum, Journal of the Atmospheric Sciences, 42, 2643-2651.

Martinson, D. G., N. G. Pisias, J. D. Hays, J. Imbrie, T. C. Moore, and N. J. Shackleton (1987), Age Dating and the Orbital Theory of the Ice Ages - Development of a High-Resolution-0 to 300,000-Year Chronostratigraphy, Quaternary Research, 27, 1-29.

Medina-Elizalde, M., and D. W. Lea (2005), The mid-Pleistocene transition in the tropical Pacific, Science, 310, 1009-1012.

Milankovitch, M. (1948), Ausbau Und Gegenwartiger Stand Der Astronomischen Theorie Der Erdgeschichtlichen Klimate, Experientia, 4, 413-418.

North, G. R. (1975), Theory of Energy-Balance Climate Models, Journal of the Atmospheric Sciences, 32, 2033-2043.

Oglesby, R. J. (1991), Springtime Soil-Moisture, Natural Climatic Variability, and North-American Drought as Simulated by the Ncar Community Climate Model-1, Journal of Climate, 4, 890-897.

Pearson, P. N., and M. R. Palmer (2000), Atmospheric carbon dioxide concentrations over the past 60 million years, Nature, 406, 695-699.

Phillipps, P. J., and I. M. Held (1994), The Response to Orbital Perturbations in an Atmospheric Model Coupled to a Slab Ocean, Journal of Climate, 7, 767-782.

Ravelo, A. C., D. H. Andreasen, M. Lyle, A. O. Lyle, and M. W. Wara (2004), Regional climate shifts caused by gradual global cooling in the Pliocene epoch, Nature, 429, 263-267.

Rind, D., R. Goldberg, and R. Ruedy (1989), Change in Climate Variability in the 21st-Century, Climatic Change, 14, 5-37.

Ruddiman, W. F., M. Raymo, and A. McIntyre (1986), Matuyama 41,000-Year Cycles - North-Atlantic Ocean and Northern-Hemisphere Ice Sheets, Earth and Planetary Science Letters, 80, 117-129.

Suarez, M. J., and I. M. Held (1979), Sensitivity of an Energy-Balance Climate Model to Variations in the Orbital Parameters, Journal of Geophysical Research-Oceans and Atmospheres, 84, 4825-4836.

Thompson, S. L., and S. H. Schneider (1979), Seasonal Zonal Energy-Balance Climate Model with an Interactive Lower Layer, Journal of Geophysical Research-Oceans and Atmospheres, 84, 2401-2414.

Zachos, J., M. Pagani, L. Sloan, E. Thomas, and K. Billups (2001), Trends, rhythms, and aberrations in global climate 65 Ma to present, Science, 292, 686-693.

# CHAPTER II

## Tropical Pacific Climate Response to Obliquity Forcing in the Pleistocene


## ABSTRACT

Marine proxy records of Pleistocene seawater temperature and productivity in the tropical Pacific Ocean vary at a 41,000 period that has been attributed to Earth's obliquity cycle. The proxy records are paradoxical both because obliquity has a small effect on low latitude insolation and because tropical seawater temperature and productivity were anti-correlated with obliquity insolation forcing. In this study, we investigate the response of the tropical Pacific climate to obliquity forcing using a coupled ocean-atmosphere model to reconcile the proxy records with climate theory. Two glacial and two modern simulations were completed with extreme high and low axial tilts of 24.5 and 22.2°. In response to an increase in axial tilt, tropical sea-surface temperatures decrease by as much as 0.8 °C due to the local reduction in insolation. Subsurface waters in the eastern and central equatorial Pacific increase by nearly 1 °C. Anomalous heating through high obliquity forcing also generates dynamical responses that weaken mean-annual mid-latitude Westerlies and subtropical trade winds, contributing to a ~20% reduction in the subtropical gyre circulation. Analyses using a Lagrangian transport model indicate that low-latitude subsurface warming

is due to a reduction in heat export from the tropics, and the advection and the advection and ventilation of anomalously warm South Pacific extratropical waters through the thermocline circulation. The model's response to obliquity is consistent with Pleistocene proxy data that indicate the tropical Walker circulation and thermocline structure were not strongly influenced by changes in axial tilt. The model results also support the hypothesis that Earth's obliquity influences climate through its control on meridional insolation gradients.

## 1.INTRODUCTION

Marine proxy records from the tropical Pacific Ocean preserve strong 41-kyr periodicities in Pleistocene seawater temperature and productivity that are attributed to fluctuations in Earth's obliquity (Clemens et al., 1991; Beaufort et al., 2001; Lea et al., 2000; Liu and Herbert, 2004; de Garidel-Thoron et al., 2005). These low-latitude records are remarkable because, unlike at high latitudes, local insolation forcing due to obliquity oscillations are quite small. Mean-annual insolation forcing at the equator differs by -3 $Wm^{-2}$ between times of high (i.e., axial tilt of 22.2°) and low obliquity (i.e., axial tilt of 24.5°) representing an annual change of approximately -0.4%. In comparison, mean-annual insolation differs by 15.4 $Wm^{-2}$ and 6.5 $Wm^{-2}$ at 90° at 65° representing increases of 9.3% and 3.0%.

In light of the small influence of obliquity on low-latitude insolation, the 41-kyr periodicities in tropical marine proxy reconstructions is unlikely to arise as a direct climate response to obliquity forcing of local insolation. Moreover, records of Pleistocene tropical seawater temperature are anti-phased with local annual

insolation: during times of high (low) axial tilt, Pacific seawater temperatures are high (low) (Lea et al., 2000; Liu and Herbert, 2004; de Garidel-Thoron et al., 2005). What then is the source of the 41-kyr periodicities in tropical proxy records? Two possibilities stand out. First, the Pleistocene tropics may have been influenced by direct obliquity forcing of high-latitude insolation (Liu and Herbert, 2004). In this case, a remote connection, possibly via atmospheric or thermocline circulation, coupled the tropics to the high latitudes. Second, the tropical climate may have been forced by other climate factors, notably atmospheric $CO_2$, that were indirectly influenced by obliquity oscillations. Ice volume changes driven by obliquity variations generated ice-proximal changes in SST, North Atlantic Deep Water formation, and dust that may have caused a strong $CO_2$ feedback (Ruddiman, 2003).

To decide between these possibilities, it is necessary to understand how the tropical climate responded to obliquity forcing in the Pleistocene. Interpretations of tropical marine proxy records provide opposing views: obliquity oscillations either triggered basin-wide dynamical adjustments in the tropics or they did not. The former view is founded on interpretations of marine records of alkenone unsaturation index ($U_{37}^{K'}$) and total alkenone abundance from Site 846 in the eastern equatorial Pacific (EEP). Liu et al. (2004) report low (high) EEP seawater temperature and high (low) EEP productivity during times of low (high) axial tilt. To explain this record, Liu and Herbert (2004) favor a mechanism that involves enhancement of the trade winds and shoaling of the thermocline during

low axial tilt, leading to increased EEP upwelling, higher productivity, and lower seawater temperature.

However, other tropical proxy records do not necessarily support obliquity-driven changes in trade wind strength and thermocline depth. Beaufort et al. (2001) report an EOF analysis of Pleistocene variations in primary productivity in the Indian and Pacific Ocean. The components of the EOF are not consistent with an increase in thermocline slope, the expected response to enhanced trade winds (Beaufort et al., 2001). de Garidel-Thoron et al. (2005) demonstrate that over glacial-interglacial cycles Mg/Ca-derived seawater temperatures in the western equatorial Pacific co-vary with the $U_{37}^{K'}$-temperatures from Site 846 in the EEP and have similar amplitudes of change. Taken together, these tropical Pacific proxy records indicate a relatively constant east-west SST gradient and imply a stable cross-Pacific thermocline structure (tilt). Many low-latitude marine proxy records from the Pacific Ocean (e.g., Perks and Keeling, 1998; Perks et al., 2002) and the Arabian Sea (e.g., Reichart et al., 1998; Budziak et al., 2000) that might be expected to preserve basin-wide changes in trade wind strength and thermocline depth either lack or have very weak 41 kyr cycles that are secondary to the 23-ky precessional cycle.

Basin-wide dynamical adjustments in the tropics may not be necessary to explain the EEP proxy records. On the basis of SST records derived from census data of radiolarian microfossils, Pisias and Mix (1997) suggest that the 41 kyr cycles in EEP SSTs are linked to the climate response of the Southern Ocean, which is transmitted through the Peru Current and/or Subantarctic Mode Water.

The purpose of this study is to clarify how the tropical Pacific Ocean responded to obliquity forcing in the Pleistocene, and to reconcile if possible the apparently contradictory proxy records. Because Pleistocene climates varied between glacial-interglacial states, we have completed two glacial and two non-glacial (modern) experiments under high- and low-obliquity conditions using a coupled ocean-atmosphere general circulation model. In the Results section, we summarize the model response to obliquity forcing with emphasis on tropical climate change. In the Discussion section, we compare the model results with the proxy evidence to substantiate our model results.

## 2. MODEL AND EXPERIMENTAL DESIGN

Glacial and modern climate experiments were completed using the Fast Ocean Atmosphere Model (FOAM) version 1.5, a fully coupled mixed-resolution ocean and atmosphere GCM. The atmospheric model is a parallelized version of the Community Climate Model 2 (CCM2) with the radiative and hydrological physics upgraded to the equivalent of CCM3 version 3.2 (Kiehl et al., 1996). The atmospheric component of FOAM was run at spectral resolution R15 (4.5° x 7.5°) with 18 vertical levels. The ocean component of FOAM (OM3) is a z-coordinate ocean general circulation model with a 128x128 point Mercator grid (1.4°x2.8°) and 24 vertical levels.

FOAM has been widely used to study climate change through geologic time (e.g., Liu et al., 2000; Poulsen et al., 2001; Harrison et al., 2003; Poulsen et al., 2003; Pierrehumbert, 2004). FOAM's simulation of modern climate shows

reasonable agreement with present day observations. In addition to the mean climate state, FOAM successfully simulates many aspects of modern interannual and interdecadal variability, including ENSO (Jacob, 1997; Liu et al., 2000; Liu et al., 2002). FOAM's most important shortcoming is an underestimation of North Atlantic Deep Water (NADW) production in the modern climate, a problem common to coupled ocean-atmosphere models. However, we do not consider this to be an important limitation for two reasons: 1) we restrict our analyses to the upper ocean circulation, and 2) a persistent bias in the thermohaline circulation will be prevalent in both sensitivity experiments and effectively filtered out by comparing (differencing) the experiments.

In a recent comparison of the simulation of global upper ocean circulation between FOAM and the NCAR Community Climate System Model (CCSM), Liu et al. (2003) showed that in many regions the two models respond consistently to Holocene orbital forcing. In fact, FOAM's sensitivity to a doubling of atmospheric $pCO_2$ is similar to that of the CCSM (Dr. Robert Jacob, personal communication, 2004), approximately 2 °C or 0.5 °C/W/m$^2$ (CCSM Science Plan, 2003).

We initially completed two glacial sensitivity experiments: high- (HOBL) and low-obliquity (LOBL) cases with axial tilts of 24.5° and 22.2°, respectively. These experiments represent continuation runs from a pre-existing Last Glacial Maximum (LGM) experiment and were each integrated for an additional 150 years to bring the upper-ocean to steady state. LGM boundary conditions include Eurasian and North American ice sheets, reduced sea level, LGM continental topography and vegetation distribution (Peltier, 1994). Orbital settings were set

to those for 18 ka based on Berger (1978). LGM greenhouse gases levels were inferred from Vostok ice cores; $CO_2$, $CH_4$, and $N_2O$ were prescribed as 200ppmv, 400ppbv, and 275ppbv, respectively (Petit et al., 1999). The FOAM LGM simulation has a global mean-annual temperature of about 8°C. Tropical Pacific SSTs in the LGM simulation are approximately 4-5°C below modern values, comparing favorably with colder SST paleo-estimates (Beck et al., 1997; Mix et al., 1999; Martinez et al., 2003).

We chose to use glacial experiments in this study to maximize the tropical response to obliquity forcing. On the basis of thermocline theory, a cold climate with shallower equatorial thermocline should be most sensitive to obliquity forcing (Philander and Federov, 2003). After analyzing the glacial obliquity experiments, two additional obliquity sensitivity experiments were conducted using present-day boundary conditions (see below). These experiments represent 150-year continuation runs of a present-day simulation. All model results described below represent averages of the last 20 years of the model integrations.

To analyze the GCM results, we developed a Lagrangian transport model to track water parcel trajectories within the interior of the ocean, a standard technique for analyzing water parcel pathways (e.g., Harper, 2000). The transport model interpolates the three-dimensional velocity field to the position of a water particle and then uses a second-order finite difference technique to predict the future position of the water particle. We linearly interpolated between monthly average velocities to calculate the time-varying velocity field at each 30-minute time step. The Lagrangian transport model only calculates transport

through advection, and therefore should be considered an approximation of the GCM-simulated flow.

# 3. RESULTS

## *3.1. Seawater temperature*

Figure 2-1 displays the seasonal and mean-annual solar insolation difference between the high (HOBL) and low (LOBL) experiments. A higher axial tilt reduces the mean-annual and seasonal meridional insolation gradient (Berger, 1978). Figure 2-2b-c illustrates the mean-annual seawater temperature difference at the surface (10m depth) and subsurface (average of 30-100m depths) between the HOBL and LOBL experiments. At the sea surface, the temperature difference is largely zonal and consistent with the local mean-annual insolation change due to an increase in Earth's axial tilt. Poleward of approximately 30°, annual SSTs increases by more than 1°C. At low latitudes, annual SSTs cool by up to 0.6 °C (Fig. 2-2b). Seasonal SST differences between the HOBL and LOBL experiments are also mainly associated with local insolation differences; for example, mid-latitude SST differences are largest during the summer when the insolation difference is greatest (Fig. 2-3). However, both mean-annual and seasonal SST differences demonstrate variations from the zonal SST pattern that are linked to dynamical changes forced by seasonal variations in insolation (see below).

Subsurface (30-100m) seawater temperatures respond very differently to an increase in obliquity. Although the local insolation is reduced, subsurface seawater temperatures are higher in a tongue that extends across the equatorial

Pacific. EEP subsurface temperatures increase by more than 0.6 °C in the HOBL experiment. In both hemispheres, subsurface waters in the subtropical Pacific are up to 1.2 °C cooler (Fig. 2-2c). Subsurface seawater temperatures show only minor seasonal variation. Cross-sectional maps of seawater temperature in the tropical Pacific (averaged from 4°N to 4°S) indicate a slight depression of the thermocline (~20m) in the central and eastern Pacific (not shown).

### *3.2. Dynamical response to obliquity forcing*

The dynamical response to obliquity forcing is complicated by the large seasonal insolation anomalies. The seasonal adjustments in heating, sea-level pressure, and winds to this insolation forcing are described below. In the mean annual, the dynamical response is conceptually much simpler. The response to an increase in axial tilt is a decrease in the mid-latitude westerlies and tropical easterlies associated with a reduction in meridional insolation and surface pressure gradients (Fig. 2-4d).

As shown in Figure 2-1, changes in obliquity significantly alter the seasonal meridional insolation distribution leading to anomalous heating at the surface, which spawns dynamical changes that influence the mean circulation of the atmosphere and ocean. During the late fall and winter, for example, the HOBL experiment is forced by anomalously low insolation in the mid-latitudes. The anomalously low insolation and surface cooling in the mid-latitudes (centered at 45°) leads to a positive surface pressure anomaly and a weakening of the mid-latitude low pressure (e.g., the Aleutian Low in the North Pacific). The surface wind response is an anti-cyclonic anomaly that includes a weakening of

the mid-latitude Westerlies and a slight intensification of the northern most trade winds in the northwestern Pacific (Fig. 2-4a).

Conversely, in the summer hemisphere, anomalous high insolation and surface heating in the extratropics leads to a weakening of the subtropical high and the trade winds (Fig. 2-4c). FOAM also predicts a slight intensification of the EEP trade winds during boreal spring (Fig. 2-4b). As pointed out by Clement et al. (2000), rapid seasonal heating along the equator preferentially warms the western Pacific warm pool, intensifying the west-east SST gradient and strengthening trade winds. However, because summer insolation dominates the mean-annual insolation anomaly, the mean-annual signal is one of weaker tropical easterlies (Fig. 2-4e). It should be noted that differences in trade wind strength primarily occur away from the equator; there is little change in the near-equatorial trade winds because there is little change in the low-latitude insolation gradients.

The obliquity-driven modifications to surface winds affect the wind-driven circulation in the Pacific Ocean. Pronounced changes include weakening of the Northern Equatorial Current and the subtropical gyre, and enhanced flow through the Northern Equatorial Countercurrent and Southern Equatorial Current. These changes are displayed as a reversal of flows in the HOBL-LOBL difference plot (Fig. 2-5). We estimate a 14% reduction in the transport volume of the Kuroshio Current at 25°N. Analysis with our Lagrangian transport model presents a consistent picture; the travel time of a water parcel through the Peru Current is 20% greater in the HOBL experiment than in the LOBL experiment. The

weakening of the subtropical gyres in the HOBL experiment can be linked to the weakening of the trades and the mid-latitude westerlies. The intensifications of the Northern Equatorial Countercurrent and Southern Equatorial Current are likely the responses to changes in zonal wind stresses according to Sverdrup theory. In the North Pacific, for example, mean-annual zonal-average trades centered on 30° latitude intensify while those centered on 15° latitude weaken (Fig. 2-6a). The anomalous wind stress caused by the change in trades promotes Ekman transport that sets up anomalous convergence at ~10°N and divergence at ~20°N. As a result of changes in sea-level height, surface pressure gradients are enhanced between 10 and 20°N, and 10°N and 0°, intensifying both the eastward-flowing NECC and the westward-flowing SEC (Fig. 2-6b).

### *3.3. Cause of tropical Pacific subsurface warming*

Several mechanisms could potentially explain the subsurface warming in the tropical Pacific under high obliquity forcing including (1) reduced EEP upwelling through a reduction in low-latitude trade wind strength; (2) a change in the source of ventilated waters in the EEP caused by a change in subsurface circulation; (3) warming of source waters through high-latitude obliquity forcing without any subsurface circulation change; and/or (4) a decrease in tropical heat transport and thermocline ventilation due to a reduction in the subtropical gyre.

Our model results do not show a significant trade wind-thermocline feedback to obliquity forcing. The absence of this feedback can be readily seen in the SST difference between experiments, which is largely zonal at low-latitude (Fig. 2-2b). Moreover, the subsurface warming in the equatorial Pacific

under high obliquity conditions persists throughout the year with little seasonal variation (Fig. 2-2c). Most significantly, the mean-annual trade wind strength near the equator shows little change between the HOBL and LOBL experiments (Fig. 2-4e). As expected from the insignificant surface wind differences, low-latitude Ekman pumping is nearly unchanged between experiments (not shown).

The model results indicate that the tropical subsurface warming is largely due to subduction and advection of anomalously warm southern mid-latitude waters through the thermocline circulation. Figure 2-7 shows the seawater temperature difference between the HOBL and LOBL experiments through a meridional cross-section in the eastern South Pacific Ocean. A warm anomaly can be traced from the surface of the mid-latitude South Pacific to the thermocline of the EEP (Fig. 2-7). To further investigate the source of the waters ventilated in the EEP, we used a Lagrangian transport model driven by the monthly-mean ocean velocities predicted by FOAM. Figure 2-2c illustrates the paths of water parcels over a 20-year integration for the HOBL and LOBL experiments. In both experiments EEP waters originate from very nearly the same location in the South Pacific and follow almost identical subsurface paths to the EEP. However, the source water temperature in the HOBL experiment is 0.6° warmer at the surface than in the LOBL experiment (Fig. 2-2b).

Two physical factors contribute to extratropical warming in the HOBL experiment, an increase in insolation and a decrease in the sea-ice distribution. At 45°S, annual insolation forcing is 0.55 $Wm^{-2}$ with a 2° increase in axial tilt. Figure 2-8 shows the sea ice distribution in two experiments. The sea-ice

distribution is very sensitive to obliquity forcing; the sea-ice distribution in the LOBL experiment is 2-10° north of that in the HOBL experiment. In the LOBL experiment, cold air advected from the sea ice surface to the ocean leads to a sensible heat loss of 1- 6 W/m$^2$ at 45°S and sea-surface cooling. In the absence of this sensible heat loss and insolation heating, the HOBL seawater temperature is higher in mid-latitudes.

The sensitivity of the EEP subsurface temperatures to South Pacific sea-ice distribution suggests that the tropical response to obliquity forcing may be very different in non-glacial climates. To test this idea, we ran two modern-day climate simulations with high (24.5°) and low (22.5°) obliquity forcing, respectively. In both modern experiments, the sea-ice line was well poleward of 70°. As in the glacial experiments, the main tropical response to obliquity forcing was a ~0.6 °C decrease in SSTs and an increase in subsurface temperatures. However, with the reduction in sea-ice, the magnitude and extent of the tropical subsurface warming was substantially reduced.

In addition to the ventilation of warmer waters, the slowing of the boundary currents may also contribute to the subsurface differences between the HOBL and LOBL experiments. The reduction in the subtropical gyres diminishes the heat transport from the equator, contributing to subsurface warming in the eastern and central tropical Pacific and subsurface cooling in subtropical temperatures in the HOBL experiment (Fig. 2-2c). The reduction in wind-driven ocean circulation under high obliquity forcing may be important to understanding oceanic paleo-productivity records from the Pacific Ocean. Our model results

provide a mechanism for generating a 41-ky productivity signal. In the modern ocean, Subantarctic Mode Water is the main channel of nutrients from the Southern Ocean to the equatorial Pacific and the main source of nutrients for the thermocline (Toggweiler et al., 1991; Sarmiento et al., 2003). We suggest that a weakening (strengthening) of the subtropical gyres would effectively reduce (enhance) the transport of nutrients in the thermocline during periods of high (low) obliquity, thereby reducing (enhancing) biological productivity.

## 4. DISCUSSION

### *4.1. Low-latitude response to obliquity forcing*

Several proxy records from the tropical Pacific preserve a 41-ky signal related to obliquity forcing. Our model results provide two mechanisms for amplifying the low-latitude obliquity forcing: 1) modifying the strength of the wind-driven ocean circulation and the advection of nutrients; and, 2) transmitting mid-latitude thermal anomalies to low latitudes through the thermocline circulation.

The thermocline response in our model is consistent with our understanding of the modern thermocline circulation. In the Pacific, tropical thermocline waters are sourced by the subduction of late winter surface waters in the mid-latitudes (Stommel, 1979; Toggweiler et al., 1991). Subducted waters reach the tropical thermocline through the eastern boundary currents and interior circulation (Harper, 2000). According to theories for the thermocline, tropical thermocline depth is dependant on the wind stress and the density gradient across the thermocline, which is determined by the temperature difference ($\Delta T$)

between the surface and the deep ocean (Bocaletti et al., 2004). In our experiments, an increase in axial tilt reduces ΔT through the subduction and advection of anomalously warm waters into the EEP, but has little effect on wind stress, leading to deepening of the thermocline as predicted by theory.

Our results are consistent with those reported by Liu et al. (2003) for orbital forcing in the Holocene. The thermocline response to Holocene orbital forcing (predominantly precessional forcing) was determined mainly by surface water subduction driven by insolation forcing in the late winter (Liu et al., 2003). In contrast to our results, the thermocline response to Holocene orbital forcing propagated to the sea surface, leading to cooler SSTs in the EEP and more La Nina-like conditions (Liu et al., 2003). The difference in the surface response is linked to the difference in orbital forcing. Because obliquity forcing has little effect on low-latitude insolation, it does little to influence trade wind strength near the equator. In contrast, by intensifying low-latitude seasonal insolation differences in the northern hemisphere, precessional forcing strengthens the trades by intensifying the summer monsoons from Asia and North America (Liu et al., 2000) and increasing the tropical east-west thermal gradient through rapid summer insolation warming of the western Pacific warm pool (Clement et al., 2000).

### *4.2. Comparison with tropical marine proxy records*

We suggest that FOAM's response to a change in obliquity is consistent with Pleistocene marine proxy records from the tropical Pacific. As indicated by the lack of an east-west productivity gradient across the tropical Pacific and

Indian Oceans (Beaufort et al., 2001) and a stable ΔSST across the tropical Pacific during glacial-interglacial oscillations (de Garidel-Thoron, 2005), marine proxy records indicate only minor changes in tropical thermocline structure in response to the obliquity cycle. FOAM also predicts only minor changes in the thermocline that do not strongly affect surface properties. Neither the proxy records nor the model support the idea that fluctuations in the axial tilt drove large-scale dynamical changes involving the Walker circulation and thermocline tilt. Rather, the FOAM results support the conclusions of Pisias and Mix (1997) that changes in tropical subsurface temperature were linked to the Southern Ocean climate response.

The tropical marine seawater proxies consistently demonstrate an anti-phased relationship with obliquity forcing of local insolation (Lea et al., 2000; Liu and Herbert, 2004; de Garidel-Thoron et al., 2005). During times of high (low) axial tilt, seawater temperatures are relatively high (low). FOAM's response is consistent with the seawater temperature proxies if they are recording subsurface (~30 m or below) temperatures rather than surface temperatures as often stated in the literature. The secretion of calcite tests by planktonic foraminfera and the growth of haptophyte algae that biosynthesize long-chained alkenones have been observed to occur over a range of depths (Be, 1977; Okada and Honjo, 1973; Okada and McIntyre, 1979; Conte et al., 1994; Ternois et al., 1997). In general, the magnitude of FOAM's seawater temperature response is consistent with that derived from radiolarian microfossils (Pisias and Mix, 1997), but is less than that indicated by either Mg/Ca or $U_{37}^{K'}$

paleothermometry (Lea et al., 2000; Liu and Herbert, 2004; de Garidel-Thoron et al., 2005). If FOAM's obliquity response is too weak, there may be several possible reasons. First, our experiments do not include variations in atmospheric $CO_2$ or global ice volume. Lea (2004) reports a strong correlation at the 41 kyr period between Cocos Ridge SST and atmospheric $CO_2$ from the Vostok ice core. We expect that including $CO_2$ variations in our experiments would have directly amplified the obliquity signal by modifying tropical radiative forcing and indirectly enhanced the obliquity signal by influencing the Southern Ocean sea-ice extent and the temperature of subducting mid-latitude waters. Second, like most medium-resolution ocean GCMs, FOAM is more diffusive than the real ocean. In a less diffusive model, it is possible that the tropical thermocline response to extratropical insolation anomalies may be stronger.

### *4.3. Obliquity forcing and ice ages*

Since Milankovitch (1941) proposed the astronomical theory for ice ages, obliquity has been implicated in the growth and decay of continental ice sheets. Milankovitch (1941) proposed that through its control on high-latitude summer insolation, obliquity determined the annual mass balance of an ice sheet. It is now well known that Milankovitch theory falls short on several accounts including its inability to explain: 1) the transition from a world dominated by 41 kyr variability at high latitudes to one dominated by 100 kyr variability in the mid-Pleistocene; and, 2) the fact that precession, rather than obliquity, dominates the summer insolation at high latitudes (Raymo and Nisancioglu, 2003).

New hypotheses that attempt to avoid the problems of the Milankovitch theory have been proposed to explain the link between obliquity and ice ages. To explain the 41 kyr period of ice ages before the mid-Pleistocene transition, Raymo and Nisancioglu (2003) suggest that obliquity primarily controlled climate change through its influence on insolation gradients rather than high latitude summer insolation. In turn, insolation gradients governed the atmospheric fluxes of heat, moisture and latent energy that controlled ice sheet growth and decay (Young and Bradley, 1994; Raymo and Nisancioglu, 2003). According to the gradient hypothesis, as obliquity decreased, the insolation gradient increased, driving greater poleward transport of moisture and promoting polar ice sheet growth.

An alternative hypothesis, here deemed the tropical-thermocline hypothesis, proposes that prior to the mid-Pleistocene transition obliquity forcing was amplified by positive feedbacks in the tropics (Philander and Federov, 2003; Ravelo et al., 2004). The tropical-thermocline hypothesis predicts that obliquity influences tropical thermocline waters through its control on mean-annual mid-latitude insolation where thermocline waters are subducted. In turn, the thermocline temperature governs the SST in regions of equatorial upwelling, leading to changes in the Walker and Hadley circulations that ultimately influence high-latitude climate through teleconnections- much in the same way that ENSO affects global climate (Cane, 1998). In either hypothesis, ice sheet growth may be amplified by ice-proximal changes in SST, NADW, and dust that stimulate a positive $CO_2$ feedback (Ruddiman, 2003).

Our model results provide insights into the role of obliquity forcing on global climate change. Most importantly, our model results predict a weak thermocline response to obliquity forcing, which does not appear at the sea surface. Zonal thermal gradients and trade wind strength vary little within the tropics in response to a change in obliquity. On the other hand, in response to low obliquity, the meridional surface-air-temperature (SAT) gradient increases, intensifying the jet stream, mid-latitude Westerlies, and subtropical ocean gyres. In both glacial and modern simulations, high-latitude regions are colder and high-latitude snowfall rates and accumulation are greater over much of the northern hemisphere under low-obliquity forcing. Jackson and Broccoli (2003) also report increased storminess and snowfall, and decreased high-latitude SAT during times of low meridional SAT gradient. They attribute the increase in northern hemisphere storminess to the accumulation of potential energy to the south of the zonal wind anomaly and the tendency for an increase in vertical shear to promote faster growth of storms (Jackson and Broccoli, 2003). Without a dynamic ice-sheet model, we can not say whether the reduction in meridional insolation gradient and enhanced snowfall might grow an ice sheet in a more favorable (i.e. pre-industrial) mean climate, but our results indicate that insolation gradient-driven moisture fluxes may amplify obliquity forcing.

## 5. SUMMARY

The response of the tropical Pacific climate to obliquity forcing is estimated using a coupled ocean-atmosphere model and compared to

Pleistocene marine proxy records from sediment cores recovered from the tropical Pacific. Two glacial simulations with high and low axial tilt were developed and analyzed. In response to an increase in axial tilt, the model predicts tropical sea-surface cooling associated with the decrease in local insolation. Extratropical surface waters warm due to the increase in local insolation and a decrease in sensible heat loss with a reduction in sea ice. Anomalous heating through high obliquity forcing also generates dynamical responses that weaken mean-annual mid-latitude Westerlies and subtropical trade winds, contributing to a ~20% reduction in the subtropical gyre circulation. Advection and ventilation of anomalously warm extratropical waters and a reduction in heat export from the tropics cause subsurface warming and a slight shoaling of the tropical thermocline in the central and eastern equatorial Pacific. Importantly, the subsurface warming in the tropical Pacific does not penetrate the sea surface, and the equatorial trade winds and Walker circulation show no systematic changes.

The model's response to obliquity forcing is consistent with tropical marine proxy data and reconciles proxy records that were seemingly at odds with each other. Lastly, the model results support the hypothesis that Earth's obliquity influences ice age climate primarily through its control on meridional insolation gradients (e.g., Raymo and Nisancioglu, 2003).

## ACKNOWLEDGMENTS

We greatly appreciate D. Lea and Z. Liu for their discussions and clarifications of the paleo-records. This work was supported by National Science Foundation grant ATM-0432503.

FIGURES: Chapter II

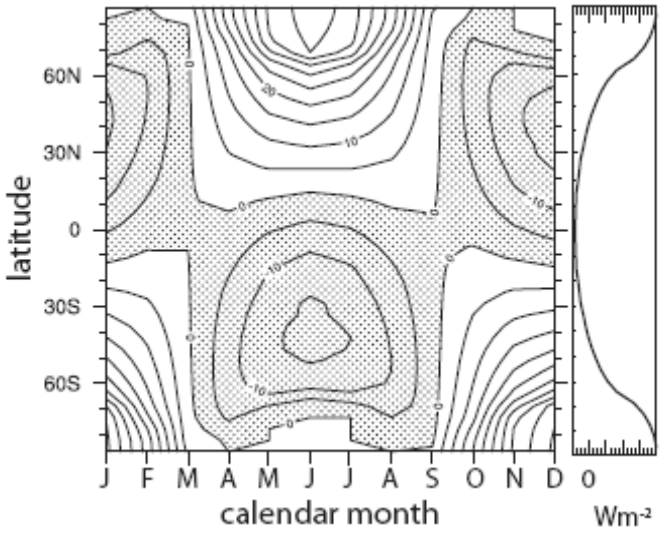


Figures 2-1. Seasonal (left) and mean-annual (right) solar insolation difference between HOBL and LOBL. Under high obliquity, seasonal and annual meridional insolation gradients are reduced. The contour interval is 10 $Wm^{-2}$.

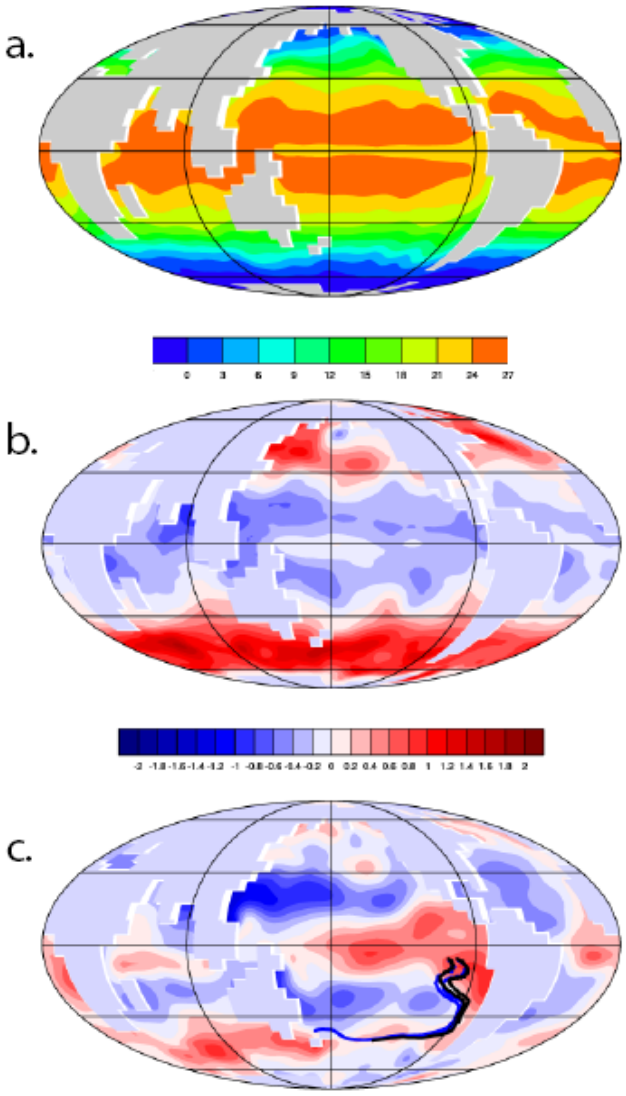


Figure 2-2. (a) Simulated mean-annual sea-surface temperature in the glacial HOBL experiment. Glacial tropical SSTs are approximately 4 °C cooler than modern SSTs. (b) Surface and (c) subsurface (30-100 m) temperature differences between the HOBL and LOBL (HOBL – LOBL) experiments. In response to an increase in obliquity, tropical SSTs cool by up to 0.6 °C, but tropical subsurface waters warm by up to 0.8 °C. Southern hemisphere water particle paths calculated using a Lagrangian transport model are shown in (c). The thick black (blue) line represents the particle trajectory in the HOBL (LOBL) experiment. The length of the trajectory indicates the speed of the flow. Thus, the trajectories indicate that flow through the subtropical gyre is faster in the LOBL experiment than the HOBL experiment. The contour interval is 3 °C in (a) and 0.2 °C in (b) and (c); the blue area in (b) and (c) represents a temperature decrease.

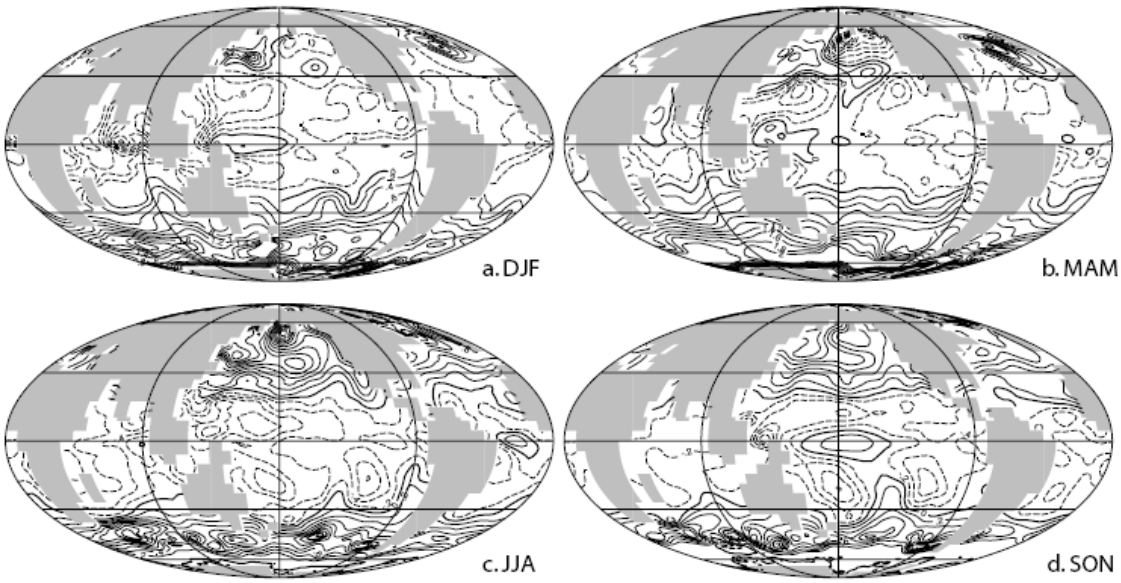


Figure 2-3. Simulated seasonal sea-surface temperature (°C) difference between HOBL and LOBL (HOBL – LOBL) experiments. Seasonal differences are linked to seasonal insolation differences or dynamical responses to seasonal insolation differences (see text). The contour interval is 0.2 °C; lower temperatures are indicated by dashed contour. (DJF = December, January, February; MAM=March, April, May; JJA=June, July, August; SON=September, October, November).

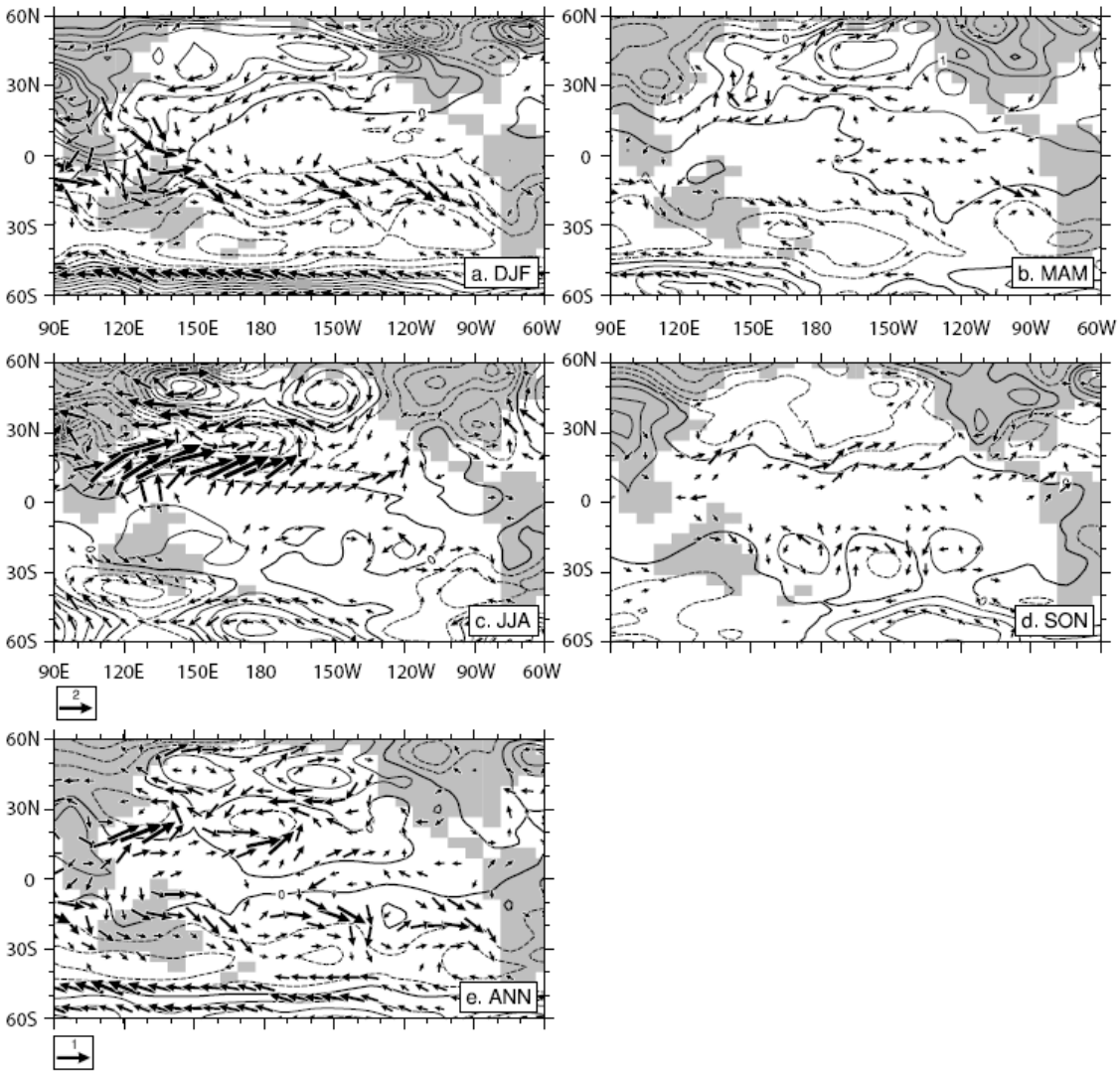


Figure 2-4. Seasonal and mean-annual differences in near-surface wind (vectors) and surface-level pressure (SLP) (contours) between HOBL and LOBL (HOBL-LOBL). Seasonal differences in insolation forcing generate SLP and near-surface wind anomalies. For example, in MAM, subtropical heating (cooling) intensifies (reduces) the subtropical high, leading to stronger (weaker) trades in the northern (southern) hemisphere. Only wind vector differences greater than 0.5 $ms^{-1}$ in (a)-(d) and 0.25 $ms^{-1}$ in (e) are displayed. The SLP contour interval is 0.5 mb; the dashed contours represent a decrease in SLP. Acronyms for the seasons are the same as in Fig. 2-3; ANN=mean-annual.

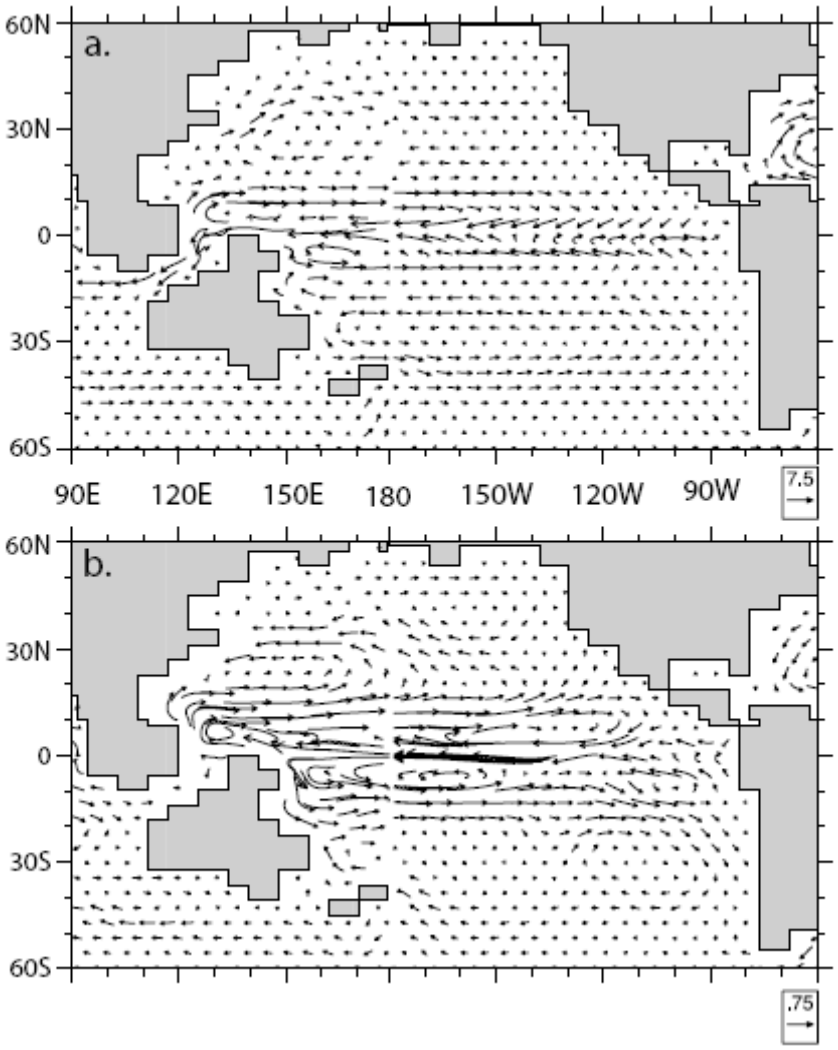


Figure 2-5. (a) Mean-annual subsurface (30-100m) flow in the HOBL experiment. (b) Difference in the subsurface flow between the HOBL and LOBL (HOBL – LOBL) experiments. As indicated by their reversal in the difference plot, the subtropical gyres slow, while the Northern Equatorial Counter Current and Southern Equatorial Current increase in speed. Note the different between the reference vectors between panels. Reference vectors are in cm $s^{-1}$.

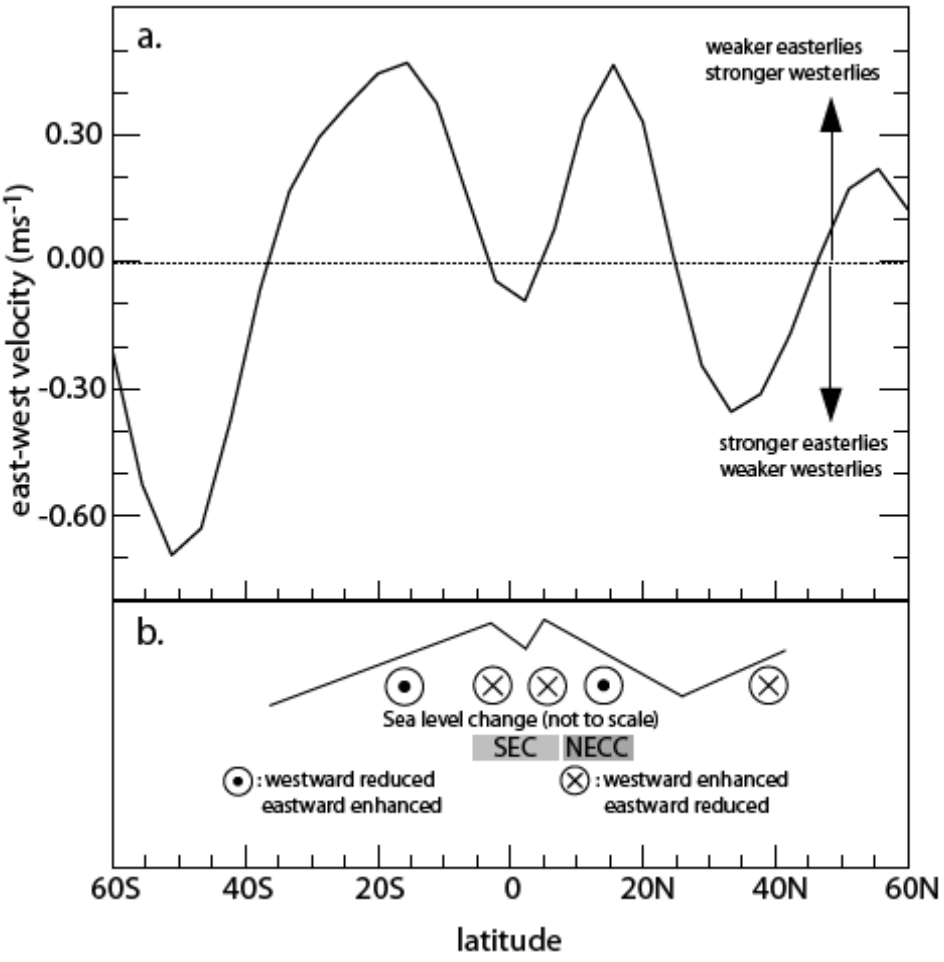


Figure 2-6. (a) Difference (HOBL – LOBL) in zonal-average mean-annual surface wind ($ms^{-1}$) over the Pacific (120°E-90°W). As indicated by the positive (eastward) wind difference, in the northern hemisphere, the off-equatorial trade winds weaken around 15° and intensify near 30° in the HOBL experiment. (b) Schematic displaying the affect of the change in zonal wind stress on the equatorial currents, according to Sverdrup theory. The solid line represents the change in relative sea-level height due to the changes in zonal wind with latitude. The symbols represent the relative change in current direction. Note that the SEC and the NECC both strengthen; the NEC weakens.

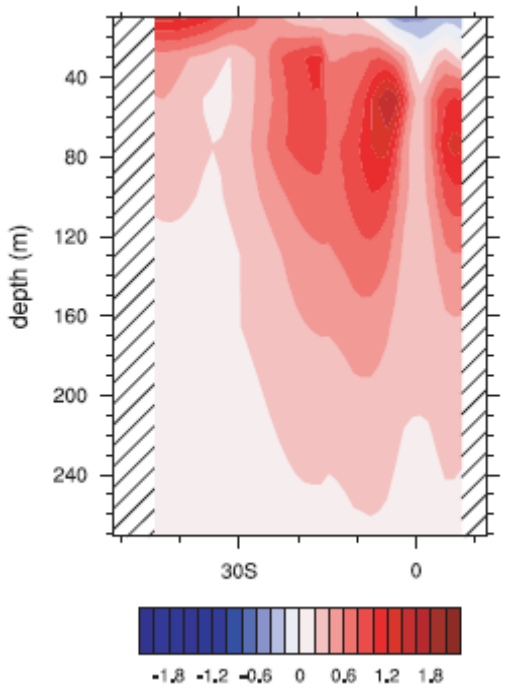


Figure 2-7. Cross-section of seawater temperature difference (HOBL – LOBL) in the eastern South Pacific (77.4°W – 91.4W). The contour interval is 0.2 °C.

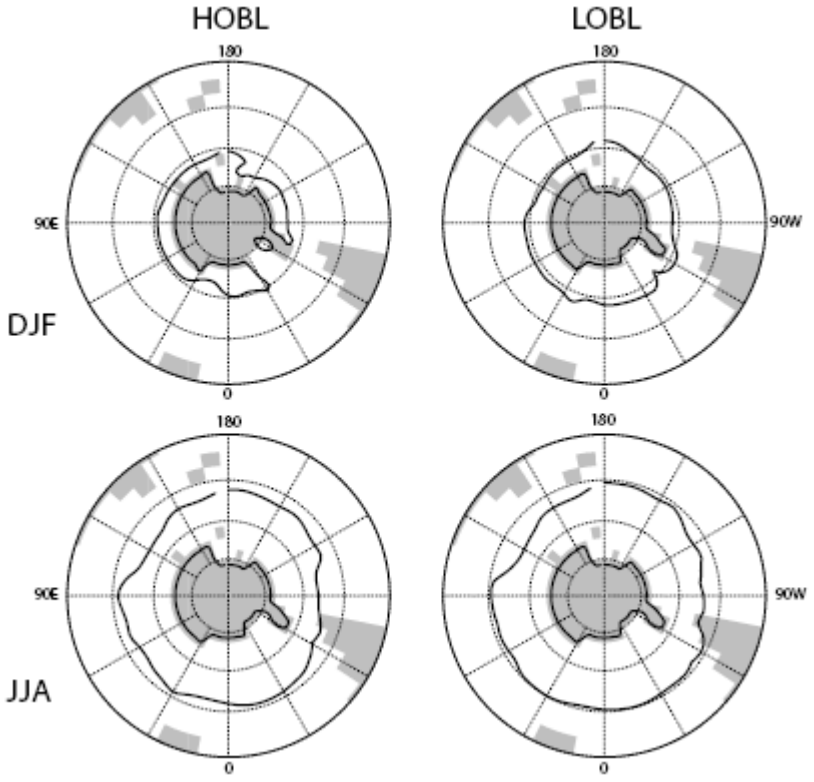


Figure 2-8. Seasonal (DJF and JJA) sea-ice distributions in the southern hemisphere for the HOBL (left column) and LOBL (right column) experiments. Note that the sea-ice distribution is farthest equatorward in the LOBL experiments. The polar projection map begins at 30 °S; the continents are shaded gray.

REFERENCES

Be, A.W.H., An ecological, zoogeographic and taxonomic review of recent planktonic foraminifera, in Oceanic Micropalaeontology, edited by A.T.S. Ramsay, pp. 1-100, Academic, San Diego, California, 1977.

Beaufort, L., T. de Garidel-Thoron, A.C. Mix, and N.G. Pisias, ENSO-like forcing on oceanic primary production during the late Pleistocene *Science*, 293, 2440-2444, 2001.

Beck, J.W., J. Recy, F. Taylor, R.L. Edwards, and G. Cabloh, Abrupt changes in early Holocene sea surface temperature derived from coral records, *Nature*, 385, 705-707, 1997.

Berger, A.L., Long term variations of daily insolation and quaternary climate change. *J. Atmos. Sci*, 35, 2362-2367, 1978.

Bocaletti G., R.C. Pakanowski, S.G.H. Philander, and A.V. Fedorov, The thermal structure of the upper ocean, *Journal of Physical Oceanography*, 34, 888-902, 2004.

Budziak, D., R.R. Schneider, F. Rostek, P. Müller, E. Bard, and G. Wefer, Late Quaternary insolation forcing on total organic carbon and C37 variations in the Arabian Sea, *Paleoceanography*, 15, 307-321, 2000.

Cane, M.A., 1998, Climate change-A role for the tropical Pacific, *Science*, 282, 56-61, 1998.

Clemens, S., W. Prell, D. Murray, G. Shimmield, and G. Weedon, Forcing mechanisms of the Indian ocean monsoon, *Nature*, 353, 720-725, 1991.

Clement, A.C., R. Seager, and M.A. Cane, Suppression of El Nino during the mid-Holocene by changes in the Earth's orbit, *Paleoceanography*, 15, 731-741, 2000.

Conte, M.H., J.K. Volkman, and G. Eglinton, Lipid biomarkers of the Haptophyta, The Haptophyte algae: Clarendon, Oxford, England, p. 351-377, 1994.

de Garidel-Thoron, T., Y. Rosenthal, F. Bassinot, and L. Beaufort, Stable sea surface temperatures in the western Pacific warm pool over the past 1.75 million years, *Nature*, 433, 294-298, 2005.

Harper, S., Thermocline ventilation and pathways of tropical-subtropical water mass exchange, *Tellus*, 52A, 330-345, 2000.

Harrison, S.P., J.E. Kutzbach, Z. Liu, P.J. Bartlein, B. Otto-Bliesner, D. Muhs, I.C. Prentice, and R.S. Thompson, Mid-Holocene climate of the Americas: a dynamical response to changed seasonality, *Climate Dynamics*, 20, 663-688, 2003.

Jackson, C.S. and A.J. Broccoli, Orbital forcing of Arctic climate: mechanisms of climate response and implications for continental glaciation, *Climate Dynamics*, 21, 539-557, 2003.

Jacob, R., Low frequency variability in a simulated atmosphere ocean system [Ph.D. thesis]: Madison, University of Wisconsin, 159p., 1997.

Kiehl, J.T., J.J. Hack, G.B. Bonan, B.A. Boville, B.P. Briegleb, D.L. Williamson, and P.J. Rasch, Description of the NCAR Community Climate Model (CCM3): Boulder, Colorado, National Center for Atmospheric Research Technical Note NCAR/TN-420+STR, 152p., 1996.

Lea, D.W., The 100000-yr cycle in tropical sst, greenhouse forcing, and climate sensitivity, *Journal of Climate*, 17, 2170-2179, 2004.

Lea, D.W., D.K. Pak, and H.J. Spero, Climate impact of Late Quaternary equatorial Pacific sea surface temperature variations, *Science*, 289, 1719-1724, 2000.

Liu, Z., and T.D. Herbert, High-latitude influence on the eastern equatorial Pacific climate in the early Pleistocene epoch, *Nature*, 427, 720-723, 2004.

Liu, Z., E. Brady, and J. Lynch-Stieglitz, Global ocean response to orbital forcing in the Holocene, *Paleoceanography*, 18, 1041, doi:10.1029/2002PA000819, 2003.

Liu, Z., J.E. Kutzbach, J.E., L. Wu, Modeling climate shift of El Nino variability in the Holocene, *Geophysical Research Letters*, 27, 2265-2268, 2000.

Liu, Z., L. Wu, R. Gallimore, and R. Jacob, Search for the origins of Pacific decadal climate variability, *Geophysical Research Letters*, 29, 10.1029/2001GL013735, 2002.

Liu, Z., S. Shin, P. Behling, W. Prell, M. Trend-Staid, S.P. Harrison, and J.E. Kutzbach, Dynamical and observational constraints on tropical Pacific sea surface temperature at the last glacial maximum, *Geophysical Research Letters*, 27, 105-108, 2000.

Martinez I., L. Keigwin, T.T. Barrows, Y. Yokyama, and J. Southon, La Nina-like conditions in the eastern equatorial Pacific and a stronger Choco jet in the northern Andes during the last glaciation, *Paleoceanography*, 18, 1011, doi:10.1029/2002PA000877, 2003.

Milankovitch, M., Canon of insolation and the ice age problem (Israel Program for Scientific Translations, Jerusalem), 1941.

Mix, A.C., A.E. Morey, N.G. Pisias, and S.W. Hostetler, Foraminiferal faunal estimates of paleotemperature: circumventing the no-analog problem yields cool ice age tropics, *Paleoceanography*, 14, 350-359, 1999.

Okada, H. and A. McIntyre, Seasonal distribution of modern coccolithophorides in the western North Atlantic ocean, *Marine Biology*, 54, 319-328, 1979.

Okada, H., and S. Honjo, The distribution of oceanic coccolithophorides in the Pacific, *Deep-Sea Research*, 20, 355-374, 1973.

Peltier,W.R., Ice age paleotopography, *Science*, 265, 195-201, 1994.

Perks, H., C.D. Charles, and R.F. Keeling, Precessionally forced productivity variations across the equatorial Pacific, *Paleoceanography*, 17, 63-69, 2002.

Perks, H.M., and R.F. Keeling, A 400 kyr record of combustion oxygen demand in the western equatorial Pacific: Evidence for a precessionally forced climate response, *Paleoceanography*, 13, 63-69, 1998.

Petit, J.R., J. Jouzel., D. Raynaud, N.I. Barkov, J.M. Barnola, I. Basile, M. Bender, J. Chappellaz, M. Davis, G. Delaygue, M. Delmotte, V.M. Kotlyakov, M. Legrand, V.Y. Lipenkov, C. Lorius, L. Pepin, C. Ritz, E. Saltzman, and M. Stievenard, Climate and atmospheric history of the past 420,000 from the Vostok ice core, Antarctica, *Nature*, 399, 429-436, 1999.

Philander, S.G., and A.V. Federov, Role of tropics in changing the response to Milankovitch forcing some three million years ago, *Paleoceanography*, 18, 1045, doi:10.129/2002PA000837, 2003.

Pierrehumbert, R., High levels of atmospheric carbon dioxide necessary for the termination of global glaciation, *Nature*, 429, 646-649, 2004.

Pisias, N.G., and A.C. Mix, Spatial and temporal oceanographic variability of the eastern equatorial Pacific during the late Pleistocene: Evidence from Radiolaria microfossils, *Paleoceanography*, 12, 381-393, 1997.

Poulsen, C.J., A.S. Gendaszek, and R. Jacob, Did the rifting of the Atlantic Ocean cause the Cretaceous thermal maximum? *Geology*, 31, 115-118, 2003.

Poulsen, C.J., R.T. Pierrehumbert, and R.L. Jacob, Impact of ocean dynamics on the simulation of the Neoproterozoic "snowball Earth", *Geophysical Research Letters*, 28, 1575-1578, 2001.

Ravelo, A.C., D.H. Andreasen, M. Lyle, A.O. Lyle, and M.W. Wara, Regional climate shifts caused by gradual global cooling in the Pliocene epoch, Nature, 429, 263-267, 2004.

Raymo, M.E., and K. Nisancioglu, The 41 kyr world: Milankovitch's other unsolved mystery, *Paleoceanography*, 18, 1011, doi:10.1029/2002PA000791, 2003.

Reichart, G.J., L.J. Lourens, and W.J. Zachariasse, Temporal variability in the northern Arabian Sea Oxygen Minimum Zone (OMZ) during the last 225,000 years, *Paleoceanography*, 13, 607-621, 1998.

Ruddiman W. F., Orbital insolation, ice volume, and greenhouse gases, *Quaternary Science Reviews*, 22, 1597-1629, 2003.

Sarmiento, J.L., N. Gruber, M.A. Brzezinski, and J.P. Dunne, High-latitude controls of thermocline nutrients and low latitude biological productivity, *Nature*, 427, 56-60, 2003.

Stommel H., Determination of water mass properties of water pumped down from the Ekmam layer to the geostrophic flow below, *Proceedings of the national academy of sciences of the united states of America*, 76, 3051-3055, 1979.

Toggweiler, J.R., K. Dixon, and W.S. Broecker, The Peru upwelling and the ventilation of the South-Pacific thermocline, *Journal of Geophysical Research-Oceans*, 96 (C11), 20467-20497, 1991.

Ternois, Y., M.A. Sicre, A. Boireau, M.H. Conte, and G. Eglinton, Evaluation of long-chain alkenones as paleo-temperature indicators in the Mediterranean Sea, *Deep-Sea Research I*, 44, 271-286, 1997.

Young, M.A., and R.S. Bradley, Insolation gradients and the paleoclimatic record, in *Milankovitch and Climate, Part2*, edited by A.L. Berger et al., pp. 707-713, D. Reidel, Norwell, Mass., 1984.

# CHAPTER III

## Sea Ice Control of Plio-Pleistocene Tropical Pacific Climate Evolution


## ABSTRACT

Marine proxies of sea surface temperature (SST) indicate that the tropical Pacific thermal gradient intensified through the Plio-Pleistocene and peaked during Pleistocene glaciations. The cause of this variability, which has been linked to the initiation of the Walker circulation, is uncertain. Here, we hypothesize that Plio-Pleistocene tropical climate variability was coupled to high-latitude Southern Hemisphere climate change, specifically sea-ice extent. We use a coupled ocean-atmosphere general circulation model to investigate the influences of sea-ice extent and atmospheric $CO_2$ on the tropical Pacific thermal structure. In the model, $CO_2$-radiative forcing in the absence of any sea-ice feedbacks has little influence on the tropical SST gradient. A 180ppm reduction in $CO_2$ causes the SST gradient to decrease by 0.4°C. In comparison, an expansion of Southern Hemisphere, high-latitude sea ice reduces tropical SSTs and enhances the SST gradient in the tropical Pacific by as much as 3.5°C. Tropical cooling is primarily due to the advection and upwelling of waters into the eastern equatorial Pacific that were cooled by sensible heat loss at the sea-ice margin in the Southern Pacific. An energy balance analysis indicates that the ocean heat flux into the eastern equatorial Pacific decreases by ~44%. This

mechanism provides an intimate coupling between the tropical Pacific and the high-latitude Southern Hemisphere through the thermocline circulation.

## 1. INTRODUCTION

The modern tropical Pacific Ocean is characterized by an east-west thermal gradient with a pool of warm water in the western equatorial Pacific (WEP) and a tongue of colder water in the eastern equatorial Pacific (EEP) associated with the upwelling of subsurface water offshore of Peru [1]. The zonal Pacific sea surface temperature (SST) gradient figures significantly in the global transport of heat and moisture because it is linked to elements of the general circulation through the Bjerknes feedback [2]. It is important to consider then that the modern tropical Pacific SST gradient is a relatively young feature and may have been absent as recently as the Pliocene [3]. Marine proxy records of tropical Pacific seawater temperature indicate that the east-west SST gradient has increased by ~2°C over the last 1.75 Ma as the EEP has gradually cooled [4][5][6][7]. However, this secular trend in the east-west SST gradient is only part of the story. Glacial-interglacial fluctuations of equivalent magnitude are superimposed on this long-term trend [5][6].

The cause of the Plio-Pleistocene evolution of the tropical Pacific is uncertain. Intensification of the tropical Pacific SST gradient and the cooling of the EEP has generally been attributed to a shoaling of the tropical thermocline and intensification of the Walker circulation [4][5][6][7][8]. The tropical thermocline depth is set by the temperature of the mid-latitude waters that source

the thermocline and the rate at which these waters are upwelled, a process that is largely controlled by the local wind stress [9]. Two specific mechanisms have been given for the long-term Plio-Pleistocene shoaling of the thermocline: 1) secular cooling of deep waters through the Cenozoic [8], and 2) intensification of the southeast trades resulting from an equatorward shift in the Antarctic Circumpolar Current after 1.83 Ma [6]. Neither of these mechanisms account for the glacial-interglacial variations in tropical SST gradient.

Glacial-interglacial variations in tropical Pacific SST gradient are not completely unexpected. Paleoclimate data indicate an increase in EEP upwelling during the Last Glacial Maximum (LGM) and earlier Pleistocene glacials [10][11][12][13][14]. Climate model simulations of the Last Glacial Maximum (LGM) support the paleo-data, predicting enhanced upwelling, cooling of EEP SST, and shallowing of the tropical thermocline [15][16][17]. However, the reduction in the east-west SST gradient can not be symptomatic of glacial conditions, because Pacific tropical climate change preceded Northern Hemisphere glaciations by several thousand years [18]. The cause of glacial-interglacial tropical Pacific SST gradient changes has not been specifically addressed in the literature. However, Medina-Elizalde and Lea [7] ascribe the general evolution of tropical SSTs between glacial and interglacial periods to direct radiative forcing by atmospheric $CO_2$.

In this contribution we propose that the evolution of the Pacific SST gradient was largely tied to the expansion and contraction of Southern Ocean sea ice. That the sea-ice margin evolved through the Plio-Pleistocene is well

documented, though the details are not highly resolved. It is known that the Pliocene sea-ice margin was substantially retracted relative to the modern [19] and protracted during the Last Glacial Maximum [20]. If the Last Glacial Maximum and present-day are representative of glacial and interglacial intervals, it is likely that the sea-ice margin expanded and contracted in concert with the Pleistocene glacial-interglacial cycles. The sea-ice margin is important because it exerts a strong control on the sensible heat loss, and consequently the temperature, of the mid-latitude seawater that is subducted and advected through the eastern boundary current to form the waters at the base of the thermocline in the EEP [23]. As demonstrated in Lee and Poulsen [23], the expansion of Southern Ocean sea ice and the reduction of mid-latitude SST lead to a cooling of EEP waters. This sea-ice-thermocline mechanism provides a strong link of communication between the Southern Hemisphere high-latitude and tropical climates, explaining the near synchronicity in proxy records from these regions. We hypothesize that this mechanism tied the secular and glacial-interglacial trends in the tropical Pacific climate to the Southern Ocean sea-ice history.

The purpose here is to provide a proof-of-concept of our hypothesis. To this end, we present results from a series of coupled ocean-atmosphere experiments in which the sea-ice extent is imposed; simulations of Pliocene and Pleistocene sea ice will be addressed in a future study. After explaining our methodology (Section 2), we describe the model results (Section 3). In Section 3.1, we explore how the tropical Pacific Ocean responds to imposed high-latitude

sea-ice forcing. In Sections 3.2 and 3.3, we describe the tropical SST response to a reduction in atmospheric $CO_2$ with and without the sea-ice feedback. In Section 4, we discuss the implications of our model results in light of Plio-Pleistocene marine proxy data and paleoceanographic evidence of sea ice evolution.

## 2. METHOD AND MODEL DESCRIPTION

### *2.1. FOAM*

This study was completed using the Fast Ocean Atmosphere Model (FOAM) version 1.5, a fully coupled mixed-resolution ocean and atmosphere GCM [24]. The atmospheric model is a parallelized version of the Community Climate Model 2 (CCM2) with the upgraded radiative and hydrological physics incorporated in CCM3.6 [25]. The atmospheric component of FOAM was run at a spectral resolution of R15 (4.5° x 7.5°) with 18 vertical levels. The oceanic component (OM3) is a z-coordinate ocean model with 128x128 point Mercator grid (1.4° x 2.8°), 24 vertical levels, and an explicit free surface. The sea-ice model in FOAM uses the thermodynamic component of the CSM1.4 sea-ice model, which is based on the Semtner 3-layer thermodynamic snow/ice model [27]. A coupler component interpolates fluxes between the atmospheric, oceanic, and sea-ice models to accommodate their different time steps and grid settings. FOAM was designed for long century-scale integrations and exhibits minimal ocean drift with no flux corrections [26]. FOAM's simulation of modern climate

shows reasonable agreement with present-day observations. FOAM has been widely used to study climate change through geological time (e.g. [28][29][30]).

### *2.2. Experimental design*

In this study, we use FOAM to estimate the tropical climate response to the extent of sea-ice in the high latitudes. To this end, three experiments were completed with extensive, moderate, and no amounts of sea ice (Table 3-1). In order to specify different sea-ice extents under otherwise identical boundary conditions, we tuned a model parameter that maps the sea-ice extent from the sea-ice model to the coupler. Under Last Glacial Maximum boundary conditions (described below) and no tuning, FOAM predicts about 10% too much sea ice in the Southern Ocean during winter. As a result, in all cases, our tuning reduced the sea-ice amount. It is important to note that by reducing the sea-ice extent, we artificially add latent energy to the high-latitude oceans with more energy added in the more highly tuned cases. This sea-ice tuning is justified by the purpose of this study, to assess the degree to which the sea-ice extent regulates the tropical Pacific climate.

The mean winter sea-ice areas predicted through our tuning procedure are listed in Table 3-1. The differences in global sea-ice distribution occur mainly in the Southern Hemisphere with only minor differences in the Northern Hemisphere (Table 3-1 and Fig.3-1). The case with the largest sea-ice extent compares well with paleo sea-ice reconstructions for the Last Glacial Maximum (LGM) with the exception that slightly more sea ice is present in the South Pacific Ocean than observed [20] [31]. The case with moderate sea-ice extent is similar

to the modern sea-ice coverage [32]. Hereafter we will refer to these cases as the LGM-ICE, MOD-ICE, and NO-ICE experiments. In addition to these three experiments, additional experiments were conducted with elevated atmospheric $CO_2$ levels (Table 3-1) to evaluate the influence of $CO_2$ on tropical Pacific climate.

We chose to use boundary conditions for the most recent glacial episode (i.e. the LGM) because it represents a time of maximum sea-ice extent and provides the greatest contrast with the Pliocene when sea-ice extent was most reduced. All FOAM experiments were initialized with LGM boundary conditions that include ice-sheet elevations and extents, sea level, topography, vegetation, orbital settings, and greenhouse gases appropriate for 21000 BP (Table 3-2). The model experiments were integrated for 200 years, bringing the surface ocean into equilibrium. Model results were averaged over the last 20 years of the experiments.

## 3. RESULTS

### *3.1. Sea-ice forcing and tropical Pacific climate*

Figure 3-1 illustrates the sea-ice extent in the LGM-ICE, MOD-ICE, and NO-ICE experiments. The high-latitude sea-ice extent has a substantial influence on both high and low latitude SSTs (Fig. 3-2). Tropical zonal average SSTs differ by about 5°C between the LGM-ICE and NO-ICE experiments and 2°C between the MOD-ICE and NO-ICE experiments. High-latitude sea-ice amounts also influence the tropical Pacific zonal thermal gradient. Larger sea-ice amounts in the Southern Ocean cause a reduction in the average tropical SST and an

enhancement of the east-west SST gradient (Fig. 3-3). For example, in comparison to the NO-ICE case, the tropical east-west SST gradients in the MOD-ICE and LGM-ICE experiments are ~1.0° and ~3.5°C greater. In both cases, the enhanced SST gradient results from greater cooling in the EEP than the WEP.

The sea-ice extent controls high-latitude SSTs mainly through its influence on sensible heat loss in the mid-latitude regions. As sea ice advances equatorward, the advection of cold air from the sea-ice surface to the sea surface enhances the mean-annual sensible heat loss. In the mid-latitude (40-50°S) Southern Ocean, mean-annual sensible heat losses are 8.4 and 4.9$Wm^{-2}$ greater and up to 28 and 12$Wm^{-2}$ higher along seasonal sea-ice margin in the LGM-ICE and MOD-ICE experiments than in the NO-ICE case. As a result, mid-latitude SSTs are 7 and 3°C lower (Fig. 3-2).

The coupling between high-latitude sea-ice area and tropical SSTs occurs through the thermocline circulation. In FOAM, mid-latitude South Pacific seawater, cooled by sensible heat loss, is subducted and advected through the eastern boundary current until it is eventually upwelled in the eastern tropical Pacific. Increasing the sea-ice extent reduces the temperature of the mid-latitude waters that source the EEP. This result is shown in Figure 3-3; in comparison to the NO-ICE case, at 90m depth subsurface waters upwelled in the EEP are 8 and 5°C colder in the LGM-ICE and MOD-ICE experiments. This mechanism for transporting high-latitude climate signals to the tropics in FOAM was previously described and diagnosed in Lee and Poulsen [23], and is consistent with modern

oceanographic processes in the Pacific Ocean [33][34]. In the modern ocean, EEP thermocline waters flow to the WEP through the equatorial currents [1]. As a consequence, the upwelling of cold mid-latitude waters into the EEP cools, to some degree, the entire tropical Pacific Ocean.

An analysis of the local energy budget provides further support that sea ice substantially impacts the ocean heat transport into the tropics. In the LGM-ICE experiment, the ocean heat flux to the EEP and WEP is reduced by 44% (39 $Wm^{-2}$) and 29% (25 $Wm^{-2}$). This reduction is a consequence of the advection of cooler waters through the tropical ocean. The reduced ocean heat flux is compensated by reductions in outgoing latent and longwave fluxes (Table 3-3). The difference in the ocean heat flux between the EEP and WEP is likely due to mixing within the tropical ocean and local radiation, which effectively heats the tropical seawater along its path from east to west.

As expected from the Bjerknes feedback [2], the increase in the east-west SST gradient intensifies the Walker circulation in the Pacific, as demonstrated by differences in the vertical pressure velocity and zonal winds between the LGM-ICE and MOD-ICE experiments (Figure 3-5). In the LGM-ICE case, upward motion in the WEP increases by up to 15%, while subsidence in the EEP is up to 30% greater. In addition, the velocity of the Trade Winds and high-level Westerlies increase (Figure 3-5), implying an increase in the Walker Circulation.

### *3.2. Atmospheric $CO_2$ forcing and tropical Pacific climate*

In this section, we explore whether the evolution of the tropical Pacific could have happened in the absence of significant sea-ice forcing. Following the

hypothesis of Medina-Elizalde and Lea [7] that the long-term depletion of atmospheric $CO_2$ controlled the tropical Pacific SSTs, we test the influence of $CO_2$-radiative forcing on the equatorial Pacific. Because the sea-ice model has been "turned off", differences in the NO-ICE and NO-ICE380 experiments exclude any sea-ice feedbacks to radiative forcing.

The reduction in atmospheric $CO_2$ from 380 to 200 ppm lowers tropical SSTs by ~0.8°C zonally in FOAM but actually decreases the tropical Pacific SST gradient by ~0.4°C (Fig. 3-6a). The tropical cooling is associated mainly with decreases in surface radiative heating and ocean heat flux (Table 3-3). However, in comparison to the sea-ice experiments (see Section 3.1), the decrease in ocean heat flux is very modest; the ocean heat flux is reduced by ~6% in both the EEP and WEP (Table 3-3). The reduced tropical SST gradient is primarily due to an increase in WEP low cloud coverage, which reduces the surface radiative heating in the WEP relative to the EEP. In sum, the model results indicate that pure radiative forcing, in the absence of sea-ice feedbacks, is not an effective mechanism for reducing the Pacific SST gradient.

### *3.3. Sea-ice and radiative forcing of tropical Pacific climate*

In section 3.1 and 3.2, we found that sea ice and $CO_2$ have opposing influences on the tropical Pacific SST gradient: Southern Hemisphere sea ice enhances the gradient; reductions in $CO_2$-radiative forcing decrease the gradient. Because radiative forcing is likely to invoke a sea-ice feedback, we evaluate the effect of reducing $CO_2$ on the tropical Pacific climate with an active sea-ice margin by comparing LGM-ICE and LGM-ICE380 experiments. Reducing

atmospheric $CO_2$ from 380 to 200ppm resulted in a 24% increase in winter sea-ice area (Table 3-1). Tropical SSTs decreased by ~2.0°C, and the east-west SST gradient increased by ~0.8°C (Fig. 3-6b). This result is consistent with Knutson and Manabe [36], which demonstrated a reduction in tropical Pacific SST gradient with an increase in atmospheric $CO_2$ from 1xPAL to 4xPAL. As in the previous experiments (Section 3.1), the intensification of the east-west SST gradient in FOAM results from upwelling of colder waters in the EEP and the associated decrease (~12%) in ocean heat flux. This result indicates that a secular decrease in atmospheric $CO_2$ could have driven the evolution of the tropical Pacific thermal gradient, but only in as much as $CO_2$ regulated Plio-Pleistocene sea ice.

# 4. DISCUSSION

## *4.1. The tropical ocean-sea ice hypothesis*

Proxy records of seawater temperature indicate that the equatorial Pacific surface temperature gradient increased by 2°C from the Pliocene to the present day due to the cooling of the EEP [4][5][6][7]. Between the Pliocene and Late Pleistocene glacial periods, the east-west SST gradient may have increased by more than 4°C [5][6]. The sea-ice sensitivity experiments described here support the hypothesis that an increase in high-latitude sea ice could account for the Plio-Pleistocene intensification of the tropical Pacific thermal gradient. Moreover, the model-predicted increase in the east-west SST gradient is consistent with the proxy data; the Pliocene to glacial increase in sea ice, represented by the LGM-

ICE and NO-ICE experiments, led to an increase of approximately 3.5°C. We reiterate that this intensification of the tropical Pacific SST gradient is due solely to a change in sea-ice area; no other boundary conditions were modified. As a result, the model results should not be considered a prediction of past SST gradients, but rather a ball-park estimate of the potential influence of sea ice on tropical Pacific SST gradients. On the basis of the $CO_2$ sensitivity experiments (see Section 3.2), it is likely that an increase in sea ice in combination with a reduction in atmospheric $CO_2$ would result in a somewhat smaller increase in Pacific SST gradient.

Sea ice is an attractive mechanism for driving tropical climate change because paleoceanographic evidence indicates that the Southern Ocean sea-ice area increased substantially through the Plio-Pleistocene and between interglacial and glacial times [19][31][37][38][39][40]. Geological evidence of reduced sea-ice coverage in the Pliocene Southern Ocean includes low abundances of diatom assemblages that are typically associated with sea ice [19][41]; the deposition of marine deposits in regions presently covered by sea ice [43]; the presence of fossils of dolphins that lived in open-water environments [44]; and a sea-ice proxy based on the chain length of marine diatoms (the *Eucampia* index) [19]. In Prydz Bay, East Antarctica, the sea-ice coverage was only ~45% of its modern extent and may at time have been completely absent [19]. Although the position of the Pliocene sea-ice edge is not known with certainty, there is considerable evidence that it was less extensive than at any time since.

Likewise, glacial-interglacial changes in sea ice are also uncertain; however differences between last glacial and modern sea-ice extents suggest that sea ice was likely more extensive during glacial intervals. From the occurrences of ice-rafted debris, changes in foraminiferal and radiolarian faunal assemblages, and lithological boundaries between diatomaceous ooze and terrigenous silt, CLIMAP [38] estimated that the LGM Southern Hemisphere sea-ice margin extended to 45°S in the Atlantic and Indian Oceans and 55°S in the Pacific Ocean. Gersonde et al. [40] used the abundance patterns of *Fragilariopsis curta* and *Fragilariopsis cylindrus* to calculate a 60-70% increase in Southern Ocean winter sea-ice coverage during the last glacial relative to the present. The cause of the increase in Southern Ocean sea ice through the Plio-Pleistocene and between interglacial-glacial cycles is not known with certainty but was likely related to reductions in atmospheric $CO_2$ and other GHGs [45][46], orbital forcing, oceanic upwelling [47], deep-ocean cooling [48], and dynamics of the Antarctic ice sheet [49]. A particularly appealing notion is that the Western Antarctic Ice Sheet, because of its location and its dynamic history (e.g., [50][51]), may have had a substantial influence on sea ice in the southern South Pacific Ocean.

### *4.2. Study limitations*

The purpose of this study is to evaluate the impact of sea ice on the equatorial Pacific rather than to simulate specific time slices. For this reason, identical model boundary conditions representing LGM conditions were used in each experiment; these boundary conditions are not, and were not intended to

be, representative of Pliocene and interglacial times. We also caution that our "tuning" of sea ice is not defensible from a physical standpoint. This device, which can be considered analogous to increasing freshwater fluxes in North Atlantic hosing experiments (e.g., [52][53][54]), was employed to obtain sea-ice margins that approximate those of glacial, interglacial, and Pliocene times. Like the North Atlantic hosing experiments, the sea-ice tuning is not strictly conservative; the artificial reduction in sea ice effectively removes latent energy of fusion (i.e., the energy that would have been used to freeze the sea ice) from the high latitudes. To further evaluate our hypothesis, climate simulations of these time slices with fully dynamic sea-ice models, and thus explicit sea-ice predictions, should be compared.

Because the purpose of this study was to examine the surface and thermocline circulations, the FOAM experiments were integrated for 200 years, not long enough to bring the deep ocean to equilibrium. However, because tropical climate change led Northern Hemisphere climate change by thousands of years [18], it is unlikely that variations in deepwater circulation were a primary control on glacial-interglacial variations in the tropical Pacific.

### *4.3. Summary and Implications for Plio-Pleistocene climate evolution*

That the tropical Pacific underwent a major reorganization in the Plio-Pleistocene is well documented [4][5][6][7]. Here, we present a specific mechanism, the cooling of the EEP through the upwelling of anomalously cold waters from the South Pacific, to explain the enhanced tropical Pacific SST gradient evidenced in marine proxy records. Our mechanism relies upon

changes in Plio-Pleistocene sea ice that have been observed in the marine record (Section 4.1). The ultimate cause of Plio-Pleistocene sea-ice evolution is uncertain, but several possibilities exist including GHG variability. The sea-ice mechanism implies that the high-latitude Southern Hemisphere has been a climate puppeteer of sorts manipulating its tropical marionette, an idea that is consistent with observations that tropical SST coincided with Antarctic air temperature in the Late Pleistocene [18].

It has been proposed that the development of a strong SST gradient across the tropical Pacific and the onset of a vigorous Walker circulation may have been instrumental in the onset and/or intensification of Northern Hemisphere glaciation, either as threshold events [6] or as a long-term conditioning [4]. Climate model results of the LGM support this idea; tropical SST patterns have been shown to have a substantial influence on glacial mass balance in the Northern Hemisphere [55]. Our model results are also generally consistent with this hypothesis; in the LGM-ICE experiment with cool tropical SSTs and an intensified SST gradient, mid- and high-latitude continental surface temperatures are several degrees cooler than in the NO-ICE case. In addition, continental snowfall is shifted southward toward the mid-latitudes. Though our experiments are highly idealized, we note that these tendencies would support the expansion of Northern Hemisphere glaciation. On the basis of these results, we speculate that conditioning for the intensification of Northern Hemisphere glaciation may have started with Southern Hemisphere cooling and sea-ice expansion. Southern Hemisphere cooling was then transmitted through the

thermocline circulation to the tropics, inducing cooling and intensification of the east-west SST gradient. Through atmospheric and oceanic teleconnections, tropical climate changes may have then favored ice-sheet growth in the high latitudes of the Northern Hemisphere.

## ACKNOWLEDGEMENTS

This research was supported by National Science Foundation grant ATM-0432503 to Poulsen. We gratefully acknowledge M. Delaney, W. Ruddiman, and two reviewers for their constructive comments.

FIGURES: Chapter III

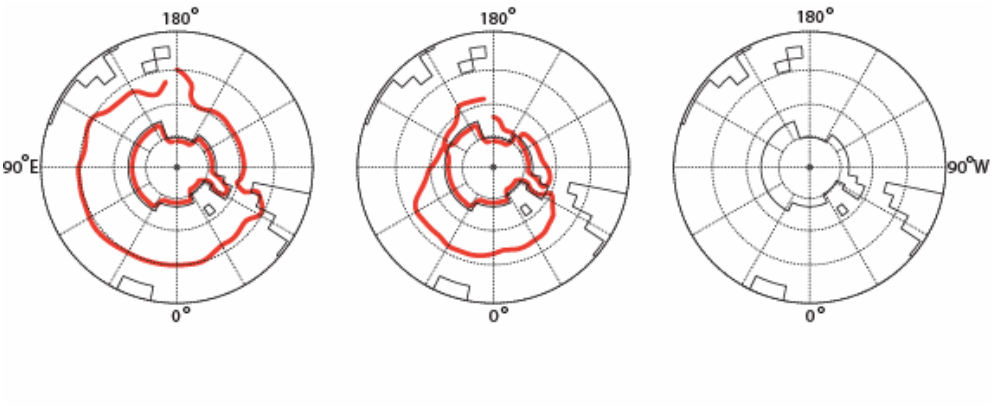


Fig. 3-1. Mean Southern Hemisphere winter (June-July-August) sea-ice distribution for the LGM-ICE (left), MOD-ICE (middle), and NO-ICE (right) experiments. The LGM-ICE winter sea-ice extent is approximately 95% greater than the MOD-ICE. NO-ICE has no sea ice by design (see Section 2.2). The polar projection map begins at 30°S.

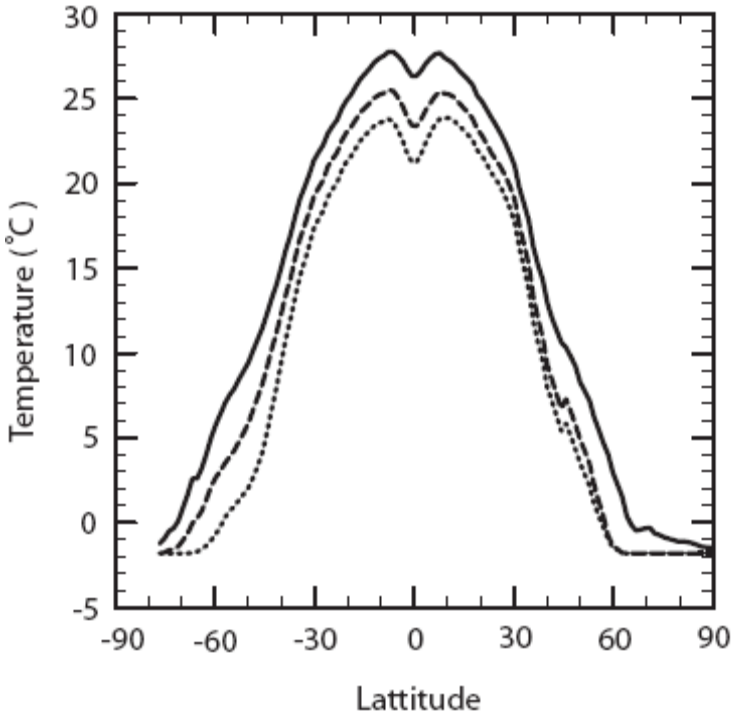


Fig. 3-2. Simulated mean-annual sea surface temperatures in LGM-ICE (dotted), MOD-ICE (dashed), and NO-ICE (solid) experiments. LGM-ICE and MOD-ICE SSTs are approximately 10 and 6°C cooler than NO-ICE at 45°S.

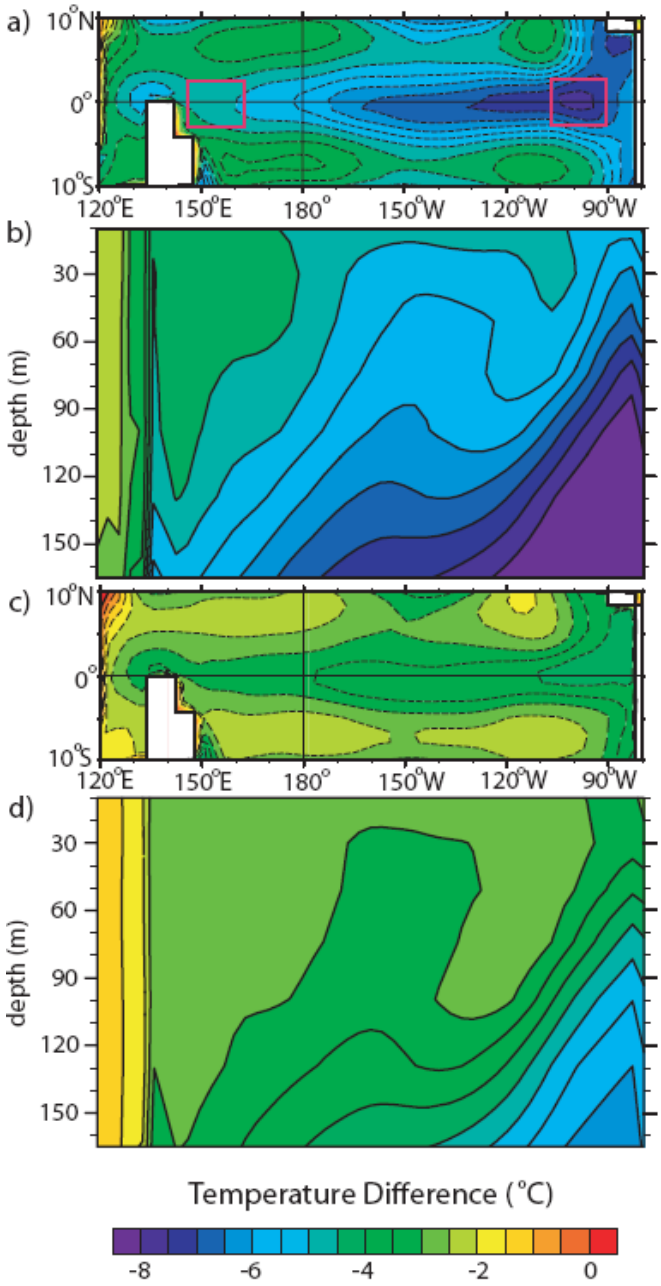


Fig. 3-3. Mean-annual SST differences (°C) in the equatorial Pacific Ocean between (a) the LGM-ICE and NO-ICE experiments, and (c) the MOD-ICE and NO-ICE experiments. In both cases, the presence of high-latitude sea ice causes tropical cooling with greater cooling in the EEP, intensifying the east-west tropical SST gradient. Cross section of mean-annual seawater temperature difference (°C) between (b) the LGM-ICE and NO-ICE experiments, and (d) the MOD-ICE and NO-ICE experiments. Pacific temperature differences are averaged between 10°N-10°S. Note that much colder waters are upwelled in the EEP in the experiments with sea ice. The contour interval is 0.5°C.

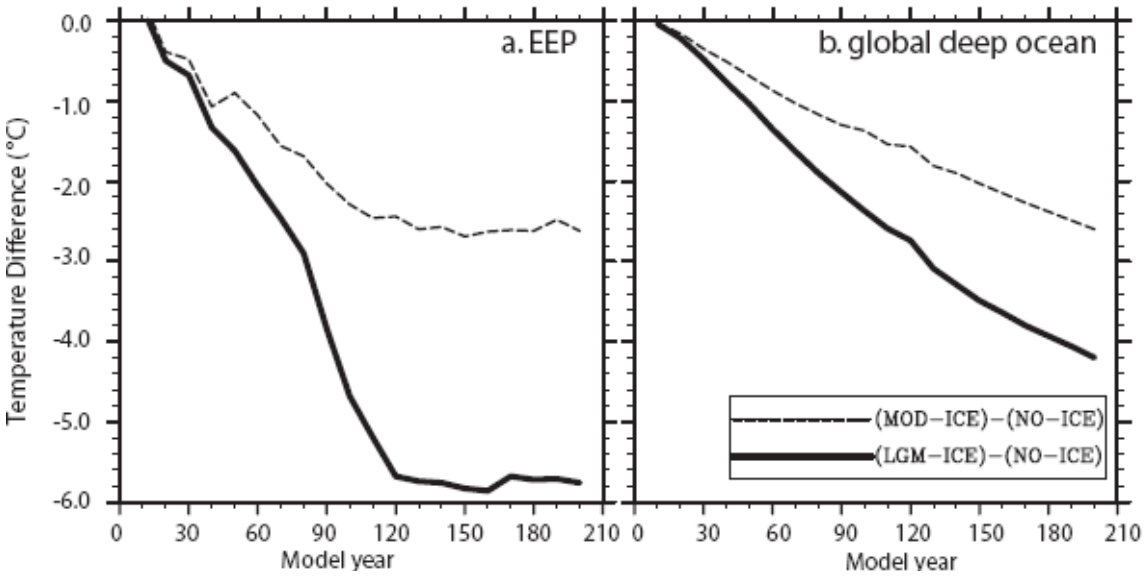


Fig. 3-4. Mean-annual sea water temperature differences (°C) in (a) the eastern equatorial Pacific upper ocean and (b) the global deep-ocean through time (model year). The EEP upper ocean temperature difference were calculated between the sea surface and a depth of 150m for the domain within 3.5°S – 3.5°N and 92°E - 103°E (Fig. 3-3a). The global deep ocean temperature differences were calculated between 200-5000 m.

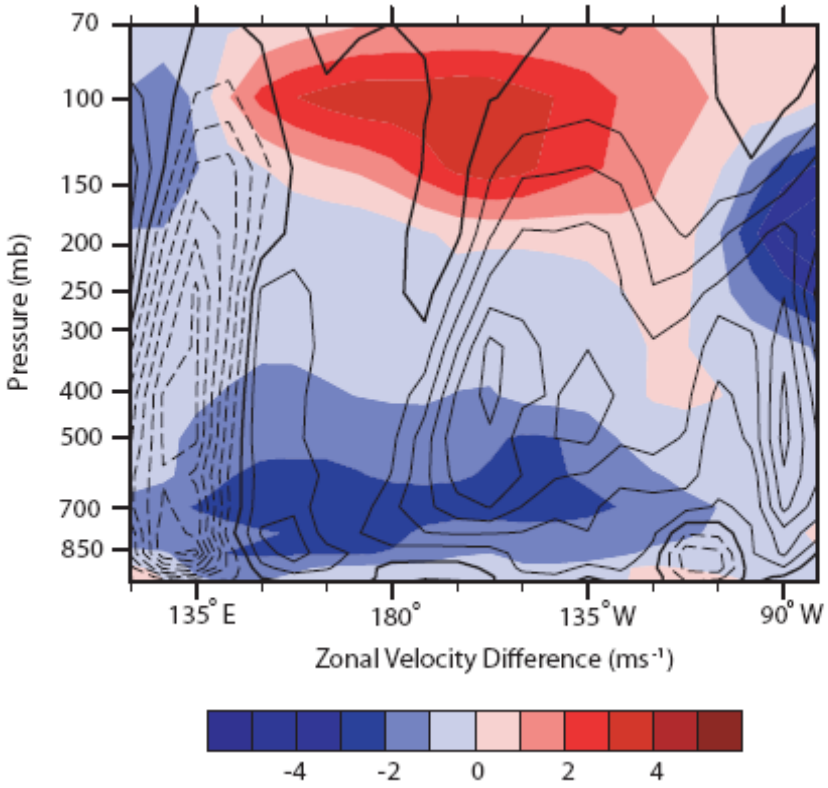


Fig. 3-5. Mean-annual vertical pressure velocity (Pa $s^{-1}$) (contours) and zonal velocity ($ms^{-1}$) (color contours) differences between the LGM-ICE and MOD-ICE experiments. Positive (negative) vertical velocity differences indicate enhanced subsidence (upward motion). Positive (negative) zonal velocity indicates increased eastward (westward) flow. Note from the vertical velocity differences that EEP subsidence and WEP upward motion is enhanced. Also, zonal velocity differences show an increase in the Trades and westward flow aloft.

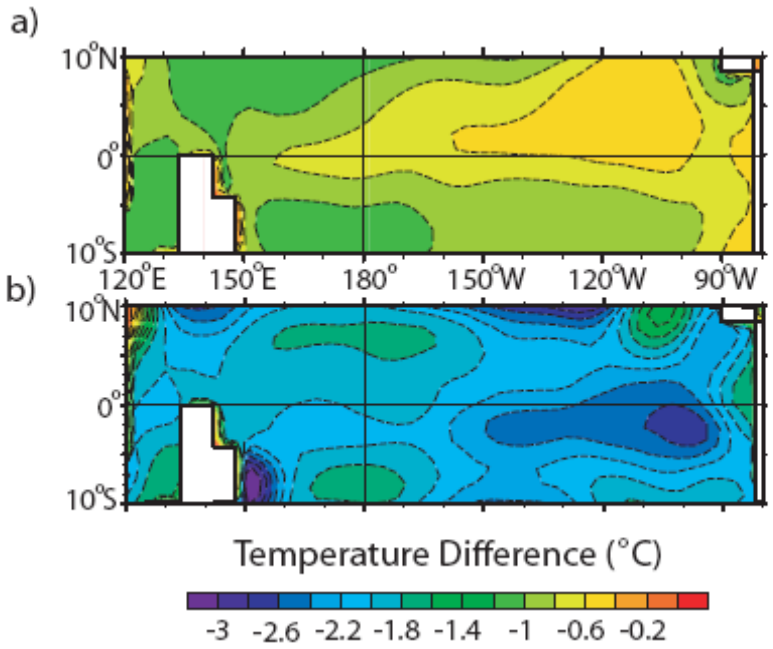


Fig. 3-6. Mean-annual SST differences (°C) in the equatorial Pacific Ocean between (a) the NO-ICE and NO-ICE380 experiments and, (b) the LGM-ICE and LGM-ICE380 experiments. Note that equatorial Pacific SST gradient is strengthened only with the presence of sea ice. The contour interval is 0.2 °C

TABLES: Chapter III

Table 3-1. Mean winter sea-ice extent ($10^7$ $km^2$) in MOD-ICE, LGM-ICE, and LGM-ICE380 experiments. See Section 2.2 for a description of our methodology for specifying the sea ice. (DJF=December, January, February; JJA=June, July, August; N.H.=northern hemisphere; S.H.=southern hemisphere)

| Experiment | $CO_2$ level (ppmv) | Mean winter sea-ice area ($10^7$ $km^2$) | |
|---|---|---|---|
| | | DJF N.H. | JJA S.H. |
| MOD-ICE | 200 | 1.76 | 2.41 |
| LGM-ICE | 200 | 2.09 | 4.68 |
| LGM-ICE380 | 380 | 1.85 | 3.61 |

Table 3-2. Summary of Last Glacial Maximum boundary conditions.

| Parameter | Reference | Description |
|---|---|---|
| Ice sheet extent | Peltier [57] | LGM Antarctic and northern hemisphere continental glacials |
| Topography | Peltier [57] | LGM condition with glacial topography and reduced sea level |
| Vegetation | Peltier [57] | LGM condition |
| $CO_2$ | Petit et al. [46] | 200 ppmv |
| $CH_4$ | Petit et al. [46] | 400 ppbv |
| $N_2O$ | Petit et al. [46] | 275 ppbv |
| Orbital setting | Berger [56] | LGM configuration |

Table 3-3. Net sea surface energy fluxes in the EEP (3.5°S-3.5°N, 92°E-103°E) and the WEP (3.5°S-3.5°N, 150°W-164°W). The domain for the EEP and WEP area averages are illustrated in Fig. 3-2a (black boxes). Positive (negative) fluxes represent gain (loss) from the sea surface (in $Wm^{-2}$). Sea surface energy fluxes are calculated for the LGM-ICE (left column) and NO-ICE experiments (center column), and the difference between the two experiments (left column). (RAD=downward surface radiation; LWV=upward longwave flux; SHF=sensible heat flux; LHF=latent heat flux; OH=ocean heat flux)

| Term | LGM-ICE | | NO-ICE | | (LGM-ICE) - (NO-ICE) | |
|---|---|---|---|---|---|---|
| | WEP | EEP | WEP | EEP | WEP | EEP |
| RAD | 620.5 | 604.6 | 644.5 | 638.0 | -24.0 | -33.4 |
| LWV | -426.5 | -413.6 | -456.3 | -450.4 | 29.8 | 36.8 |
| SHF | -0.2 | -2.2 | -4.8 | -4.3 | 4.6 | 2.1 |
| LHF | -84.0 | -61.2 | -98.7 | -94.7 | 14.7 | 33.5 |
| OH | -109.8 | -127.6 | -84.7 | -88.6 | -25.1 | -39.0 |

## REFERENCES


[1] G.L. Pickard, W.J. Emery, Descriptive Physical Oceanography, fifth ed., Butterworth Heinemann, Burlington,1990.

[2] J. Bjerknes, Atmospheric teleconnections from the equatorial Pacific, Monthly Weather Review 97 (1969) 163-172.

[3] P. Molnar, M.A. Cane, El Niño's tropical climate and teleconnections as a blueprint for pre-Ice Age climates, Paleoceanography 17, doi:10.1029/2001PA000663 (2002).

[4] A.C. Ravelo, D.H. Andreasen, M. Lyle, A.O. Lyle, M.W. Wara, Regional climate shifts caused by gradual global cooling in the Pliocene epoch, Nature 429 (2004) 263-267.

[5] T. de Garidel-Thoron, Y. Rosenthal, F. Bassinot, L. Beaufort, Stable sea surface temperatures in the western Pacific warm pool over the past 1.75 million years, Nature 433 (2005) 294-298.

[6] E.L. McClymont, A. Rosell-Melé, Links between the onset of modern Walker circulation and the mid-Pleistocene climate transition, Geology 33 (2005) 389-392.

[7] M. Medina-Elizalde, D.W. Lea, The Mid-Peistocene Transition in the Tropical Pacific, Science 310 (2005) 1009-1012.

[8] S.G. Philander, A.V. Federov, Role of tropics in changing the response to Milankovitch forcing some three million years ago, Paleoceanography 18,1045 doi:10.1029/2002PA000837 (2003).

[9] G. Bocaletti, R.C. Pakanowski, S.G.H. Philander, A.V. Federov, The thermal structure of the upper ocean, Journal of Physical Oceanography 34 (2004) 888-902.

[10] M. Sarnthein, K. Winn, J-C Duplessy, M.R. Fontugne, Global variations of surface ocean productivity in low and mid latitudes: Influence on $CO_2$ reservoirs of the deep ocean and atmosphere during the last 21,000 years, Paleoceanography 3, (1988) 361-399.

[11] N.G. Pisias, D.K. Rea, Late Pleistocene paleoclimatology of the central equatorial Pacific: Sea surface response to the southeast tradewinds, Paleoceanography 3, (1988) 21-37.

[12] D.K. Rea, The paleoclimate record provided by eolian deposition in the deep sea: the geologic history of wind, Reviews of Geophysics 32 (1994) 159-195.

[13] D.J. Andreasen, A.C. Ravelo, Tropical Pacific ocean thermocline depth reconstructions for the last glacial maximum, Paleoceanography 12, (1997) 395-413.

[14] L. Beaufort, T. de Garidel-Thoron, A.C. Mix, and N.G. Pisias, ENSO-like forcing on oceanic primary production during the Late Pleistocene, Science 293, (2001) 2440-2444.

[15] A.B.G. Bush, S.G.H. Philander, The role of ocean-atmosphere interactions in tropical cooling during the Last Glacial Maximum, Science 279 (1998), 1341-1344.

[16] C.D. Hewitt, R.J. Stouffer, A.J. Broccoli, J.F.B. Mitchell, and P.J. Valdes, The effect of ocean dynamics in a coupled GCM simulation of the Last Glacial Maximum, Climate Dynamics 20 (2003) 203-218.

[17] A. Timmermann, F. Justino, F.-F. Jin, U. Krebs, H. Goosse, Surface temperature control in the North and tropical Pacific during the last glacial maximum, Climate Dynamics 23 (2004) 353-370.

[18] D.W. Lea, D.K. Pak, H.J. Spero, Climate impact of Late Quaternary equatorial Pacific sea surface temperature variations, Science 289 (2000) 1719-1724.

[19] J.M. Whitehead, S. Wotherspoon, S.M. Bohaty, Minimal Antarctic sea ice during the Pliocene, Geology 33 (2005) 137-140.

[20] CLIMAP Project members, The surface of the Ice-Age Earth, Science 191 (1976) 1131-1137.

[21] H.Gildor, E. Tziperman, Sea ice as a glacial cycles' climate switch: role of seasonal and orbital forcing, Paleocenography 15 (2000) 605-515.

[22] E. Tziperman, H. Gildor, On the mid-Pleistocene transition to 100-kyr glacial cycles and the asymmetry between glaciation and deglaciation times, Paleoceanography 18 1001 doi:10.1029/2001PA000627 (2003).

[23] S.-Y. Lee, C.J. Poulsen, Tropical Pacific climate response to obliquity forcing in the Pleistocene, Paleoceanography 20 PA4010 doi:10.1029/2005PA001161 (2005).

[24] R.L. Jacob, Low frequency variability in a simulated atmosphere-ocean system, PhD Thesis University of Wisconsin, (1997) 159 p.

[25] J.T. Kiehl, J.J. Jack, G.B. Bonan, B.A. Boville, D.L. Williamson, and P.J. Rasch, The national center for atmospheric research community climate model: CCM3, Journal of Climate 11, (1998) 1131-1149.

[26] L. Wu, Z. Liu, R.G. Gallimore, R. Jacob, D. Lee, and Y. Zhong, A coupled modeling study of Pacific decadal variability: the Tropical mode and the North Pacific mode, Journal of Climate 15, (2003) 1101-1120.

[27] A.J. Semtner, A model for the thermodynamic growth of sea ice in numerical investigations of climate, Journal of Atmospheric Science 6, (1976) 379-389.

[28] Z. Liu, S. Shin, P. Behling, W. Prell, M. Trend-Staid, S.P. Harrison, J.E. Kutzbach, Dynamical and observational constraints on tropical Pacific sea surface temperature at the last glacial maximum, Geophysical Research Letters 27 (2000) 105-108.

[29] C.J. Poulsen, R.T. Pierrehumbert, R.L. Jacob, Impact of ocean dynamics on the simulation of the Neoproterozoic “snowball Earth”, Geophysical Research Letters 28 (2001) 1575-1578.

[30] S.P. Harrison, J.E. Kutzbach, Z. Liu, P.J. Bartlein, B. Otto-Bliesner, D. Muhs, I.C. Prentice, R.S. Thompson, Mid-Holocene climate of the Americas: a dynamical response to changed seasonality, Climate Dynamics 21 (2003) 663-688.

[31] X. Crosta, J.J. Pichon, Reappraisal of Antarctic seasonal sea-ice at the Last Glacial Maximum, Geophysical Research Letters 25 (1998) 2703-2706.

[32] P. Gloersen, W.J. Campell, D.J. Cavalierei, J.C. Comiso, C.L. Parkinson, H.J. Zwally, Arctic and Antarctic sea ice, 1978-1987: Satellite passive-microwave observations and analysis: Washington D.C., NASA Special Publication 511 (1992) 290.

[33] J.R. Toggweiler, K. Dixon, W.S. Broecker, The Peru upwelling and the ventilation of the South-Pacific thermocline, Journal of Geophysical Research-Oceans 96 (1991) 20467-20497.

[34] S. Harper, Thermocline ventilation and pathways of tropical-subtropical water mass exchange, Tellus 52A (2000) 330-345.

[35] R.T. Pierrehumbert, Climate change and the tropical Pacific, the sleeping dragon wakes, Proc. Nat. Acad. Sci. 97 (2000) 1355-1358.

[36] T.R. Knutson, S. Manabe, Time-Mean Response over the Tropical Pacific to Increased $CO_2$ in a Coupled Ocean-Atmosphere Model, Journal of Climate 8 (1995) 2181-2199.

[37] J.D. Hays, J. Imbrie, N. J. Shackleton, Variation in the Earth's orbit: pacemaker of the ice ages, Science 194 (1976) 1121-1132.

[38] CLIMAP Project members, Seasonal reconstructions of the Earth's surface at the Last Glacial Maximum, Geological Society of America Map and Chart Series (1981) MC-36.

[39] D.W. Cooke, J.D. Hays, Estimates of Antarctic ocean seasonal ice-cover during glacial intervals, Antarctic Geoscience 131 (1982) 1017-1025.

[40] R. Gersonde, A. Abelmann, U. Brathauer, S. Becquey, C. Bianchi, G. Cortese, H. Grobe, G. Kuhn, H.-S. Niebler, M. Segl, R. Sieger, U. Zielinski, D.K. Fütterer, Last glacial sea surface temperatures and sea-ice extent in the Southern Ocean (Atlantic-Indian sector): A multiproxy approach, Paleoceanography 18, 1061 doi:10.1029/2002PA000809 (2003).

[41] A.D. Mahood, J.A. Barron, Late Pliocene diatoms in a diatomite from Prydz Bay, East Antarctica, Micropaleontology 42 (1996) 285-302.

[42] J.M Whitehead, P. Quilty, D.M. Harwood, A. McMinn, Early Pliocene palaeoenvironment of the Sorsdal Formation, Vestfold Hills, based on diatom data, Marine Micropaleontology 41 (2001) 125-152.

[43] J.M. Whitehead, B.C. McKelvey, The stratigraphy of the Pliocene-early Pleistocene Bardin Bluffs Formation, Amery Oasis, northern Prince Charles Mountains, Antarctica, Antarctica Science 13 (2001) 79-86

[44] P.G. Quilty, Coastal East Antarctic Neogene sections and their contribution to the ice sheet evolution debate, American Geophysical Union Antarctic Research Series 60 (1993) 251-264.

[45] M.E. Raymo, B. Grant, M. Horowitz, G.H. Rau, Mid-Pliocene warmth: Stronger greenhouse and stronger conveyor, Marine Micropaleontology 27 (1996) 313-326.

[46] J.R. Petit, J. Jouzel, D. Raynaud, N.I. Barkov, J.M. Barnola, I. Basile, M. Bender, J. Chappellaz, M. Davis, G. Delaygue, M. Delmotte, V.M. Kotlyakov, M. Legrand, V.Y. Lipenkov, C. Lorius, L. Pepin, C. Ritz, E. Saltzmen, M. Stievenard, Climate and atmospheric history of the past 420,000 from the Vostok ice core, Antarctica, Nature 399 (1999) 429-436.

[47] J.R. Marlow, C.B. Lange, G. Wefer, A. Rosell-Mele, Upwelling intensification as part of the Pliocene-Pleistocene climate transition, Science 290 (2000) 2288-2291.

[48] C.H. Lear, H. Elderfield, P.A. Wilson, Cenozoic deep-sea temperatures and global ice volumes from Mg/Ca in benthic foraminiferal calcite, Science 287 (2000) 269-272.

[49] P.J. Bart, J.B. Anderson, Relative temporal stability of the Antarctic ice sheets during the late Neogene based on the minimum frequency of outer shelf grounding events, Earth and Planetary Science Letters 182 (2000) 259-272.

[50] R.P. Scherer, A. Aldahan, S. Tulaczyk, G. Possnert, H. Engelhardt, and B. Kamb, Pleistocene collapse of the West Antarctic Ice Sheet, Science 281 (1998) 82-85.

[51] H. Conway, B.L. Hall, G.H. Denton, A.M. Gades, and E.D. Waddington, Past and future grounding-line retreat of the West Antarctic Ice Sheet, Science 286 (1999) 280-283.

[52] K. Dahl, A. Broccoli, R. Stouffer, Assessing the role of North Atlantic freshwater forcing in millennial scale climate variability: a tropical Atlantic perspective, Climate Dynamics 24 (2005) 325-346.

[53] A.X. Hu, G.A. Meehl, Bering Strait throughtflow and the thermohaline circulation, Geophysical Research Letters 32 L24610 doi:10.1029/2005GL024424 (2005).

[54] S. Rahmstorf, M. Cruicfix, A. Ganopolski, H. Goosse, I. Kamankovich, R. Knutti, G. Lohmann, R. Marsh, L.A. Mysak, Z. Wang, A.J. Weaver, Thermohaline circulation hysteresis, Geophysical Research Letters 32 L23605 doi:10.1029/2005GL023655 (2005).

[55] J.H. Yin and D.S. Battisti, The importance of tropical sea surface temperature patterns in simulations of Last Glacial Maximum climate, Journal of Climate 14, (2001) 565-581.

[56] A.L. Berger, Long term variations of daily insolation and Quaternary climatic changes, Journal of the Atmospheric Sciences 35 (1978) 2362-2367.

[57] W.R. Peltier, Ice age paleotopography, Science 265 (1994) 195-201.

# CHAPTER IV

## Amplification of Obliquity Forcing Through Mean-annual and Seasonal Atmospheric Feedbacks


## ABSTRACT

Pleistocene benthic $\delta^{18}O$ records exhibit strong spectral power at ~41 kyr, indicating that global ice volume has been modulated by Earth's axial tilt. This feature, and weak spectral power in the precessional band, has been attributed to the influence of obliquity on mean-annual and seasonal insolation gradients at high latitudes. In this study, we use a coupled ocean-atmosphere general circulation model to quantify changes in continental snowfall associated with mean-annual and seasonal insolation forcing due to a change in obliquity. Our model results indicate that insolation changes associated with a decrease in obliquity amplify continental snowfall in three ways: (1) Local reductions in air temperature enhance precipitation as snowfall. (2) An intensification of the winter meridional insolation gradient strengthens zonal circulation (i.e the Aleutian low), promoting greater vapor transport from ocean to land and increased snow precipitation. (3) An increase in the summer meridional insolation gradient enhances summer eddy activity, increasing vapor transport to high-latitude regions. In our experiments, a decrease in obliquity leads to an annual snowfall

increase of 25.0 cm; just over one-half of this response (14.1 cm) is attributed to seasonal changes in insolation. Our results indicate that the role of insolation gradients is important in amplifying the relatively weak insolation forcing due to a change in obliquity. Nonetheless, the total snowfall response to obliquity is similar to that due to a shift in Earth's precession, suggesting that obliquity forcing alone can not account for the spectral characteristics of the ice-volume record.

## 1. INTRODUCTION

It has long been known that the Quaternary global ice-volume record, archived in benthic $\delta^{18}O$, varies at orbital frequencies (Hays et al., 1976; Imbrie, 1980, 1985; 1993). One of the most puzzling features of this record is the prominence of variability at the obliquity period (Raymo and Nisancioglu, 2003; Lisiecki and Raymo, 2005; Cortijo et al., 1999; Vimeux et al., 2001). Traditionally, orbital cycles in global ice volume have been linked to summer insolation at 65ºN (Milankovitch, 1948, Berger et al., 1993). However, high-latitude summer insolation is influenced most strongly by Earth's precession with a period of ~23 kyr. It is perplexing then that spectral power in benthic $\delta^{18}O$ is greater in the obliquity band than the precessional band.

To explain this paradox, two types of hypotheses have been proposed, (i) those that are generally consistent with Milankovitch's original hypothesis and (ii) those that call upon internal climate processes to amplify orbital, and specifically obliquity, forcing. In the first category, Huyber (2006) suggests that obliquity

primarily controlled ice volume changes through the integrated summer energy. Precession greatly influences absolute summer insolation but the short duration of the precessional summer leads to lower summer energy than that of obliquity. Raymo et al. (2006) proposes that the change in benthic $\delta^{18}O$ due to the increase in the NH ice volume was offset by the melting of the West Antarctic Ice Sheet due to the out-of-phase precessional insolation forcing between the two hemispheres. The strong 41kyr ice-volume signal was also attributed to the fact that obliquity has nearly twice the period than precession, and therefore twice the time to accumulate snow/ice (Ruddiman, 2003). In the second category, it has been proposed that climate feedbacks, mainly associated with meridional heat and vapor transports (Khodri et al., 2001; Crucifix and Loutre, 2002; Raymo and Nisancioglu, 2003; Loutre et al., 2004; Vettoretti and Peltier, 2004; Kukla and Gavin, 2004; Risebrobakken et al, 2006) and $CO_2$-ice volume interaction (Ruddiman, 2006), may have modulated the insolation forcing, enhancing the ice volume response to orbital forcing.

The focus on climate feedbacks on orbital forcing arises from recognition that obliquity and precession affect Earth's insolation in different ways. In contrast to precession, obliquity alters the mean-annual equator-to-pole insolation gradient. A reduction in axial tilt from the Plio-Pleistocene maximum (24.5°) to minimum (22.2°) reduces annual insolation by up to ~16 $Wm^{-2}$ (~8%) at high latitudes and increases it by ~3 $Wm^{-2}$ (<0.5%) at the equator (calculated from Berger and Loutre, 1991). Loutre et al. (2004) show that mean-annual insolation has significant spectral power at the obliquity band and hypothesize

that paleo-climate records of sea-surface temperature and global ice volume can be interpreted as a response to changes in mean-annual insolation and insolation gradients.

Obliquity also has a substantial influence on seasonal insolation. A reduction in Earth's obliquity from the Plio-Pleistocene maximum to minimum reduces solar heating in summer and fall by up to 48 $Wm^{-2}$ at high latitude and increases it by 7 $Wm^{-2}$ near the equator, enhancing the equator-to-pole insolation gradient by 55 $Wm^{-2}$. A number of studies have suggested that an increase in the seasonal equator-to-pole insolation gradient might have enhanced snowfall over ice sheets due to greater latent heat transport and internal climate processes (e.g. ENSO-like oscillation) (Johnson, 1991; Khodri et al., 2001; Vettoretti and Peltier, 2003, 2004; Kukla and Gavin, 2004). In support of these ideas, Raymo and Nisancioglu (2003) show that summer equator-to-pole insolation gradient is strongly correlated to glacial-interglacial ice-volume variations from 3.0 to 0.8 Ma.

Although insolation gradient changes have been frequently linked to ice volume variability, this mechanism has not been explicitly tested. The goal of this study is to systematically quantify the influence of both mean-annual and seasonal insolation changes resulting from Earth's obliquity on continental snowfall, and to determine the climate mechanisms that respond to these insolation variations. To do this, we have developed coupled ocean-atmosphere model experiments that represent: (1) mean-annual and seasonal insolation changes due to a reduction in Earth's axial tilt; and (2) mean-annual only insolation changes due to a reduction in Earth's axial tilt. To be clear, the

insolation conditions in (2) are idealized and provide a useful sensitivity experiment, but would not have occurred anytime during Earth history. By comparing results from these two scenarios, we distinguish the climate responses to mean-annual and seasonal forcings.

Our model results indicate that seasonal and mean-annual insolation forcings associated with a decrease in axial tilt generate comparable changes in annual continental snowfall. In section 3, we describe the snowfall differences and explain the physical mechanisms that account for these changes. In section 5, we compare the snowfall response due to changes in Earth's obliquity and precession, and discuss the implications of these results for global ice volume variability.

## 2. EXPERIMENTAL DESIGN

This study was completed using the Fast Ocean Atmosphere Model (FOAM) version 1.5, a fully coupled mixed-resolution ocean and atmosphere general circulation model (GCM) (Jacob, 1997). The atmospheric model is a parallelized version of the Community Climate Model 2 (CCM2) with the upgraded radiative and hydrological physics incorporated in CCM3.6 (Kiehl et al., 1996). The atmospheric component of FOAM was run at a spectral resolution of R15 (4.5° x 7.5°) with 18 vertical levels. The oceanic component (OM3) is a z-coordinate ocean model with 128x128 point Mercator grid (1.4° x 2.8°), 24 vertical levels, and an explicit free surface. FOAM was designed for long century-scale integrations and exhibits minimal ocean drift with no flux corrections (Wu et

al., 2003). FOAM's simulation of modern climate shows reasonable agreement with present-day observations and NCAR CSM (Harrison et al., 2003). FOAM has been widely used to study climate change through geological time (e.g. Liu et al., 2000; Poulsen et al., 2001; Lee and Poulsen, 2006).

A change in Earth's axial tilt alters the distribution of insolation, significantly influencing both mean-annual and seasonal meridional insolation gradients. A decrease in Earth's obliquity from 24.5 to 22.2°, for instance, increases the mean-annual equator-to-pole insolation gradient by ~30 $Wm^{-2}$, the summer equator-to-pole insolation gradient by ~55$Wm^{-2}$, and reduces the winter equator-to-pole insolation gradient by ~10$Wm^{-2}$. We have designed two sets of experiments to estimate the climate response to each of these components. The first experimental set is straightforward and includes experiments with high (24.5º; *hobl*) and low (22.2º; *lobl*) axial tilt (Table 1). We have used Earth's maximum and minimum obliquities over the last five million years (Berger and Loutre, 1991). The difference between *hobl* and *lobl* experiments yields the climate response resulting from both mean-annual and seasonal insolation changes, which we refer to as ΔTOTAL.

A second set of experiments was designed to estimate the climate response to just mean-annual insolation forcing caused by a change in axial tilt. In this case, we first computed the difference in mean-annual insolation between our high (*hobl*) and low (*lobl*) obliquity experiments, and a present day experiment. We then added these mean-annual, zonal insolation anomalies to two present-day experiments. These insolation adjustments increase the annual

equator-to-pole insolation in one experiment (*higrad*) and decrease it in the second (*lograd*) (Table 1), but seasonal insolation and insolation gradients are nearly identical between experiments and unchanged from the present day. In the *higrad* case, the high-latitude insolation anomaly is negative. Adding this negative insolation anomaly during polar night causes the incoming insolation to become negative, which is unreasonable and not allowed by the model. To avoid this problem, the minimum insolation was set to 0 $Wm^{-2}$ during polar night. This correction slightly affects the winter season (polar night) insolation and equator-to-pole gradient at 70-90°, but does not have an appreciable influence on the snowfall response (which is mainly centered at 60-65°). The difference between *higrad* and *lograd* experiments yields the climate response to obliquity's mean-annual forcing, which we refer to as ΔMA.

It is important to note that mean annual insolation in the *higrad* and *lograd* experiments are identical to those in the *hobl* and *lobl* experiments, respectively, and that only seasonal insolation differs between these experiments (Fig. 1). As a result, the mean-annual insolation difference in ΔTOTAL and ΔMA are also the same. Thus, to estimate the climate response to seasonal insolation only (ΔSEA), we difference our two sets of experiments. In summary:

ΔTOTAL = *lobl* – *hobl*; represents total insolation difference due to a reduction in axial tilt

ΔMA = *higrad* – *lograd*; represents the mean-annual insolation difference due to a reduction in axial tilt

ΔSEA = ΔTOTAL – ΔMA; represents the seasonal insolation difference due to a reduction in axial tilt.

Because our ultimate objective is to explain variability in the ice-volume record, we focus on the climate response comparison between ΔTOTAL and ΔMA here.

Other than insolation, all model boundary conditions were set to modern values including trace gas concentrations and geography. The experiments were each integrated for 200 years, bringing the surface ocean into quasi-equilibrium. We tested the quasi-equilibrium state by comparing decadal-averaged global and high-latitude (50ºN – 90ºN) sea surface temperatures. The sea-surface temperatures respond to the imposed orbital forcing in the initial 40-110 years. After model year 120, global and high-latitude sea-surface temperature trends are 0.02 and 0.05ºC/decade, respectively. The model results presented here were averaged over the last 50 model years.

## 3. RESULTS

### *3.1. Snowfall response*

To quantify the possible contribution made by mean-annual and seasonal forcing to ice-sheet mass balance, we examine the high-latitude continental snowfall responses to both ΔTOTAL and ΔMA. In ΔTOTAL, zonal continental snowfall increases by 25.0 cm (sum of upper and lower panel of Fig. 2a). In contrast, in ΔMA, annual snowfall increases by 10.9 cm (sum of upper and lower panel of Fig. 2b). The global seasonal snowfall response (ΔSEA shown in Fig.

2c) is 14.1 cm, indicating that mean-annual and seasonal insolation changes contribute almost equally to the total continental snowfall response. In both ΔTOTAL and ΔMA, the snowfall response occurs mainly during the summer half-year. In the northern hemisphere, for example, a reduction in obliquity (ΔTOTAL) enhances summer half-year snowfall by 78% and winter half-year snowfall by 22% (Fig. 2b).

Differences in snowfall are mainly due to differences in non-convective stable snowfall which are closely related to temperature and moisture transport. Non-convective precipitation in FOAM model forms when an air parcel exceeds vapor saturation, and becomes snow when the lowest level of the atmosphere and the land surface are below the freezing point of water (Kiehl et al., 1996). Obliquity alters insolation in two ways that might enhance the total snow formation in ΔTOTAL relative to ΔMA: (1) by decreasing insolation and temperature at high latitudes; and/or (2) by enhancing the seasonal meridional insolation gradient and moisture transport. We examine each of these factors below.

### *3.2. Winter snowfall response*

The winter snowfall response in ΔTOTAL accounts for one-quarter of the total annual snowfall difference. Continental snowfall increases in mid-latitude from 40-60ºN and decreases poleward of 70ºN (Fig 2a). In contrast, snowfall response in ΔMA does not have systematic latitudinal distribution (Fig 2b).

The winter snowfall difference between ΔTOTAL and ΔMA can be attributed to dynamical adjustments to the seasonal insolation forcing. In

ΔTOTAL, mid-latitude insolation is increased (Fig. 1), enhancing meridional insolation (Fig. 1a) and surface temperature gradients at high latitudes (Fig. 3a). The dynamical response to the changes in radiative heating is an intensification of the meridional circulation (i.e. polar cell) and the associated stationary patterns, including the Aleutian low in the North Pacific (Fig. 3b-c). These adjustments lead to anomalous low-level winds (Fig. 3b). Anomalous northwesterly flow intensifies the flow of polar air over the northwestern Pacific Ocean, enhancing the local latent heat flux (Fig. 3d). This anomalous moisture is transported by the prevailing winds from the Pacific to North America, and can be identified as a region of enhanced relative humidity stretching across the mid-latitudes (Fig. 3e). An additional source of moisture can also be identified over central North America (Fig. 3d), and arises from enhanced radiative heating over the continent (Fig. 3a). These two moisture sources provide the vapor that contributes to enhanced snowfall over North America (Fig. 3f).

In the absence of winter heating in ΔMA, there is no significant change in circulation, latent heat flux (not shown), or snowfall (Fig. 2b).

### *3.3. Summer snowfall response*

In summer, snowfall increases due to both (1) a decrease in air temperature due to a reduction in NH insolation and (2) an increase in seasonal poleward moisture transport. Summer (June) insolation at 80°N decreases by 48 and 25 $Wm^{-2}$ in ΔTOTAL and ΔMA, leading to decreases in zonal-averaged SATs by 2.5 and 0.5°C, respectively (Fig. 4a). The larger reduction in SAT in ΔTOTAL is mainly due to a greater summer sea-ice extent in the *lobl* experiment,

which increases local albedo. The reduction in air temperature can partially explain the snowfall responses in ΔTOTAL and ΔMA through (1) the transformation of rainfall to snowfall, and (2) an increase in local atmospheric saturation due to a decrease in saturation vapor pressure following the Clausius-Clapeyron relationship. In support of (2), lower troposphere relative humidity increases over most of the northern mid- and high-latitude regions (Fig. 5a-b).

However, two lines of evidence indicate that the local temperature decrease only partially explains the summer snowfall increase ΔTOTAL. First, the increase in (water-equivalent) snowfall is twice the simulated decrease in rainfall (Fig. 4b-c), indicating the existence of another moisture source. Second, changes in lower troposphere relative humidity do not directly track changes in temperature. In ΔTOTAL, for example, the greatest increases in relative humidity occur in the mid-latitudes near 45°N (Fig. 5a), while insolation and temperature reductions are greatest at high latitudes (Fig. 1a and Fig. 4a).

In addition to absolute insolation, the summer equator-to-pole gradient also changes in ΔTOTAL and ΔMA. A reduction in the axial tilt (ΔTOTAL) enhances the summer equator-to-pole insolation gradient by up to 55 $Wm^{-2}$ (Fig. 1a) leading to a 3°C increase in summer meridional temperature gradient (Fig. 4a). In contrast, in ΔMA, the summer equator-to-pole gradient is enhanced by only 30 $Wm^{-2}$ (Fig. 1b) leading to a 0.5°C increase in summer meridional temperature gradient (Fig. 4a). As a result of differential heating between low- and high-latitudes, the baroclinicity increases in both cases. In the modern climate, transient eddies increase with baroclinicity and are responsible for

transporting heat and moisture between the subtropics and mid-latitude (Trenberth and Stepaniak, 2003). FOAM responds in a similar manner; summer mid-latitude baroclinicity is greater in ΔTOTAL than ΔMA. The high baroclinicity in ΔTOTAL enhances the transient eddy activity leading to a 200% increase in summer poleward transient eddy vapor transport at 40°N and an enhancement in the total vapor transport (Fig. 5c and 5d). The increase in summer vapor transport provides the moisture for additional boreal continental snowfall, and is reflected in changes in relative humidity (Fig. 5a). As noted above, in ΔTOTAL, the largest increases in relative humidity coincide with regions of enhanced baroclinicity at ~40°N. In contrast, in ΔMA, changes in relative humidity grossly track insolation changes, and remain essentially unchanged (small decreases and increases) at ~40°N.

## 4. SUMMARY AND CAVEATS

Changes in obliquity cause variations in both mean-annual and seasonal insolation. We have designed numerical experiments to evaluate the relative importance of these insolation changes on continental snowfall. Our model results indicate that the influence of mean annual and seasonal obliquity forcing are approximately equal and account for 44% and 56% of global annual continental snowfall, respectively. We show in Section 3 that the response to insolation forcing through obliquity is amplified in FOAM through winter ocean-to-land vapor transport and summer transient eddy activity (Fig. 3 and 5). Our results highlight the importance of equator-to-pole insolation gradients, and

demonstrate that changes in insolation gradients can generate dynamical changes that influence moisture transport and continental snowfall. For perspective, it is worth noting that a decrease in axial tilt (ΔTOTAL) led to polar zonal SAT decreases of 6 and 2.5ºC in NH winter and summer, respectively. Yet, the snowfall response was 3.5x greater in the NH summer, mainly due to enhanced moisture transport through transient eddies.

In our experimental design and analysis, we have made several assumptions that warrant discussion. First, throughout our analysis and interpretation, we assume that an increase in snowfall translates into an increase in ice volume. In reality, the ice volume results from a combination of snowfall accumulation and summer ablation. Ablation is often quantified using the positive-degree-day index (PDD), an estimate of melt based on the number of days with near-surface air temperature above the melting point and a local melt factor. The change in PDD will be much larger in ΔTOTAL since the change in summer insolation (Fig. 1) and continental surface temperature (Fig. 4a) is much larger. As a result, the inferred ice-volume changes between our ΔTOTAL and ΔMA cases are probably too small. We have not calculated the absolute change in PDD here because the values are sensitive to the mean high-latitude climate, which is strongly influenced by our choice of (modern) trace gas values, and to local melt factors that are not well constrained. In the absence of a dynamic ice-sheet component in our model, it is not possible to calculate the exact ice-volume change that would result from the changes in insolation forcing prescribed here;

consequently, our results may be better viewed as continental ice accumulation potential.

In addition, since we simulate the climate response to obliquity insolation changes under present-day boundary conditions, the snowfall response described here does not account for Pleistocene boundary conditions (e.g $CO_2$, $CH_4$, and land surface types), which varied between glacial and interglacial. In a cold climate with low $pCO_2$, it is unclear if the snowfall response to insolation forcing would increase. A decrease in mid-latitude surface temperature would likely cause an increase in summer snowfall and an enhanced moisture transport due to a stronger meridional thermal gradient. However, a decrease in surface temperature might also reduce specific humidity due to a decrease in saturation vapor pressure in a cold climate. Finally, the FOAM experiments were integrated for 200 years; the surface ocean has reached a quasi-steady state but the deep ocean is still equilibrating. Because we focus our analysis on surface and tropospheric condition, the deep ocean condition should have little effect on surface temperature and continental snowfall.

## 5. IMPLICATION FOR THE ICE VOLUME RECORD

Changes in annual and seasonal meridional insolation gradients and associated atmospheric and vapor responses have been hypothesized to cause ice-volume variability (e.g. Khodri et al., 2001; Crucifix and Loutre, 2002; Raymo and Nisancioglu, 2003; Loutre et al., 2004; Vettoretti and Peltier, 2004; Kukla and Gavin, 2004; Risebrobakken et al., 2006). However, this hypothesis has not been

explicitly tested in a systematic way before. Our results demonstrate that changes in mean annual and seasonal insolation resulting from a decrease in axial tilt have comparable influences on continental snowfall, and presumably global ice volume. Changes in mean-annual insolation influence snowfall mainly through a local (high latitude) decrease in temperature and increase in vapor saturation. In contrast, seasonal changes in insolation drive enhanced circulation and vapor transport, increasing snowfall.

To directly compare the snowfall response to obliquity and precession, we have completed two additional precessional sensitivity experiments. In these experiments, northern hemisphere summer is positioned at aphelion (cold NH summer orbit) and perihelion (warm NH summer orbit), respectively, in an eccentric orbit (eccentricity = 0.056, which represents the maximum value over the last 3 Ma (Berger et al., 1993)). Precessional oscillation from warm to cold NH summer orbits increases the continental snowfall in the NH by 14.3 cm (Fig. 6). Snowfall variations over a processional oscillation result from both thermal and dynamical effects. During the summer half-year, the thermal effect dominates. Snowfall increases (decreases) when NH (SH) summer insolation and surface temperature decrease (increase) (Fig. 6). The dynamical effect is most apparent during winter when an increase in meridional thermal gradient enhances storm activity, leading to an increase in high-latitude snowfall (Lee, unpublished data). The simulated snowfall response in FOAM to precession is largely similar to climate sensitivities described in Jackson and Broccoli (2003) using a AGCM coupled to a slab ocean model.

The precessional shift in the orbital position of NH summer leads to a NH continental snowfall response that is 85% of that calculated due to a change in axial tilt (ΔTOTAL). In comparison to a change in obliquity, a change in precession does not influence mean-annual insolation and has only a small influence on summer insolation gradients. However, it has a very large effect (up to ~70 $Wm^{-2}$) on absolute summer insolation, which contributes to the large snowfall response. This comparison has important implications for the insolation gradient hypothesis. While mean-annual and summer meridional insolation gradient changes associated with a decrease in obliquity may amplify relatively weak insolation forcing, their influence may not be sufficiently large to account for the spectral nature of the ice volume record.

In sum, this contribution systematically identifies climate mechanisms that amplify the climate response to obliquity forcing, and demonstrates that both mean-annual and seasonal changes in the meridional distribution of insolation play important roles in amplifying this forcing. Nonetheless, our model results suggest that these climate feedbacks can not fully explain the large spectral power of the 41-kyr cycles in the ice-volume record, and the 41-kyr paradox remains just that.

ACKNOWLEDGEMENTS

This research was supported by National Science Foundation grant ATM-0432503 to C.J. Poulsen, and the University of Michigan Barbour Fellowship and Scott Turner Research Fund to S.-Y. Lee.

FIGURES: Chapter IV

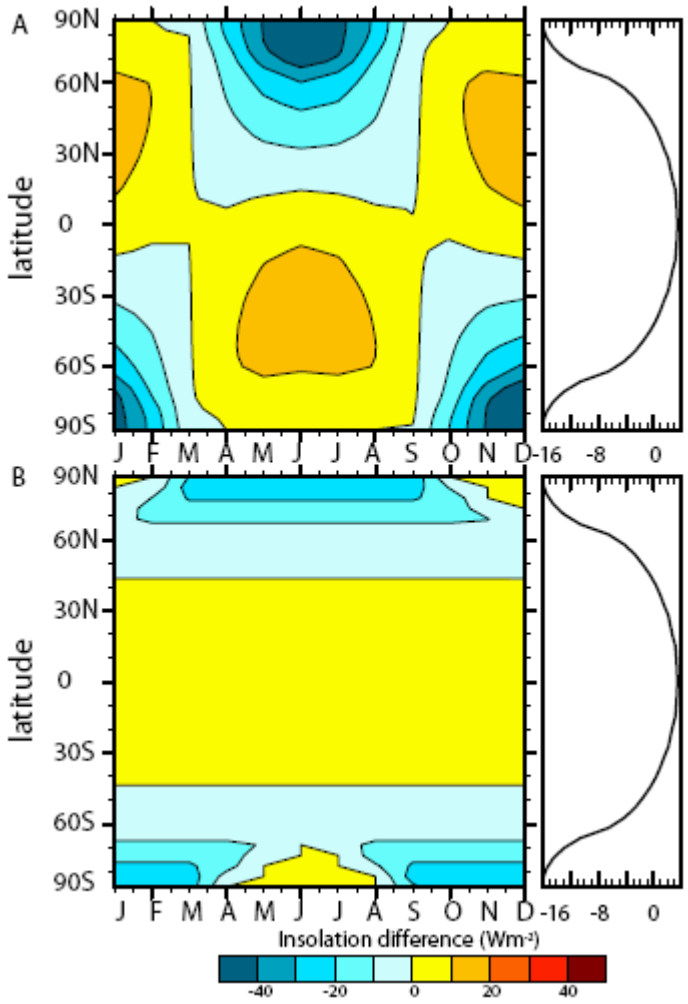


Figure 4-1. Mean monthly and annual (right column) insolation difference ($Wm^{-2}$) between ΔTOTAL (A. *lobl* – *hobl*) and ΔMA (B. *higrad* – *lograd*) experiments. The insolation difference in ΔMA yields the climate response to obliquity's mean-annual forcing. Contour interval is 10 $Wm^{-2}$. Although seasonal insolation differs between these experiments sets, mean-annual insolation is identical between ΔTOTAL and ΔMA.

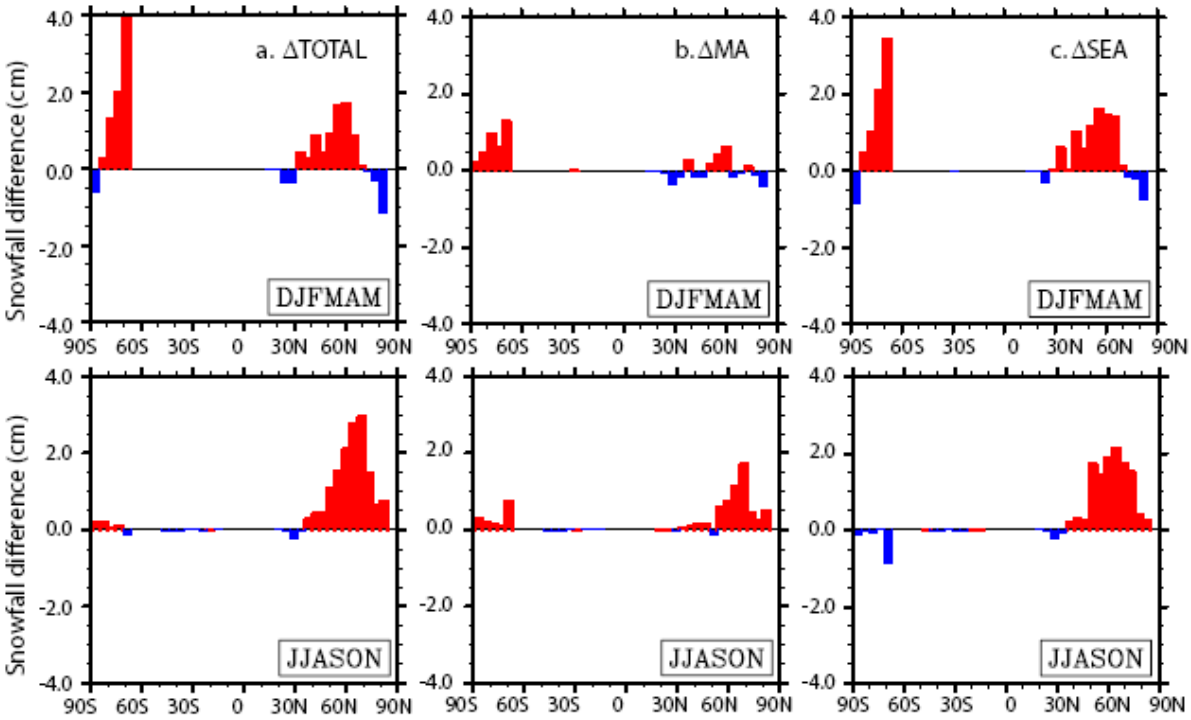


Figure 4-2. Continental snowfall response to orbital forcing. Zonally averaged half-year (December through May and June through November) differences in total snowfall (cm): (a) ΔTOTAL (*lobl-hobl*), (b) ΔMA (*higrad-lograd*), and (c) ΔSEA (ΔTOTAL - ΔMA).

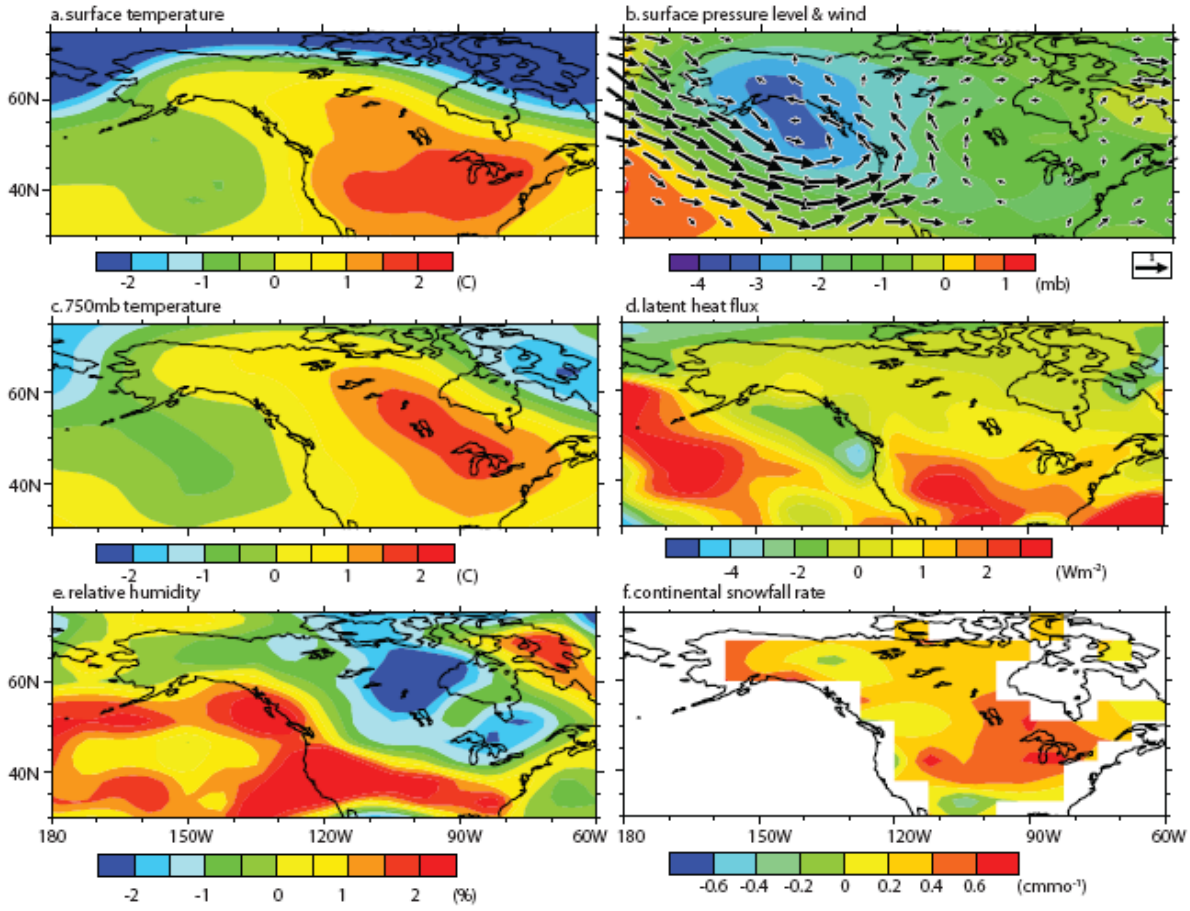


Figure 4-3. Differences in January-February-March atmospheric conditions over North America due to a decrease in obliquity (ΔTOTAL). (a) surface air temperature (in degree Celsius), (b) lower tropospheric wind (vectors; averaged from surface to 750 mb) and surface level pressure (contour; in mb), (c) lower tropospheric (750 mb) air temperature (in degrees Celsius), (d) latent heat flux (in $Wm^{-2}$), (e) relative humidity (in %), and (f) continental snowfall rate (in cm $month^{-1}$).

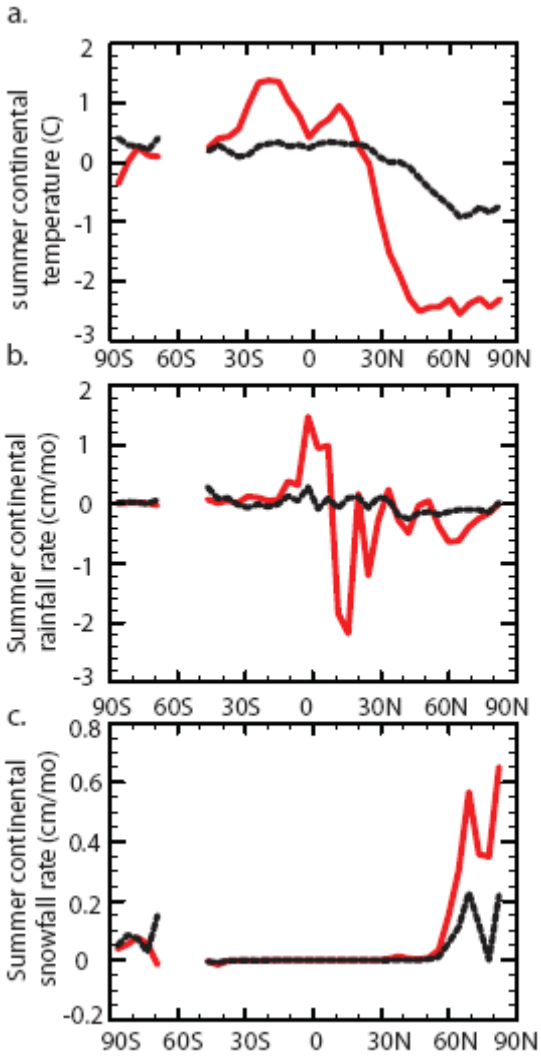


Figure 4-4. Differences in zonally-averaged June-July-August (a) continental surface air temperature (in degree Celsius), (b) continental rainfall rate (in cm month$^{-1}$), and (c) continental snowfall rate (in cm day$^{-1}$) between experimental sets. Results from ΔTOTAL and ΔMA experiments are shown in red-solid and black-dash line, respectively.

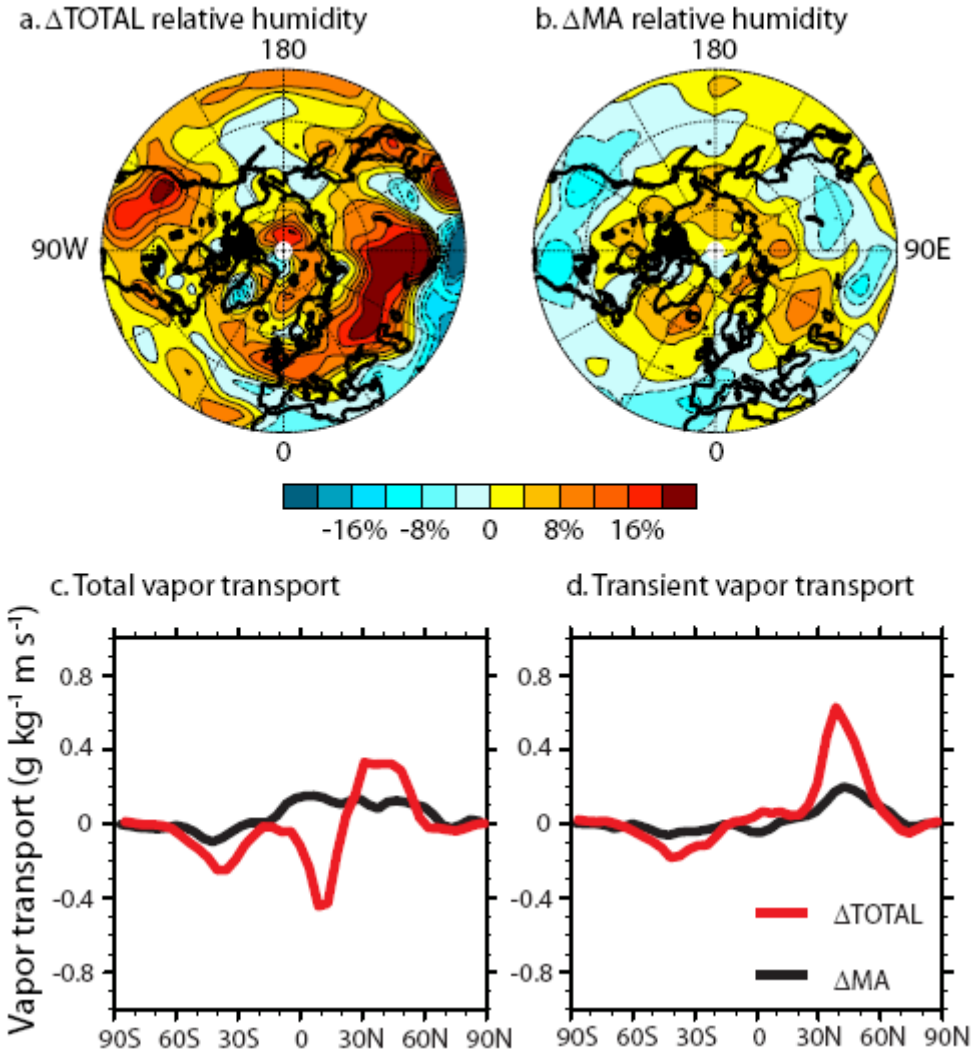


Figure 4-5. Response of vapor transports and tropospheric relative humidity to orbital changes. (a-b) Difference maps in lower tropospheric (750 mb) June-July-August relative humidity (%) as a result of a decrease in air temperature and an increase in vapor tranport in (a) ΔTOTAL and (b) ΔMA. The polar projection map begins at 30ºN and the contour interval is 4%. (c-d) Difference in zonal-average June-July-August atmospheric meridional vapor transport (g $kg^{-1}$ m $s^{-1}$) by (A) all processes (mean meridional + stationary eddies + transient eddies) and through (B) transient eddies between experimental sets. Results from ΔTOTAL and ΔMA experiments are shown in red and black line, respectively. Positive values represent an increase in the northward vapor transport or a reduction in the southward vapor transport.

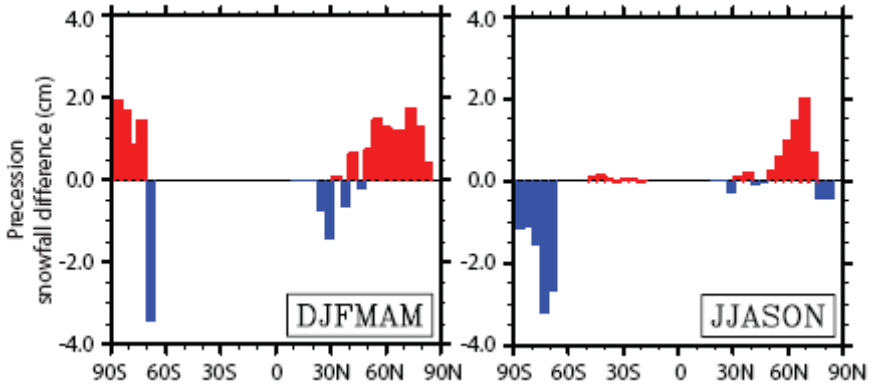


Figure 4-6. Zonally averaged half-year continental snowfall response to precessional forcing. Snowfall differences is shown in cm.

TABLE: Chapter IV

Table 4-1. Numerical Climate Experiments

| **Experiments** | **Obliquity** | **Anomaly** | **Note** |
|---|---|---|---|
| *lobl* | 22.2 | | ΔTOTAL = *lobl* – *hobl* Total changes due to obliquity's mean-annual & seasonal forcing. |
| *hobl* | 24.5 | | |
| *higrad* | 23.4 | Anomaly increasing the mean-annual insolation gradient so that it is the same in *lobl* | ΔMA = *higrad- lograd* Changes due to obliquity's mean-annual forcing. ΔSEA = ΔTOTAL – ΔMA Changes due to obliquity's seasonal forcing |
| *lograd* | 23.4 | Anomaly increasing the mean-annual insolation gradient so that it is the same in *hobl* | |

# REFERENCES

Berger, A. and Loutre, M.F.: Insolation Values for the Climate of the Last 10000000 Years. Quaternary Science Reviews, 10, 297-317, 1991.

Berger, A., Loutre, M.F. and Tricot, C.: Insolation and Earths Orbital Periods. Journal of Geophysical Research-Atmospheres, 98, 10341-10362, 1993.

Cortijo, E., Lehman, S., Keigwin, L., Chapman, M., Paillard, D. and Labeyrie, L.: Changes in meridional temperature and salinity gradients in the North Atlantic Ocean (30 degrees-72 degrees N) during the last interglacial period. Paleoceanography, 14, 23-33, 1999.

Crucifix, M. and Loutre, M.F.: Transient simulations over the last interglacial period (126-115 kyr BP): feedback and forcing analysis. Climate Dynamics, 19, 417-433, 2002.

Harrison, S.P., Kutzbach, J.E., Liu, Z., Bartlein, P.J., Otto-Bliesner, B., Muhs, D., Prentice, I.C. and Thompson, R.S.: Mid-Holocene climates of the Americas: a dynamical response to changed seasonality. Climate Dynamics, 20, 663-688, 2003.

Hays, J.D., Imbrie, J. and Shackleton, N.J.: Variations in Earths Orbit - Pacemaker of Ice Ages. Science, 194, 1121-1132, 1976.

Huybers, P.: Early Pleistocene glacial cycles and the integrated summer insolation forcing. Science, 313, 508-511, 2006.

Imbrie, J.: A Theoretical Framework for the Pleistocene Ice Ages. Journal of the Geological Society, 142, 417-432, 1985.

Imbrie, J. and Imbrie, J.Z.: Modeling the Climatic Response to Orbital Variations. Science, 207, 943-953, 1980.

Imbrie, J., Mix, A.C. and Martinson, D.G.: Milankovitch Theory Viewed from Devils Hole. Nature, 363, 531-533, 1993.

Jackson, C. S., and A. J. Broccoli: Orbital forcing of Arctic climate: mechanisms of climate response and implications for continental glaciation, Climate Dynamics, 21, 539-557, 2003.

Jacob, R., 1997. Low frequency variability in a simulated atmosphere ocean system, University of Wis.-Madison, Madison, 159 pp.

Johnson, R.G.: Major Northern-Hemisphere Deglaciation Caused by a Moisture Deficit 140-Ka. Geology, 19, 686-689, 1991.

Khodri, M., Leclainche, Y., Ramstein, G., Braconnot, P., Marti, O. and Cortijo, E.: Simulating the amplification of orbital forcing by ocean feedbacks in the last glaciation. Nature, 410, 570-574, 2001.

Kiehl, J.T., Hack, J.J., Bonan, G.B., Boville, B.A., Briegleb B.P., Williamson, D.L., Rasch, P.J., 1996. Description fo the NCAR Community Climate Model (CCM3) pp. 152.

Kukla, G. and Gavin, J.: Milankovitch climate reinforcements. Global and Planetary Change, 40, 27-48, 2004.

Lee, S.Y. and Poulsen, C.J.: Sea ice control of Plio-Pleistocene tropical Pacific climate evolution. Earth and Planetary Science Letters, 248, 253-262, 2006.

Lisiecki, L.E. and Raymo, M.E.: A Pliocene-Pleistocene stack of 57 globally distributed benthic delta O-18 records. Paleoceanography, 20, 2005.

Liu, Z.Y., Kutzbach, J. and Wu, L.X.: Modeling climate shift of El Nino variability in the Holocene. Geophysical Research Letters, 27, 2265-2268, 2000.

Loutre, M.F., Paillard, D., Vimeux, F. and Cortijo, E.: Does mean annual insolation have the potential to change the climate? Earth and Planetary Science Letters, 221, 1-14, 2004.

Milankovitch, M.: Ausbau Und Gegenwartiger Stand Der Astronomischen Theorie Der Erdgeschichtlichen Klimate. Experientia, 4, 413-418, 1948.

Poulsen, C.J., Pierrehumbert, R.T. and Jacob, R.L.: Impact of ocean dynamics on the simulation of the Neoproterozoic "snowball Earth". Geophysical Research Letters, 28, 1575-1578, 2001.

Raymo, M.E., Lisiecki, L.E. and Nisancioglu, K.H.: Plio-pleistocene ice volume, Antarctic climate, and the global delta O-18 record. Science, 313, 492-495, 2006.

Raymo, M.E. and Nisancioglu, K.: The 41 kyr world: Milankovitch's other unsolved mystery. Paleoceanography, 182003.

Risebrobakken, B., Balbon, E., Dokken, T., Jansen, E., Kissel, C., Labeyrie, L., Richter, T. and Senneset, L.: The penultimate deglaciation: High-resolution paleoceanographic evidence from a north-south transect along the eastern Nordic Seas. Earth and Planetary Science Letters, 241, 505-516, 2006.

Ruddiman, W.F.: Orbital insolation, ice volume, and greenhouse gases. Quaternary Science Reviews, 22, 1597-1629, 2003.

Ruddiman, W. F.: Ice-driven $CO_2$ feedback on ice volume, Climate of the Past, 2, 43-55, 2006.

Trenberth, K.E. and Stepaniak, D.P.: Seamless poleward atmospheric energy transports and implications for the Hadley circulation. Journal of Climate, 16, 3706-3722, 2003.

Vettoretti, G. and Peltier, W.R.: Post-Eemian glacial inception. Part II: Elements of a cryospheric moisture pump. Journal of Climate, 16, 912-927, 2003.

Vettoretti, G. and Peltier, W.R.: Sensitivity of glacial inception to orbital and greenhouse gas climate forcing. Quaternary Science Reviews, 23, 499-519, 2004.

Vimeux, F., Masson, V., Delaygue, G., Jouzel, J., Petit, J.R. and Stievenard, M.: A 420,000 year deuterium excess record from East Antarctica: Information on past changes in the origin of precipitation at Vostok. Journal of Geophysical Research-Atmospheres, 106, 31863-31873, 2001.

Wu, L., Liu, Z., Gallimore, R., Jacob, R., Lee, D. and Zhong, Y.: Pacific decadalvariability: The tropical Pacific mode and the North Pacific mode. Journal of Climate, 16, 1101-1120, 2003.

# CHAPTER V

## Obliquity and precessional forcing of continental snow fall and melt


## ABSTRACT

Milankovitch theory posits that Earth's orbital cycles were the primary forcing of Pleistocene ice-age cycles through their strong influence on summer insolation at high latitudes. However, the early Pleistocene global ice volume varied mainly at the obliquity period with weak variability at the precessional period suggesting that traditional Milankovitch theory is not sufficient to explain the ice-age cycles. Here we describe the results from a series of coupled ocean-atmosphere general circulation model experiments, using the Fast Ocean Atmosphere Model, that systematically investigate the influence of precession and obliquity on continental snow fall and potential ablation.

Our model results identify three factors that would tend to magnify the influence of obliquity forcing on the global ice volume: First, high-latitude snowfall variability is dominated by changes in Earth's axial tilt. Second, hemispheric changes in net snowfall due to Earth's precession are out-of-phase, and largely cancel to produce a very small global snowfall change. Third, net snow accumulation variability over Antarctica responds greatly to changes in obliquity through its control on snowfall and melt. We discuss the implications of these

factors for existing hypotheses that account for the variability in the ice-volume record.

## 1. INTRODUCTION

The waxing and waning of Northern Hemisphere (NH) ice sheets has been the major source of climate variability during the past 2.7 Myrs. The benthic $\delta^{18}O$ record, a proxy for global ice volume, contains significant variance at orbital periods of ~100, ~41, and ~21 kyrs, implicating Earth's orbital fluctuations in glacial-interglacial climate change (Milankovitch, 1941). Both the 21 and 41 kyrs fluctuations in ice volume have been traditionally characterized as linear responses to orbital variations of precession (with cycles of ~21 kyr) and obliquity (with cycles of ~41 kyr), while the 100 kyr cycles have been commonly attributed to non-linear responses between the ice sheet and climate feedback that were phase locked by eccentricity (Imbrie et al., 1992; Imbrie et al., 1993).

Milankovitch's theory of the ice ages has been widely accepted to explain the orbital control on advances and retreats of the NH ice sheets. According to the theory, changes in high-latitude summer insolation are the main control on ice sheet expansion and contraction. If snow and ice survive the summer, the ice sheet will grow causing ice volume to increase; otherwise, ablation will dominate and the ice sheet will shrink. Because precession and obliquity fluctuations both strongly influence high-latitude (65°N) summer insolation (Fig. 5-1), Milankovitch theory would predict global ice volume to vary with both orbital cycles. Orbital setting favors the growth of ice sheets during times with low obliquity and cold summer precession condition. However, for most of the Pleistocene (until ~0.8

Ma) global ice volume varied predominantly at the obliquity period with only feeble variance in the precession band (Raymo et al., 1994; Raymo and Nisancioglu, 2003; Lisiecki and Raymo, 2005). Even when the ~100 kyr oscillation dominated the benthic $\delta^{18}O$ record during the late Pleistocene, variance at the obliquity period was nearly three times as great as that at the precessional period (Raymo et al., 2006).

This discrepancy between Milankovitch theory and the global ice volume record has been coined the "41 kyr problem" (Raymo and Nisancioglu, 2003). The prevalence of the obliquity signal in Pleistocene global ice volume record has been attributed to factors including the state of the tropical Pacific Ocean (Philander and Federov, 2003; Ravelo et al., 2004), the size of NH ice sheets (Clark and Pollard, 1998; Berger et al., 1999; Huyber and Wunsch, 2005), summer and mean annual equator-to-pole insolation gradients (Paillard, 2001; Crucifix and Loutre, 2002; Raymo and Nisancioglu, 2003; Loutre et al., 2004; Kukla and Gavin, 2004; Vettoretti and Peltier, 2004), and the strength and duration of high latitudes summer insolation (Huyber, 2006). The "41 kyr problem" can also be viewed as a "21 kyr problem" in which the precessional signal is unexpectedly weak in the global ice volume record. The "21 kyr problem" may have arisen because precessional insolation changes are out-of-phase between the hemispheres; ice accumulation in the NH was partly offset by melting in the SH leaving only a small signal in the global ice volume record (Raymo et al., 2006).

The goal of this study is to examine climate responses to orbital forcing that might reconcile the apparent contradiction between the global ice volume record and Milankovitch theory. Our approach then is to systematically quantify the continental snowfall response to obliquity and precession variations using a coupled ocean-atmosphere general circulation model. In Section 2, we describe our model and experimental design. In Section 3, we present the results of continental snowfall differences associated with the obliquity and precessional forcings. Section 4 shows the cumulative positive degree day melting that influences snow preservation and ice sheet growth. In Section 5, we discuss the implications of our results to ice ages theory with previous hypotheses and our model limitations. In our final analysis, we suggest that obliquity signal is amplified in the ice volume record through enhanced meridional insolation gradient, hemispheric asymmetry of snowfall response to orbital forcing, and snow accumulation over Antarctica.

## 2. MODEL DESCRIPTION & EXPERIMENTAL DESIGN

### *2.1. FOAM*

This study was completed using the Fast Ocean Atmosphere Model (FOAM) version 1.5, a fully coupled mixed-resolution ocean and atmosphere general circulation model (Jacob, 1997). The atmospheric model is a parallelized version of the Community Climate Model 2 (CCM2) with the upgraded radiative and hydrological physics incorporated in CCM3.6 (Kiehl, 1996). The atmospheric component of FOAM was run at a spectral resolution of R15 (4.5° × 7.5°) with 18

vertical levels. The oceanic component (OM3) is a z-coordinate ocean model with 128×128 point Mercator grid (1.4° × 2.8°), 24 vertical levels, and an explicit free surface. FOAM was designed for long century-scale integrations and exhibits minimal ocean drift with no flux corrections (Wu et al., 2003). FOAM's simulation of modern climate shows reasonable agreement with present-day observations. FOAM has been widely used to study climate change through geological time (e.g. Liu et al., 2000; Poulsen et al., 2001; Harrison et al., 2003; Lee and Poulsen, 2005).

### *2.2. Experimental design*

In this study, we use FOAM to estimate the continental snowfall and temperature responses to obliquity and precession variations in the high latitudes. Two series of experiments were completed to independently evaluate the influence of obliquity and precessional cycles on climate (Table 5-1). In each series, we systematically varied the orbital parameter over the full range of orbital variations for the last 5 million years (Berger, 1991). In the first series, the precessional index (a combination of precession and eccentricity) was varied in six increments from its Plio-Pleistocene minima (extreme warm NH summer) to its maxima (extreme cold NH summer). In the second series, the axial tilt was varied in six steps from its Pleistocene maxima (24.5°) to its minima (22.2°). Figure 5-2 shows the monthly-average zonal insolation differences between the minimum and maximum cases in each series of experiments.

All other boundary conditions were prescribed at present-day values (Table 5-1). Each experiment was run for 200 years. After several decades, the

upper ocean temperatures have reached quasi-equilibrium and the global averaged sea surface temperature show drifts within 0.1 ºC. The deep ocean is still equilibrating in these experiments, but this has little effect on sea-surface temperatures and continental snowfall. The results described below represent the climatology of the final 50 years of these experiments.

Ultimately our goal is to understand how orbital cyclicity is expressed in the global ice volume record, and whether the mechanism and the magnitude of the expression differ for obliquity and precessional cycles. Because a single orbital cycle is bounded by some minimum and maximum orbital condition (Table 5-1), we quantify (in Sections 3 and 4) the snow accumulation response over a cycle by analyzing the difference between experiments with maximum and minimum orbital conditions. For economy of presentation, we focus our discussion on the experimental pairs with the largest orbital change, i.e., hobl-A and lobl-A; nhcs-high and nhhs-high, and refer to these cases as Δobl-max and Δprec-max. Because the climate response to obliquity and precession is linear (as described in Section 3.1), the differences between the other experimental pairs with smaller orbital changes (e.g. hobl-B,C, and lobl-B,C, nhcs-med,low, and nhhs-med,low) are similar but reduced in magnitude.

## 3. SNOW ACCUMULATION

### *3.1. Orbital cycles and snowfall distribution*

The accumulation of continental snowfall in FOAM is directly controlled by orbital conditions. In the model, a decrease in axial tilt increases continental

snowfall in both the NH and the SH (Fig. 5-3; Table 5-2); precessional oscillations from warm to cold NH summer increase snowfall mainly in the NH (Fig. 5-4; Table 5-2). In both obliquity and precession experiments, a majority of the NH snowfall response occurs over the former locations of the Laurentide and Fennoscandian ice sheets, indicating a meaningful comparison between our model results and the ice volume record.

Our model results suggest that the NH high-latitude snowfall response to obliquity or precession variations in the model is linear (Fig. 5-5). Moreover, the rate of snowfall change due to variations in obliquity and precession are very similar (Fig. 5-5). The annual continental snowfall responses in the NH are 17.0 cm $yr^{-1}$ and 14.3 cm $yr^{-1}$ in Δobl-max and Δprec-max, respectively (Table 5-2). At 65°N, the critical latitude in traditional Milankovitch theory, continental snowfall increase by 1.3 cm $yr^{-1}$ (Δobl-max) and 1.5 cm $yr^{-1}$ (Δprec-max). Although the annual snowfall response is similar, the seasonal changes in snowfall are quite different between the two orbital forcings. A reduction in obliquity leads to enhanced high-latitude snowfall mainly during the boreal summer and fall seasons (compare NH snowfall in upper and lower panels of Fig. 5-3). In contrast, a shift from warm to cold NH summer orbits increases snowfall more effectively in winter and spring seasons (Fig. 5-4).

SH snowfall responds very differently to obliquity and precessional variations. In the Δobl-max case, a decrease in tilt increases snowfall accumulation in austral summer and fall with little changes in winter and spring, leading to an 8.1 cm increase in net annual snowfall (Fig. 5-3, Table 5-2). In

contrast, in the Δprec-max case, the precessional shift greatly reduces snowfall south of 70°S during austral winter and spring with minor increases in summer and fall, leading to a 6.2 cm decrease in net annual snowfall over Antarctica (Fig. 5-4, Table 5-2).

On a global basis, continental snowfall is ~3x more sensitive to variations in obliquity than to precession. In the Δobl-max case, global continental snowfall increases by 25.1 cm as a result of positive snow accumulation in both the NH and the SH. In the Δprec-max case, due to the negative snow accumulation in the SH, global continental snow increases by only 8.1 cm (Table 5-2). The snowfall differences to orbital forcing are closely tied to the atmospheric vapor and heat transport forced by seasonal insolation variations (see Section 3.2 and 3.3).

### *3.2. Absolute insolation forcing and surface temperature*

Our results indicate that insolation influences continental snowfall through its control on surface air temperature, which increases relative humidity and promotes snowfall in high latitudes. In the Δprec-max case, changes in orbital configuration reduce summer insolation by up to 90$Wm^{-2}$ in the NH high latitudes (Fig. 5-2). Reduced seasonal insolation subsequently cools the surface air temperature, leading to an increase in low-level air relative humidity. The increase in NH high latitude relative humidity can be linked exclusively to temperature since the specific humidity decreases in mid- and high-latitude regions over North America and Eurasia (Fig. 5-8c). Increasing low level saturation in turn leads to greater snowfall response (Fig. 5-4d). The snowfall

response in the Δprec-max demonstrates this effect: one-third of the annual snowfall difference occurs during summer and fall seasons (Fig. 5-4).

The decrease in high-latitude summer insolation due to precessional changes is greater than that of obliquity changes at the latitudes of peak snowfall response (60-70ºN). This implies that the absolute insolation forcing and the resulting reduction in atmospheric temperature is not the main reason for the large difference in the snow response. In both Δobl-max and Δprec-max, large snowfall differences are associated with differences in non-convective stable snowfall. Non-convective precipitation in the model forms when an air parcel exceeds vapor saturation, and becomes snow when the lowest level of the atmosphere and the land-surface are below the freezing temperature. Prescribed orbital changes alter insolation in two ways that might influence non-convective snow formation: (1) by reducing insolation at high latitudes; and (2) by increasing the meridional insolation gradient. The decreases in high-latitude summer insolation are $-40 Wm^{-2}$ and $-80 Wm^{-2}$ for the Δobl-max and Δprec-max, respectively (Fig. 5-2). However, the Δobl-max case has much greater snowfall response (13.3 cm) during the summer half-year than that in the Δprec-max case (5.0 cm). This result indicates that the cold surface temperature resulting from orbital forcing cannot be the primary reason for the difference in modeled snowfall. If atmospheric cooling was primarily responsible for increasing snowfall, the precessional experiments would have the larger response.

### *3.3. Meridional insolation gradient and moisture transport*

In the modern climate, transient eddies are responsible for most of the heat and moisture transport between subtropics and mid-latitude. As evidenced by the modern seasonal cycle in the number of extratropical storms, transient eddy activity increases with baroclinicity. FOAM responds in a similar manner. In the NH summer, the equator-to-pole insolation gradient increases by up to 55 $Wm^{-2}$ in the Δobl-max case (Fig. 5-2a), increasing summer baroclinicity and enhancing eddy vapor transport. In the Δobl-max case, summer eddy vapor transport increases at 40°N (Fig. 5-6b) causing a net increase in the total vapor transport (Fig. 5-6d). The increase in summer vapor transport provides the moisture for additional snowfall. This seasonal meridional vapor transport is also evident by a decrease (increase) in summer atmospheric equivalent water content in tropics (subtropics).

The annual cycle of snowfall response is closely linked to differences in seasonal meridional insolation gradient. As shown in the Δobl-max case, changes in obliquity significantly alter the seasonal meridional insolation distribution (Fig. 5-2a), leading to strengthening in equator-to-pole eddy vapor transport, which influences continental snowfall. The meridional insolation gradient reaches a maximum during the summer season in the Δobl-max case. In response, meridional vapor transport increases during boreal and austral summers, leading to enhanced snowfall precipitation (Fig. 5-3 and Fig. 5-6). We note that the SH meridional temperature gradient is less sensitive to orbitally-driven insolation change than the NH in the Δobl-max case due to the presence

of the Antarctic Ice Sheets, which dominate the regional climate. As a result, the eddy response is weaker in the SH than in the NH (Fig. 5-6).

In the Δprec-max case, the winter equator-to-pole insolation gradient increases by up to 50$Wm^{-2}$ in the NH and decreases by ~50$Wm^{-2}$ in the SH (Fig. 5-2b). The enhanced seasonal equator-to-pole insolation gradient strengthens mid-latitude baroclinicity. As a result, total and eddy vapor transports increase over the mid-latitude continents (Fig. 5-6a and 5-6c), providing the moisture for boreal winter snowfall (Fig. 5-4). In contrast, due to the reduction in the SH insolation gradient, SH winter mid-latitude eddy activity decreases significantly leading to a reduction in total vapor transport (Fig. 5-6b and 5-6d), and Antarctic snowfall (Fig. 5-4).

The vapor transport from mid-latitudes ultimately reaches the high latitudes through the mean meridional circulation, and is aided by seasonal vapor transport from ocean to land. In summer time, diabatic heating sets up a zonal ocean-to-land surface pressure gradient and drives geostrophic flow that would increases tropospheric northward vapor transport over the continent in our simulations (Fig. 5-7). In the NH, the enhanced moisture transport through transient eddy activity and the large-scale circulation can be recognized as increases in lower tropospheric relative humidity (Fig. 5-8) that extend across the mid- and high-latitudes of North America and are associated with regions of enhanced or only slightly reduced specific humidity (Fig. 5-9). Vettoretti and Peltier (2003) report a similar increase in vapor transport during the Post-Eemian and refer to this as the cryospheric moisture pump.

### *3.4. Seasonal solar heating*

In addition to changes in the meridional temperature gradient (Section 3.3), changes in seasonal solar heating may also influence transient eddy transport. The growth of baroclinicity increases with enhanced meridional temperature gradient and reduced static stability (Lindzen and Farrell, 1980). Static instability occurs when a warm air parcel rises due to positive buoyancy, and is enhanced by latent heating during condensation (Gutowski et al., 1992). As the axial tilt decreases, heating in the mid-latitudes of the winter hemisphere increases seasonal baroclinicity in two ways: (1) by slightly increasing the meridional insolation gradient north of 40ºN (Fig. 5-2a); and, (2) by reducing static stability and increasing the latent heat flux. As a result, FOAM predicts enhanced transient eddy vapor transport and a small snowfall increase during the NH winter and spring in the Δobl-max case, in contrast to major change during summer and fall (Fig. 5-3 and Fig. 5-6). Similarly, snowfall differences during austral summer in the Δprec-max case (Fig. 5-4) are also attributed to seasonal solar heating (Fig. 5-2) that strengthens the mid-latitude baroclinicity and drives SH transient eddy transport at 50ºS (Fig. 5-6a).

## 4. SNOW ABLATION

In the absence of a continental ice-sheet model, we use the positive degree-day (PDD) index to estimate the potential ablation differences between experiments. The PDD index is based on the observed correlation between near ground air temperature and the rate of snow and ice melt, and is calculated by

summing daily above-freezing temperatures over a year (Braithwaite, 1995). Thus, unlike snowfall, orbital changes in potential ablation are primarily controlled by local temperature change driven by local insolation variations. Both a decrease in axial tilt and a shift toward maximum precession reduce the PDD and, by inference, the ablation potential (Fig. 5-2).

Precession has a much (254%) greater influence on ablation than obliquity in the NH. In the Δprec-max case, in response to changes from minimum to maximum precession, the annual PDD in the NH decreases by 973 degree-days, from 2203 degree-days (nhhs-high) to 1230 degree-days (nhcs-high). In comparison, the NH annual PDD in the Δobl-max case decreases by 383 degree-days from 1611 degree-days (hobl-C) to 1228 degree-days (lobl-A) with a decrease in obliquity. The PDD changes in the SH hemisphere, however, are quite different from those in the NH. The annual PDDs change by 30 in the Δprec-max case and 54 in the Δobl-max case (Table 5-3). The small change in PDD is a result of low air temperature over Antarctic.

To convert Antarctic PDD to snow melt, we use a melt factor of 0.8 cm per PDD (Braithwaite, 1995; Lefebre et al., 2002). This melt factor is based on field measurements from Greenland that range from 0.3 to 4.0 cm with a typical value of 0.8 cm. We emphasize that this factor has a large natural range; using a single global value as we do is only justifiable as a way of grossly illustrating the approximate balance between snowfall and ablation. Using this melt factor, we estimate that SH snow accumulation increases by 43 cm in response to a decrease in axial tilt. In contrast, the snow accumulation difference between

maximum and minimum precession is 24 cm. Thus our calculations indicate that obliquity has a ~45% greater influence on Antarctic snow accumulation.

It is important to note that because our experiments include present-day greenhouse gas (GHG) levels, perennial snow cover occurs only in the SH and not in the NH. Consequently, the PDD can be used to estimate differences in absolute ablation over the SH (as described above). In the NH, converting PDD to ablation would result in very high numbers that simply indicate that snow can not survive melting season. In experiments with sufficiently reduced GHGs, the NH PDD would be substantially lower (e.g., compare SH and NH PDDs, Table 5-3) and perennial snow cover would occur. Here, we use the differences in NH PDD as a relative estimate of insolation influence on continental snow ablation. Because the climate responses to orbital changes are nearly linear, as described in section 3.1, we do not expect the relative climate responses to the orbital forcing to significantly differ under lower GHGs.

# 5. DISCUSSION

## *5.1. Orbital forcing and meridional insolation gradient*

Previous studies hypothesize that the large 41kyr variance in the global ice volume record is due to changes in seasonal or annual equator-to-pole insolation gradients rather than high latitude summer insolation (Young and Bradley, 1984; Paillard, 2001; Crucifix and Loutre, 2002; Raymo and Nisancioglu, 2003; Loutre et al., 2004; Kukla and Gavin, 2004; Vettoretti and Peltier, 2004). According to the gradient hypothesis, as obliquity decreases, the insolation

gradient increases, driving greater poleward moisture transport and promoting ice sheet growth in the northern high latitudes. In contrast, precessional fluctuations induce very large insolation changes (twice that of changes in axial tilt) at northern high latitudes, but cause small changes in the meridional insolation gradient. As a result of the small changes in meridional insolation gradient, changes in poleward moisture flux are minor and the growth of ice sheets is limited.

Though FOAM's snow response to orbital forcing is consistent with the hypothesis that enhanced meridional insolation gradient leads to strengthening in poleward moisture flux, the absolute difference in snowfall is so small (approximately 16%) that it is unlikely to independently account for the ice volume variability and could not explain the difference in power at precessional and obliquity periods or the growing of precessional power after 1 Ma. Our model results show that the equator-to-pole insolation gradient influences large scale meridional moisture transport: in both experimental cases, increase in continental snowfall is associated with seasonal increases in the equator-to-pole insolation gradient (Fig.5-2, Fig. 5-3, and Fig. 5-4). However, the snowfall response to obliquity and precession is comparable. In the Δobl-max case, a decrease in axial tilt causes a 17.0 cm of continental snowfall difference, only 2.7 cm greater than that in the Δprec-max case (Table 5-2).

### *5.2. Hemispheric snowfall asymmetry*

A second explanation for the "41 kyr problem" is that because the precessional influence on ice volume is out-of-phase between hemispheres, the

precessional influence on the global ice volume is small (Raymo et al., 2006). Precessional maximum, for instance, causes cold summer conditions in the NH that promote snowfall accumulation and warm summer conditions in the SH that promote ablation. On a global scale, these two effects would approximately cancel, eliminating the precessional signal from the benthic $\delta^{18}O$ records of global ice volume. In contrast, the obliquity influence on ice volume is in-phase between hemispheres and therefore, this periodicity stands out in the benthic $\delta^{18}O$ records. Raymo et al. (2006) suggests that the ice volume record was susceptible to precessional masking prior to the mid-Pleistocene transition when the East Antarctic Ice Sheet was primarily marine-based and thus vulnerable to melting. After the mid-Pleistocene transition, the East Antarctic Ice Sheet was apparently sufficiently cold that ablation was limited and the precessional signal appeared in the benthic $\delta^{18}O$ records.

The FOAM results provide support for this hypothesis. In response to a change from minimum to maximum precession, snowfall accumulation differences are positive in the NH (14.3 cm) and negative in the SH (-6.2 cm) (Fig. 5-4 and Table 5-2). Globally, the annual snowfall increases by 7.1 cm, while ablation increases by ~24 cm in the SH. In contrast, a decrease in axial tilt enhances the annual global snowfall by up to 25.1 cm, more than three times that of the precession response, while snow melt decreases by ~43 cm in the SH. Because ice volume variance is dependent on the amplitude of the net accumulation response to orbital forcing, it follows that axial tilt, with more

snowfall and less SH ablation, will have a more prominent signal than precession, with less snowfall accumulation but increased SH ablation.

The hypothesis that precessional changes in ice volume are masked by the out-of-phase responses between the NH and SH ice sheets is predicated on the presence of NH continental ice sheets. The NH continental ice sheets appeared around 2.7 Ma and continued to grow through the late-Pleistocene (Shackleton and Hall, 1984), but were relatively small prior to the mid-Pleistocene transition (0.8 Ma). During times when NH ice sheets were small or absent and therefore unable to effectively offset any changes in Antarctic ice volume, the global ice volume record should display substantial variability in both precession and obliquity bands. Yet, this is not the case; precessional variability in the benthic $\delta^{18}O$ record is weak even prior to the mid-Pleistocene transition (Lisiecki and Raymo, 2007; Raymo et al., 2006). We suggest that other mechanisms must have accounted for the absence of strong precessional variability in the benthic $\delta^{18}O$ records before the onset of Northern Hemisphere glaciation.

### *5.3. Antarctic ice volume response to orbital forcing*

Based on the different snowfall responses to obliquity and precessional forcing in the NH and SH, we suggest that snow accumulation in Antarctica might be an alternative explanation for the obliquity signal in the global ice volume record. In our experimental sets using FOAM, the snowfall response to precession and obliquity in the NH is similar. In contrast, in the SH, precessional and obliquity changes lead to very different snow accumulations. In comparison

to precessional changes, a reduction in axial tilt increases Antarctic snowfall by 23% (1.9 cm) and decreases melt by 45% (19 cm), leading to an increase in SH net snow accumulation (Table 5-2, 5-3). In our model results, the absolute change in SH snowfall is small (~45%) compared to that of the NH, and far from balancing the NH ice volume. However, Antarctic snow has a much greater influence on isotopic mass balance than the NH snow because Antarctic snow has low $\delta^{18}O$. A unit ice volume change on Antarctica has up to 4x the effect on benthic $\delta^{18}O$ as the same ice volume change in the NH (Raymo et al., 2006). Consequently the depleted mean snow $\delta^{18}O$ over Antarctica would have amplified the net accumulation response expressed in the benthic $\delta^{18}O$. In sum, based on the SH snow accumulation results, we suggest that the absence of precessional variability prior to 1 Ma (when NH ice sheets were small) might be due to the fact that the global ice volume primarily reflects orbitally-driven changes in Antarctic accumulation.

Studies of benthic $\delta^{18}O$ show that precessional power of global ice volume increased significantly after 1 Ma (Raymo et al., 2006; Lisieck and Raymo, 2007). We suggest that the increase of spectral power in precessional band ~1 Ma marked the transition of NH domination over the global ice volume record. As the NH ice sheets gradually expanded since 2.7 Ma, the benthic $\delta^{18}O$ signal would have increasingly reflected NH ice volume for two reasons: (1) Ice volume variations would have been increasingly influenced by snowfall and ablation in the NH. Based on our results, NH ablation is very sensitive to precessional forcing. This increase in ice volume variation transfers into high spectral power in

precessional band because power variance is an exponential function of variance magnitude in spectral analysis. To illustrate this concept, we created two synthetic records containing both precession and obliquity signals but different magnitude of variations at the precessional period. Spectral analysis of the two records demonstrates a 4x increase in precessional spectral power with a doubling of the precession-related signal (Fig. 5-10). The absence of precessional variability in the early Pleistocene may represent the fact that global ice volume was mainly obliquity-driven changes in Antarctic ice volume (Fig. 5-10a). After the expansion of NH ice sheets, precessional power may have been significantly enhanced as the ice volume variation increased (Fig. 5-10b). (2) The $\delta^{18}O$ of snow/ice over the NH ice sheets would have progressively decreased as the ice sheets grew. In modern Antarctica, for example, $\delta^{18}O$ values of firn range between -20‰ to -55‰ (Graf et al., 1999). These very low values result from vapor fractionation due to the very low temperatures and high elevations of the Antarctic ice sheet. Snow falling on the Northern Hemisphere ice sheets would have experienced a similar fractionation history.

### *5.4. Model limitation*

The purpose of this study is to evaluate the influence of orbital parameters on continental snow accumulation. For this reason, we systematically altered only one orbital parameter in each experiment to decipher the changes made by obliquity and precession variations. In reality, these cycles overlapped, complicating the climate response to orbital forcing. Also, $pCO_2$ was maintained at present-day levels in our experiments; our experiments therefore do not

account for $CO_2$ feedbacks. Reducing the $CO_2$ in these experiments would increase the net snow accumulation by decreasing the potential ablation. It is unclear if the snowfall response to orbital forcing would increase in a low $CO_2$ climate. However, as explained in Section 4, we do not expect the relative climate responses to orbital forcing to significantly differ under lower GHGs.

Because our model does not currently include a dynamic ice-sheet component, it is not possible to calculate ice-sheet flow or to predict ice-volume changes resulting from the orbital changes that might influence our results (DeConto and Pollard, 2003; Levis et al., 2004). Throughout our analysis and interpretation we assume that an increase in snowfall translates into an increase in ice volume. Our results may be better viewed as a continental snow accumulation potential. Future climate experiments of orbital forcing will need to incorporate dynamic ice-sheet model to make direct comparisons with the ice volume record.

## 6. SUMMARY & CONCLUSION

The benthic $\delta^{18}O$ record of global ice volume has varied mainly at the obliquity period (~41 kyrs) with relatively weak variance at the precession period (~21 kyrs) through most of the Pleistocene indicating that summer insolation is not sufficient to regulate ice-age cycles. Here, we present a suite of coupled ocean-atmosphere GCM experiments that quantify orbital influences on continental snowfall and potential ablation. We show that snowfall and ablation variations are closely linked to seasonal insolation forcing. Our model results

identify three ways though which the global ice volume record is more sensitive to variations in obliquity than precession. First, vapor transport and continental snowfall is most directly linked to the equator-to-pole insolation gradient, which varies strongly with the axial tilt. Second, changes in snowfall and potential ablation due to precessional shifts are out-of-phase between the hemispheres, resulting in only small changes in net global snow fall. Third, Antarctic snow accumulation has greater response to obliquity than precession, because annual increase of snowfall is amplified by summer decrease of melt.

We suggest that prior to the mid-Pleistocene transition obliquity-driven change in Antarctic snow accumulation was likely controlling the global ice volume variability. After the growth of Northern Hemisphere ice sheets, both precession and obliquity had significant influences on snowfall accumulation and thus continental ice volume. However, because snowfall accumulation linked to precession is out-of-phase between hemispheres, the global ice volume change due to precession would have largely canceled and been subsidiary to obliquity.

## ACKNOWLEDGEMENTS

This research was supported by National Science Foundation grant ATM-0432503 to C.J. Poulsen, and the University of Michigan Barbour Fellowship and Scott Turner Research Fund to S.-Y. Lee.

FIGURES: Chapter V

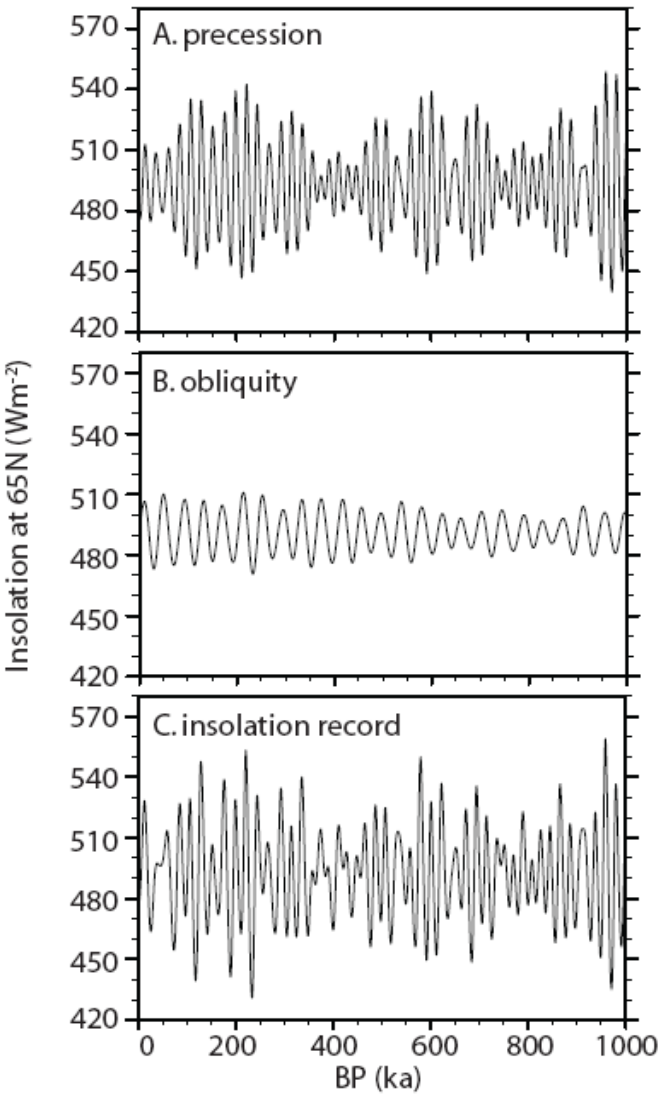


Figure 5-1. June 21 insolation at 65ºN for the past 1 million years. Insolation was calculated for orbits with (A) fixed (23.5°) obliquity and time varying eccentricity and precession, (B) fixed eccentricity/precession and time varying obliquity, and (C) time varying eccentricity, precession, and obliquity. The summer insolation at 65ºN is dominated by precession signal. The insolation records were created using code contributed to us by D. Pollard (personal communication) and based on celestial mechanics from Danby (1967) using the orbital solutions of Berger (1991) .

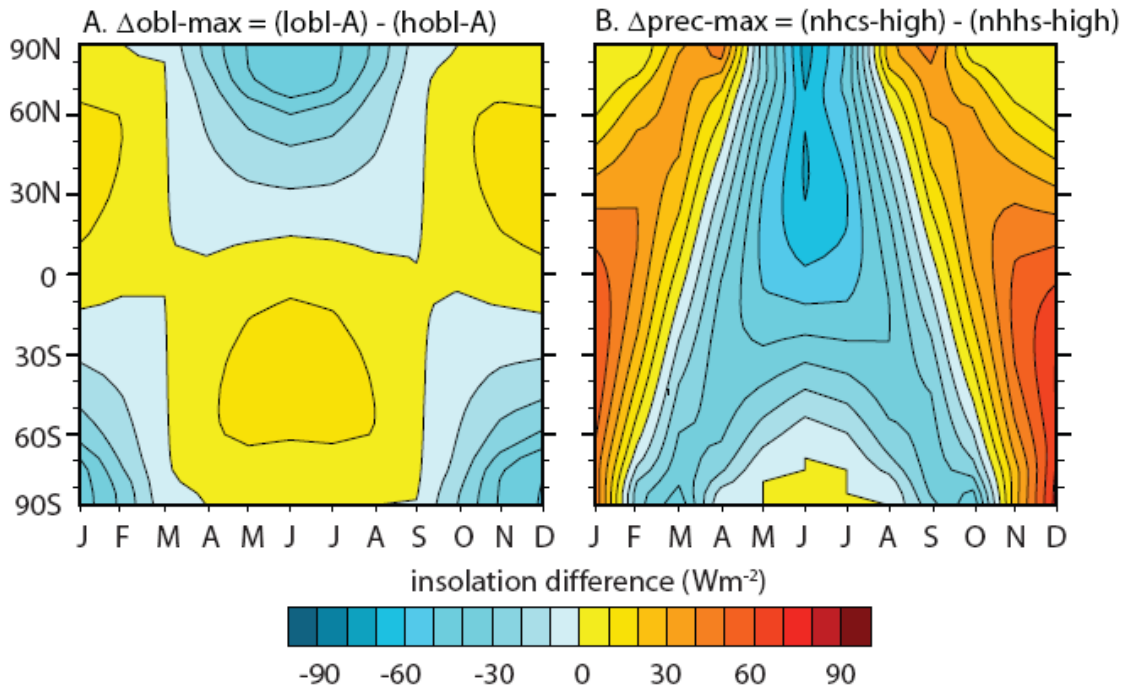


Figure 5-2. Mean monthly insolation difference ($Wm^{-2}$) between obliquity (A. Δobl-max = lobl-A – hobl-A) and precessional (B. Δprec-max = nhcs-high – nhhs-high) experiments. Contour interval is 10 $Wm^{-2}$.

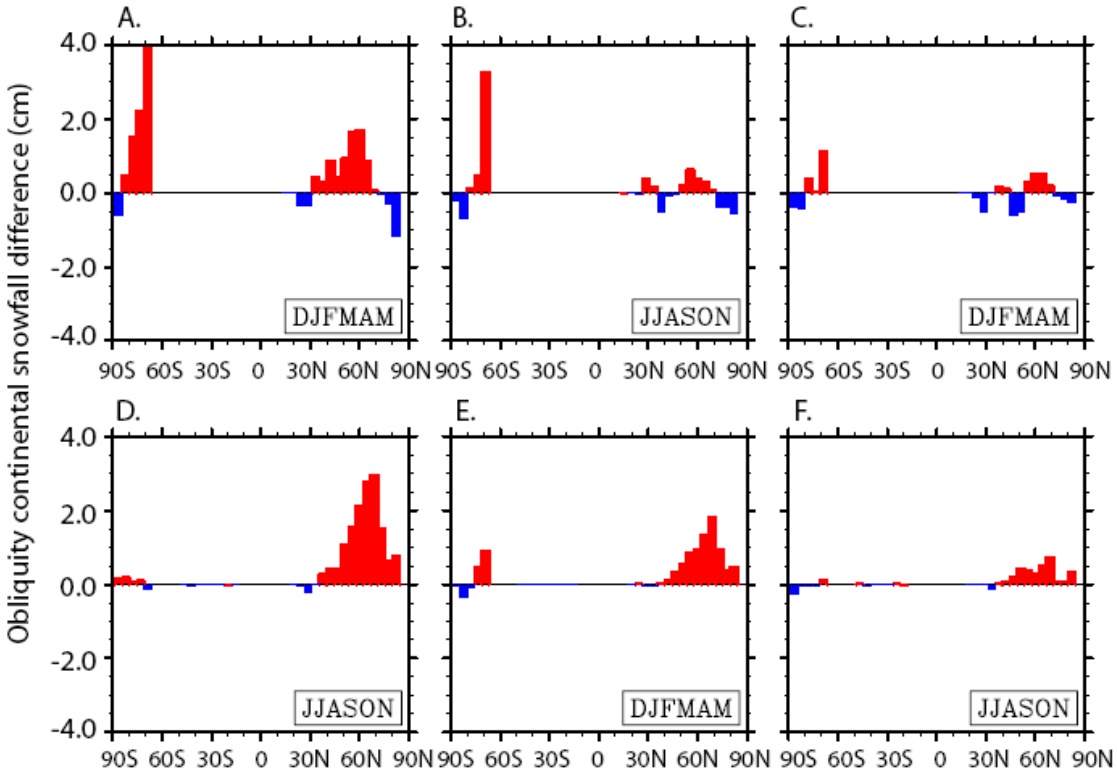


Figure 5-3. Cumulative continental snowfall responses to obliquity forcing. Zonally-averaged half-year (December through May and June through November) differences in total snowfall (cm) (A,D) ∆obl-max, (B,E) lobl-B – hobl-B, and (C,F) lobl-C – hobl-C.

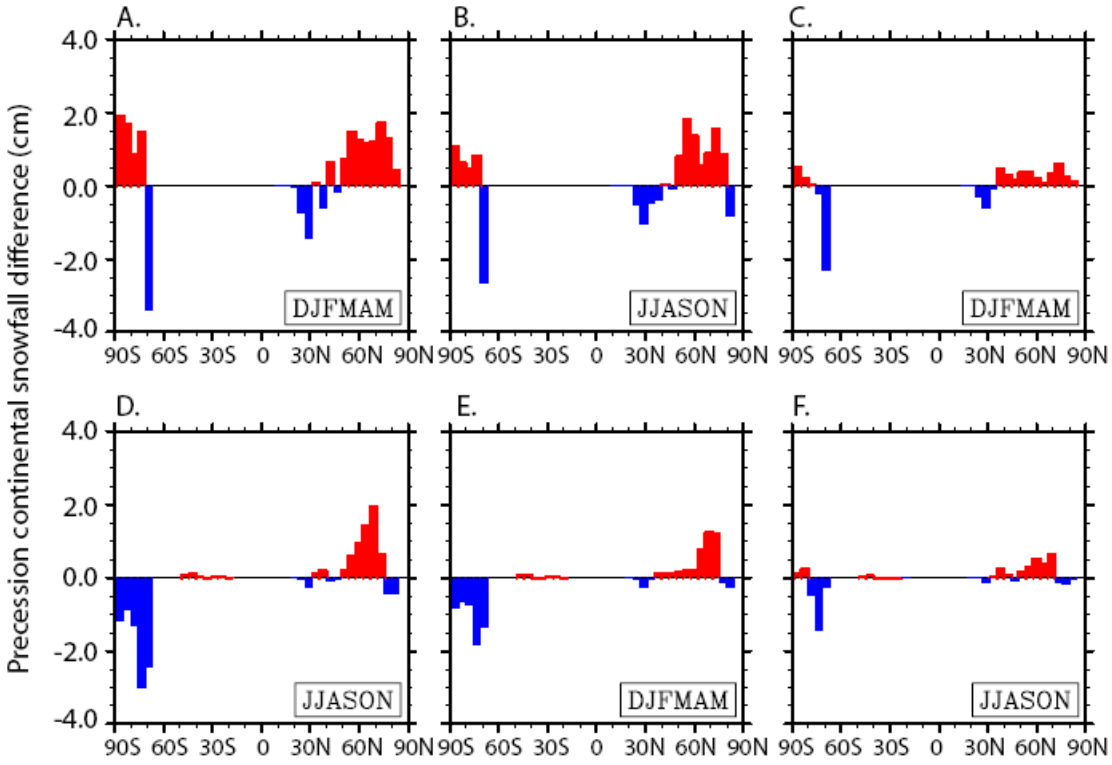


Figure 5-4. Cumulative continental snowfall responses to precession forcing. Zonally-averaged half-year (December through May and June through November) differences in total snowfall (cm) (A,D) ∆perc-max, (B,E) nhcs-med – nhhs-med, and (C,F) nhcs-low – nhhs-low.

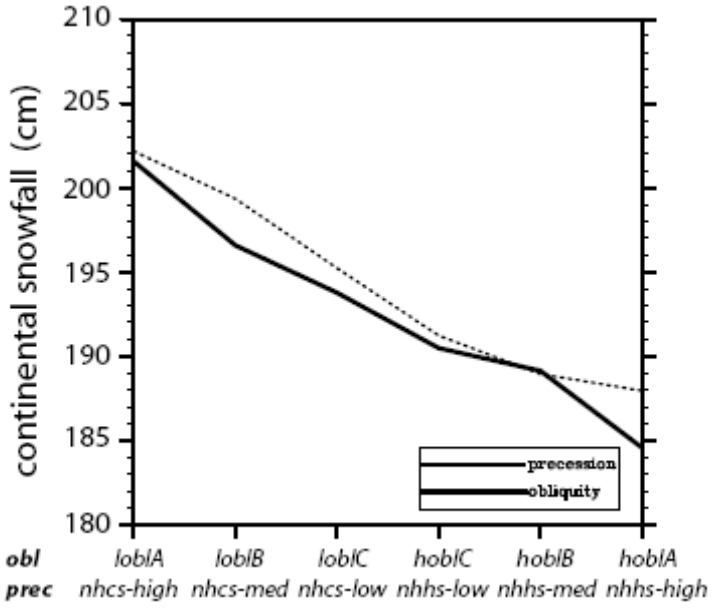


Figure 5-5 Annual NH continental snowfall (cm) in each experiment. Note that the snowfall response to obliquity and precession in the model is largely linear.

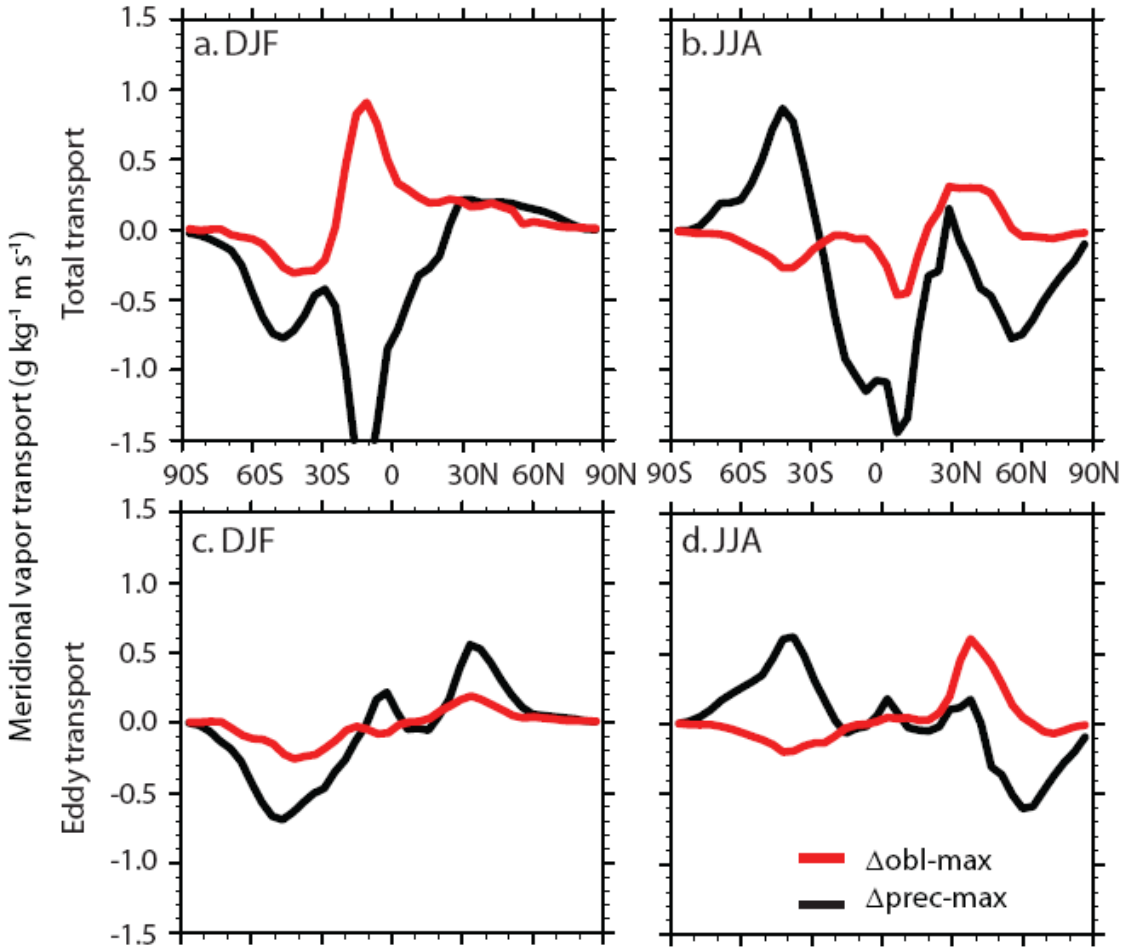


Figure 5-6 Response of meridional vapor transport to orbital forcing. Differences in zonally average seasonal meridional (A-B) total vapor transport (including mean meridional circulation, stationary eddies, and transient eddies) between experiments (Δobl-max: red line; Δprec-max: black line) and (C-D) transient eddy vapor transport (g $kg^{-1}$ m $s^{-1}$). Positive values represent an increase in the northward vapor transport or a reduction in the southward vapor transport.

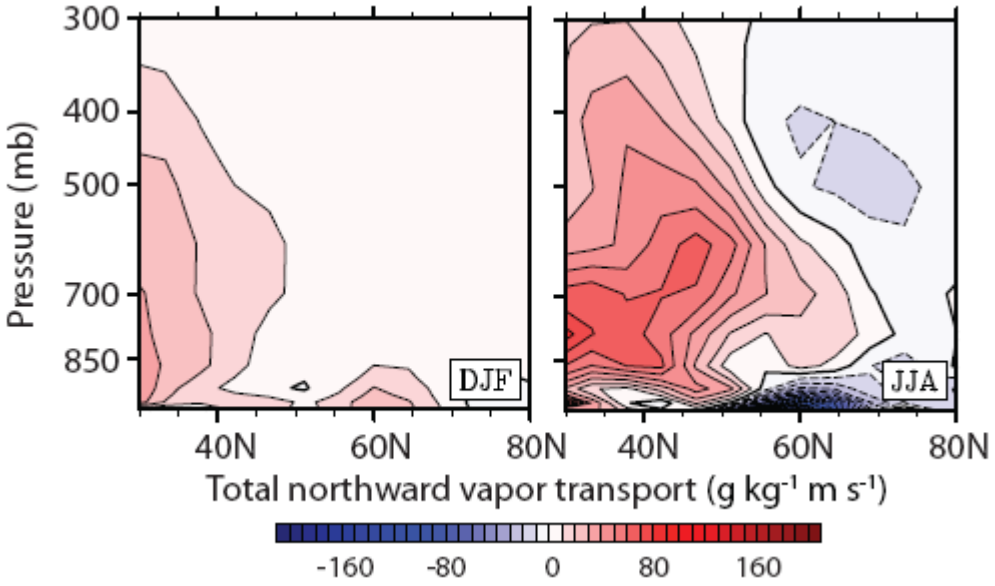


Figure 5-7 Difference in total northward vapor transport over Northern Hemisphere continents. Difference in mean (A) December-January-February and (B) June-July-August meridonal vapor transport due to a reduction in obliquity (Δobl-max). Positive values represent greater northward vapor transport. In June-July-August, the enhanced northward transport corresponds to increase continental snowfall (Fig. 3A). The contour interval is 10 cm $s^{-1}$ g $kg^{-1}$.

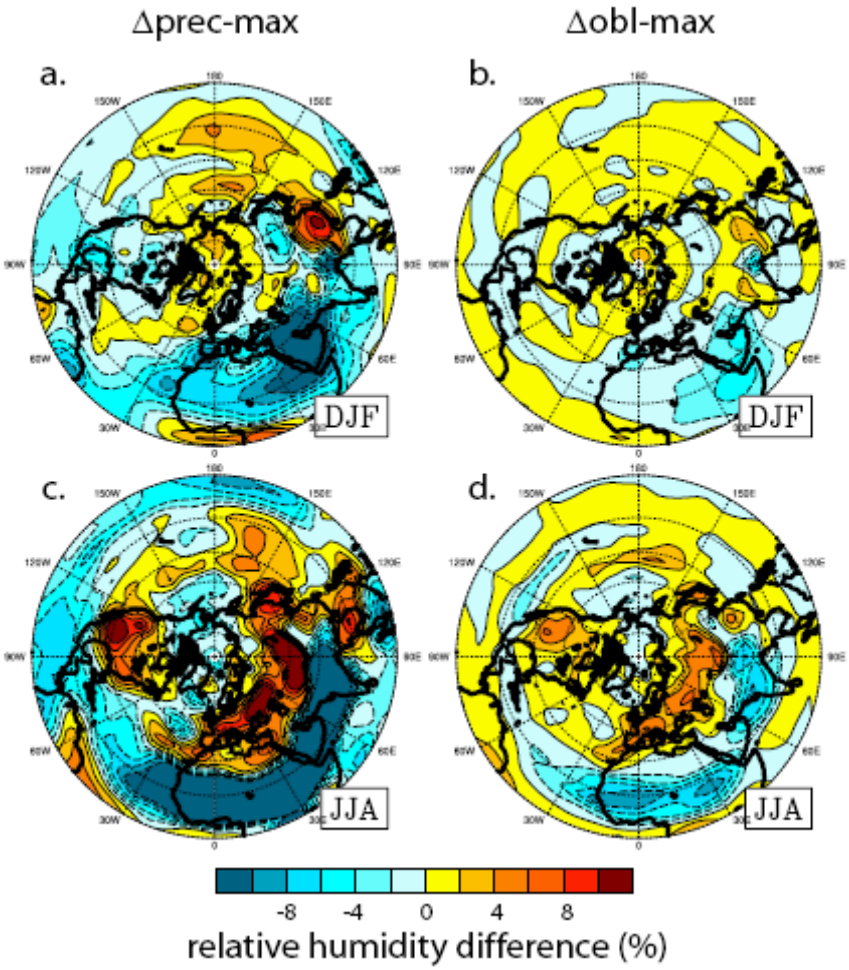


Figure 5-8 Response of tropospheric relative humidity to orbital forcing. Difference maps of seasonal lower tropospheric (700mb) relative humidity (%) in (A,C) Δprec-max and (B,D) Δobl-max. The contour interval is 2%. The enhanced moisture transport through orbital-forced transient eddy activity can be recognized as increases in lower tropospheric relative humidity across North America.

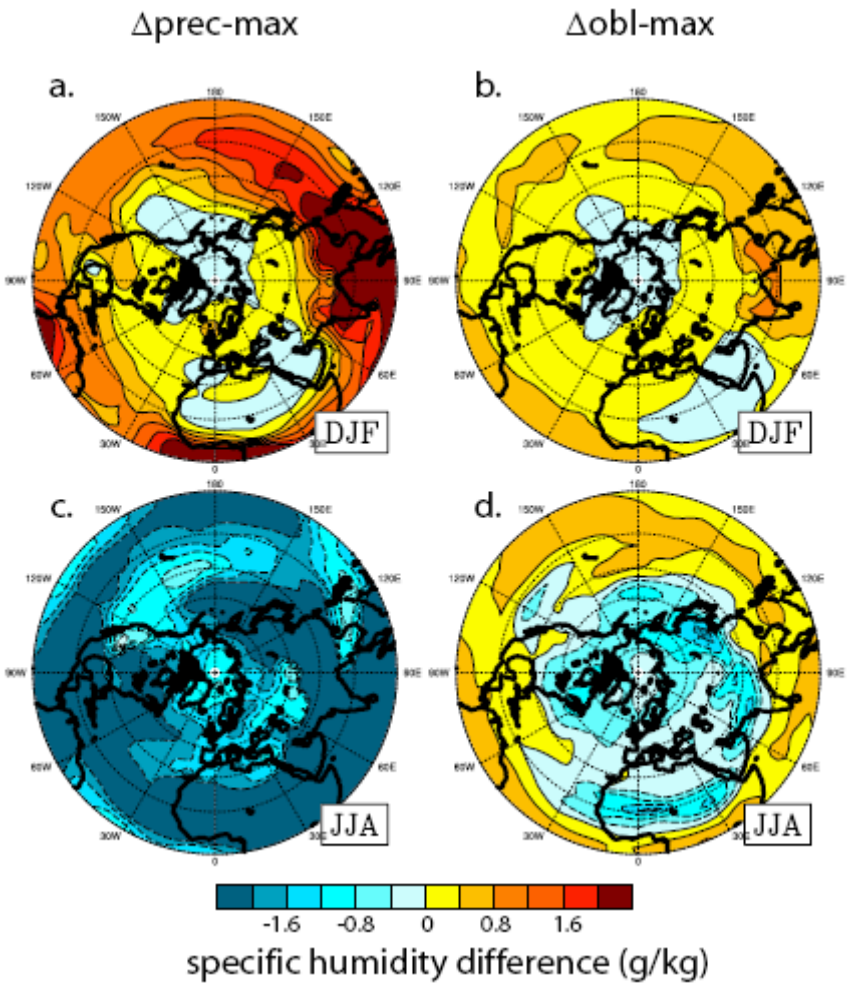


Figure 5-9. Response of tropospheric specific humidity to orbital forcing. Difference maps of seasonal lower tropospheric (700mb) specific humidity (g $kg^{-1}$) in (A,C) Δprec-max and (B,D) Δobl-max. The contour interval is 0.4 g $kg^{-1}$. The different spatial pattern between relative and specific humidity indicates difference in saturation and moisture transport.

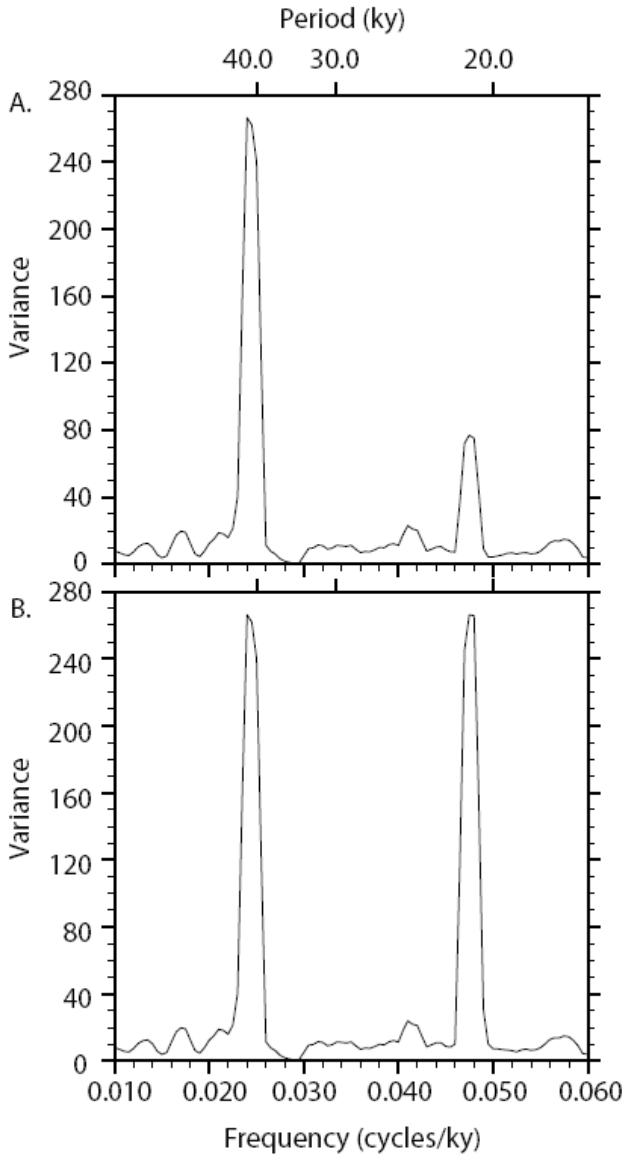


Figure 5-10 Spectral analyses of synthetic records contain both obliquity and precessional signals and random noise. (A) shows a spectral analysis of fix variance amplitude in obliquity band and 1x variance amplitude in precessional band. (B) shows a spectral analysis of fix variance amplitude in obliquity band and doubled variance amplitude in precessional band compare to (A). Note the significant increase of power variance at the precessional period from (A) to (B). The spectral analyses illustrate how increase in global ice volume variability in precessional band may have enhanced precessional power expression in global ice volume record after 1 Ma.

TABLES: Chapter V

Table 5-1. List of numerical climate experiments and orbital parameters. Orbital parameters were modified one at a time; other orbital settings were prescribed at present-day value with eccentricity of 0.017, obliquity of 23.45º, and precession of 168º. (nhcs = NH cold summer; nhhs = NH hot summer; hobl = high obliquity; lobl = low obliquity)

| Experiment | Eccentricity | Obliquity | Precession |
|---|---|---|---|
| nhcs-high | 0.056 | 23.45 | 180 |
| nhcs-med | 0.037 | 23.45 | 180 |
| nhcs-low | 0.017 | 23.45 | 180 |
| nhhs-high | 0.056 | 23.45 | 0 |
| nhhs-med | 0.037 | 23.45 | 0 |
| nhhs-low | 0.017 | 23.45 | 0 |
| hobl-A | 0.017 | 24.50 | 168 |
| hobl-B | 0.017 | 24.12 | 168 |
| hobl-C | 0.017 | 23.73 | 168 |
| lobl-A | 0.017 | 22.20 | 168 |
| lobl-B | 0.017 | 22.58 | 168 |
| lobl-C | 0.017 | 22.97 | 168 |

Table 5-2. Continental snowfall differences between experimental pairs. Positive (negative) numbers represent greater (less) continental snowfall (in cm $yr^{-1}$).

| | **Obliquity** | | | **Precession** | | |
|---|---|---|---|---|---|---|
| | Δobl-max | B | C | Δprec-max | med | low |
| **NH** | | | | | | |
| **DJFMAM** | 3.7 | 0.2 | 0.5 | 9.3 | 7.0 | 2.3 |
| **JJASON** | 13.3 | 7.2 | 2.8 | 5.0 | 3.4 | 1.7 |
| **ANN** | 17.0 | 7.4 | 3.3 | 14.3 | 10.4 | 4.0 |
| **SH** | | | | | | |
| **DJFMAM** | 7.7 | 2.9 | 0.7 | 2.5 | 0.3 | -0.8 |
| **JJASON** | 0.4 | 0.9 | -0.3 | -8.7 | -5.4 | -1.8 |
| **ANN** | 8.1 | 3.8 | 0.4 | -6.2 | -5.1 | -2.6 |

Δobl-max = (lobl-A) – (lobl-A)
Obliquity B = (lobl-B) – (lobl-B)
Obliquity C = (lobl-C) – (lobl-C)
Δprec-max = (nhcs-high) – (nhhs-high)
Precession B = (nhcs-med) – (nhhs-med)
Precession C = (nhcs-low) – (nhhs-low)

Table 5-3. Annual and seasonal PDD indexes for each experiment. The indexes are calculated by summing daily above-freezing temperatures over a year. In the NH, the indexes were derived from area north of 60ºN.

| | | | **Precession** | | | |
|---|---|---|---|---|---|---|
| | nhcs-high | nhcs-med | nhcs-low | nhhs-high | nhhs-med | nhhs-low |
| **NH** | | | | | | |
| **JJASON** | 1228 | 1423 | 1507 | 2200 | 2049 | 1828 |
| **ANN** | 1230 | 1427 | 1514 | 2203 | 2054 | 1832 |
| **SH** | | | | | | |
| **DJFMAM** | 103 | 100 | 82 | 72 | 72 | 82 |
| **ANN** | 104 | 101 | 83 | 74 | 73 | 83 |

| | | | **Obliquity** | | | |
|---|---|---|---|---|---|---|
| | lobl-A | lobl-B | lobl-C | hobl-C | hobl-B | hobl-A |
| **NH** | | | | | | |
| **JJASON** | 1226 | 1304 | 1482 | 1600 | 1727 | 1857 |
| **ANN** | 1228 | 1308 | 1487 | 1611 | 1749 | 1880 |
| **SH** | | | | | | |
| **DJFMAM** | 62 | 64 | 73 | 97 | 109 | 115 |
| **ANN** | 63 | 65 | 74 | 98 | 110 | 117 |

# REFERENCES


Bart, P. J. (2001). Did the Antarctic ice sheets expand during the early Pliocene? Geology 29(1): 67-70.

Berger, A.L. and M.F. Loutre (1991), Insolation values for the climate of the last 10 million years, Quaternary Science Reviews, 10: 297-317.

Berger, A., Li, X.S., Loutre, M.F. (1999). Modelling northern hemisphere ice volume over the last 3 Ma. Quaternary Science Review 18: 1-11.

Braithwaite, R. J. (1995). Positive degree-day factors for ablation on the Greenland ice-sheet studied by energy-balance modeling. Journal of Glaciology 41(137): 153-160.

Clark, P. U., Pollard, D. (1998). Origin of the middle Pleistocene transition by ice sheet erosion of regolith. Paleoceanography 13: 1-9.

Danby, J.M.A. (1962), Fundamentals of celestial mechanics, Macmillan, New York, 348 pp.

Gutowski, W. J., Branscome, L.E., Stewart, D.A. (1992). Life-cycles of moist baroclinic eddies. Journal of the Atmospheric Sciences 49(4): 306-319.

Haq, B. U., Hardenbol, J., Vail, P.R. (1987). Chronology of fluctuating sea levels since the Trissic. Science 235(4793): 1156-1167.

Harrison, S., Kutzbach, J., Liu, Z., Bartlein, P., Otto-Bliesner, B., Muhs, D., Prentice, I.C., Thompson, R.S. (2003). Mid-Holocene climates of the Americas: a dynamical response to changed seasonality. Climate Dynamics 20: 663-688.

Huyber, P. (2006) Early Pleistocene glacial cycles and the integrated summer insolation forcing. Science 313(5786): 508-511.

Huyber, P., Wunsch, C. (2005). Obliquity pacing of the late Pleistocene glacial termination. Nature 434: 491-494.

Imbrie, J., Berger, A., Boyle, E.A., Clemens, S.C., Duffy, A., Howard, W.R., Kukla, G., Kutzbach, J., Martinson, D.G., McIntyre A., Mix, A.C., Mofino, B., Morley, J.J., Peterson, L.C., Pisias, N.G., Prell, W.L., Raymo, M.E., Shackleton, N.J., Toggweiler, J.R. (1992). On the structure and origin of major glaciation cycles, 1. Linear responses to Milankovitch forcing. Paleoceanography 7: 701-738.

Imbrie, J., Berger, A., Boyle, E.A., Clemens, S.C., Duffy, A., Howard, W.R., Kukla, G., Kutzbach, J., Martinson, D.G., McIntyre A., Mix, A.C., Mofino, B., Morley, J.J., Peterson, L.C., Pisias, N.G., Prell, W.L., Raymo, M.E., Shackleton, N.J., Toggweiler, J.R. (1993). On the structure and origin of major glaciation cycles 2. the 100,000-year cycle. Paleoceanography 8(6): 699-735.

Jacob, R. (1997). Low frequency variability in a simulated atmosphere ocean system. Madison, University of Wis.-Madison. Ph.D. dissertation, 159pp.

Khodri, M., Leclainche, Y., Ramstein, G., Braconnot, P., Mart,i O., Cortijo, E. (2001). Simulating the amplification of orbital forcing by ocean feedbacks in the last glaciation. Nature 410(6828): 570-574.

Kiehl, J. T., Hack, J.J., Bonan, G.B., Boville, B.A., Briegleb B.P., Williamson, D.L., Rasch, P.J. (1996). Description fo the NCAR Community Climate Model (CCM3) NCAR Tech. Note, 152pp.

Lee, S.-Y., Poulsen, C.J. (2005). Tropical Pacific climate response to obliquity forcing in the Pleistocene. Paleoceanography 20: PA4010, doi:10.1029/2005PA001161.

Levis, S., G. B. Bonan, C. Bonfils, 2004: Soil feedback drives the Mid-Holocene North African monsoon northward in fully coupled CCSM2 simulations with a dynamic vegetation model. Climate Dynamic, 23, doi: 10.1007/s00382-004-0477y, 791- 802.

Lindzen, R. S., Farrell, B. (1980). The role of Polar-regions in global climate, and a new parameterization of global heat transport. Monthly Weather Review 108(12): 2064-2079.

Lisiecki, L. E., Raymo, M.E. (2005). A Pliocene-Pleistocene stack of 57 globally distributed benthic δ18O record. Paleoceanography 20.

Liu, Z., Kutzbach J., Wu, L. (2000). Modeling climate shift of El Nino variability in the Holocene. Geophys. Res. Lett. 27(15): 2265-2268.

Loutre, M.-F., D. Paillard, et al. (2004). Does mean annual insolation have the potential to change the climate? Earth and Planetary Science Letters 221(1-4): 1-14.

Milankovitch, M. (1941). "Canon of insolation and the ice-age problem."

Paillard, D. (2001). Glacial cycles: Toward a new paradigm. Reviews of Geophysics 39(3): 325-346.

Peltier, W. R. (2004). Global glacial isostasy and the surface of the ice-age Earth: the ICE-5G (VM2) model and GRACE. Annual Review of Earth and Planetary Sciences 32: 111-149.

Philander, S. G., Federov, A.V. (2003). Role of tropics in changing the response to Milankovitch forcing some three million years ago. Paleoceanography 18(2): 1045.

Poulsen, C. J., Pierrehumbert, R.T., Jacob, R.L. (2001). Impact of ocean dynamics on the simulation of the Neoproterozoic "snowball earth". Geophys. Res. Lett. 28(8): 1575-1579.

Ravelo, A. C., Andreasen, D.H., Lyle, M., Lyle, A.O., Wara, M.W. (2004). Regional climate shifts caused by gradual global cooling in the Pliocene epoch. Nature 429(6989): 263-267.

Raymo, M. E. (1994). The initiation of Northern-hemisphere glaciation. Annual Review of Earth and Planetary Sciences 22: 353-383.

Raymo, M. E., Lisiecki L.E., Nisancioglu K. (2006). Plio-Pleistocene ice volume, Antarctic climate, and the global δ18O record. Science 313: 492-495.

Raymo, M. E., Nisancioglu, K. (2003). The 41 kyr world: Milankovitch's other unsloved mystery. Paleoceanography 18(1): 1011.

Renssen, H., Goosse, H., Muscheler, R. (2006). Coupled climate model simulation of Holocene cooling events: solar forcing triggers oceanic feedback. Climate of the Past 2: 209-232.

Ruddiman, W. F. (2003). Orbital insolation, ice volume, and greenhouse gases. Quat. Sci. Rev. 22: 1597-1629.

Ruddiman, W. F. (2006). Ice-driven CO2 feedback on ice volume. Climate of the Past 2: 43-78.

Shackleton, N. J., HALL, M.A. (1984). Oxygen and carbon isotope stratigraphy of Deep-Sea Drilling Project Hole-552A - Plio-Pleistocene glacial history. Initial reports of the Deep Sea Drilling Project 81: 599-609.

Shackleton, N. J., Hall, M.A., Pate, D. (1995). Pliocene stable isotope stratigraphy of site 846. College Station, Texas.

Vettoretti, G., Peltier, W.R. (2003). Post-Eemian glacial inception. Part II: Elements of a cryospheric moisture pump. J. Clim. 16: 912-927.

Wu, L., Liu, Z., Gallimore, R., Jacob, R., Lee, D., Zhong, Y. (2003). Pacific decadal variability: the tropical Pacific mode and the North Pacific mode. Journal of Climate 16(8): 1101-1120.

Young, M. A., Bradley, R.S. (1984). Insolation gradient and paleoclimate record. Springer, New York.

# Chapter VI

## Summary

The glacial-interglacial cycles of the past 2.7 Myr represent one of the largest and most significant climate phenomena during the late Cenozoic. Traditional Milankovitch theory fails to explain several prominent features of the Pleistocene benthic $\delta^{18}O$ record. Among these, the dominance of the obliquity frequency in the early Pleistocene; and the absence of prominent spectral power in the precessional frequency pose challenges to the Milankovitch theory and to our understanding of orbital influences on climate. Data and modeling studies support the idea that Earth's climate system does not always respond linearly to external forcing; small changes in insolation forcing may be amplified by internal climate feedbacks. In this study, a series of experiments were developed and analyzed to determine the climate response to orbital forcing and the internal pathways as well as feedbacks that propagate and amplify orbital forcing during Plio-Pleistocene.

In response to an increase in axial tilt, the model predicts tropical sea-surface cooling associated with a decrease in local insolation. Extratropical sea-surface temperature warms because of the increase in local insolation and a decrease in sensible heat loss with a reduction in sea ice. Anomalous heating through high-obliquity forcing results in weakening of both mean-annual mid-

latitude westerlies and subtropical trade winds. Advection and ventilation of anomalously warm extratropical water causes subsurface warming in the central and eastern tropical Pacific. Because the subsurface warming does not penetrate to the sea surface, the equatorial trade winds and Walker circulation do not have systematical changes.

Marine proxies of sea surface temperature (SST) indicate that the tropical Pacific thermal gradient intensified through the Plio-Pleistocene and peaked during Pleistocene glaciations. The influence of Southern Ocean sea ice to mid-latitude and eastern equatorial Pacific oceanic condition has an implication to Plio-Pleistocene tropical Pacific oceanic reorganization. We present a specific mechanism, the cooling of the eastern equatorial Pacific through the upwelling of anomalously cold waters from the Southern Ocean, to explain the enhanced tropical Pacific SST gradient evidenced in marine proxy records.

The strong spectral power of Pleistocene benthic $\delta^{18}O$ at ~41kyr indicates that global ice volume has been modulated by Earth's axial tilt. This feature has been attributed to the influence of obliquity on mean-annual and seasonal insolation gradients at high latitudes. In response to obliquity changes, our modeling results indicate that insolation variations associated with a decrease in obliquity amplify continental snowfall in two ways: (1) An increase in high-latitude winter insolation is enhanced through a low-cloud feedback, resulting in colder air temperatures and increased snow precipitation. (2) An increase in the summer insolation gradient enhances summer eddy activity, increasing vapor transport to

high-latitude regions. In our experiments, just over one-half of the annual snowfall increase is attributed to seasonal changes in insolation suggesting that mean-annual insolation forcing is an equally important factor on influencing continental snowfall as seasonal insolation forcing.

By comparing two series of sensitivity experiments investigating the influence of precession and obliquity on continental snow fall and melt, we identify three factors that tend to magnify the influence of obliquity forcing on global ice volume. First, high-latitude snowfall is dominated by changes in Earth's axial tilt. Second, hemispheric changes in net snowfall due to Earth's precession are out-of-phase producing a very small global snowfall change. Third, net snow accumulation variability over Antarctica responds greatly to changes in obliquity through snowfall and ablation.

This study seeks to understand the climate response to orbital forcing. Pleistocene and modern simulations were developed and analyzed to determine the mechanisms that provide feedbacks on insolation forcing and link various climate components. This study identifies (1) a high-latitude-tropical connection through the South Pacific surface gyre circulation that explains much of the tropical climate variability in the Plio-Pleistocene proxy record and (2) internal feedbacks that amplify climate response to orbital forcing that might have contributed to the large sensitivity of Pleistocene global ice volume to obliquity.